THE BIOCHEMISTRY AND STRUCTURE OF A NOVEL NITRIC OXIDE SYNTHASE FROM CYANOBACTERIA

A Dissertation

Presented to the Faculty of the Graduate School

of Cornell University

in Partial Fulfillment of the Requirements for the Degree of

Doctor of Philosophy

by

Angela Picciano

December 2019

THE BIOCHEMISTRY AND STRUCTURE OF A NOVEL NITRIC OXIDE SYNTHASE FROM CYANOBACTERIA

Angela Picciano, Ph.D.

Cornell University 2019

Nitric oxide synthases (NOS) are monooxygenase enzymes that catalyze the oxidation of L-arginine to L-citrulline and nitric oxide (NO). They are composed of a catalytic heme-binding domain (NOS_{ox}) and a flavin-binding domain (NOS_{red}) responsible for electron transfer and heme activation. NOS-derived NO serves as a signaling molecule in animals, controlling vascular tone, immune response, and neuronal signaling. NOS are also found in bacteria and are involved in various roles, including biofilm formation, recovery from UV damage, and protection from oxidative stress. However bacterial NOS sequences only contain a NOS_{ox} domain, and must rely on nonspecific reductases for activation. Recently, sequences for a unique NOS-like protein have been identified in cyanobacteria. These proteins are the first bacterial NOS to contain a mammalian-like NOS_{red}, and also contain a globin-like domain (NOS_g) which has not been observed in any other NOS. This work confirms that the NOS from the cyanobacteria *Synechoccocus* sp. PCC 7335 (syNOS) is a true NOS, and produces NO from L-arginine. However, the factors governing syNOS activation deviate from our current knowledge of NOS enzymology. syNOS requires Ca^{2+} and tetrahydrobiopterin for NO production, and $syNOS_g$ rapidly oxidizes all NO to nitrate. $syNOS_{red}$ facilitates the reduction of $syNOS_{ox}$ and $syNOS_g$ independent of one another, which indicates direct electron

transfer between $syNOS_g$ and $syNOS_{red}$. The reduction of $syNOS_g$ can also be mediated by $syNOS_{FAD}$, in a manner analogous to flavohemoglobin proteins, and does not require $syNOS_{FMN}$, as in NOS_{ox} reduction. The structures of $syNOS_{FAD}$ and $syNOS_{FMN}$ have been determined, and homology modeling of $syNOS_g$ confirms that $syNOS_{FAD}$ – $syNOS_g$ domain interactions are possible. The function of syNOS has yet to be identified, but genomic analysis of other syNOS homologues suggests it may participate in signal transduction pathways. The presence of $syNOS_g$ and its Ca^{2+} dependence may serve as a switch to turn on/off such signaling pathways.

BIOGRAPHICAL SKETCH

Angela Picciano was born in June of 1990 to Sara (Maccherone) Picciano and Anthony Picciano, and was raised in Swedesboro, NJ with her sister, Gina. Angela attended St. Margaret's elementary & middle school, and Padua Academy high school, where her interest in chemistry began. Angela majored in biochemistry at Rowan University, where she worked in the labs of Dr. Gregory Caputo, studying the design of antimicrobial peptides and their permeabilization of bacterial membranes, and Dr. Timothy Vaden, investigating the potentially therapeutic interaction of amyloid β peptides with copper and curcumin. These experiences motivated her to pursue research; after graduating magna cum laude in 2013 she began graduate studies at Cornell University. When she is not in the lab, Angela volunteers at the Tompkins County SPCA and is a member of the Finger Lakes Mineral Club.

ACKNOWLEDGMENTS

I would first like to thank my family for their unconditional support despite the large distance separating us. Thank you to my advisor, Brian Crane, for your immense patience and endless advice. It has been a privilege to work with you. I would also like to thank my lab mate Mike Lynch for giving me a reason to laugh every day, even when my results were disappointing. Thank you to Roselynn Cordero, who has been an incredible friend and source of support for all the ups and downs of graduate school. And last but not least, thank you to my lab mate Estella Yee, for listening to all my questions and complaints these past six years.

TABLE OF CONTENTS

LIST OF TABLES

LIST OF FIGURES

Chapter One

Chapter Two

Chapter Three

Appendix B

Appendix C

CHAPTER ONE

Introduction

1.1 A Brief History of Nitric Oxide Biology

Nitric oxide (NO) is a gaseous diatomic free radical, with an unpaired electron delocalized between the nitrogen and oxygen atoms in a π* molecular orbital; NO readily reacts with other organic radical species, including triplet oxygen and metal ions (1). Since its discovery in the 1770's (2), NO has been largely known as a potent greenhouse gas produced by anthropogenic sources, primarily combustion (3). The identification of NO as a biologically relevant molecule came almost 200 years after its discovery and has been an active field of research ever since.

The field of NO biology began with the discovery of its role in the denitrification cycle of bacteria and plants. NO was proposed to be an intermediate between the reduction of NO_2^- to N_2O as early as the 1950's (4) but the concept remained controversial for decades. Heavy debate revolved about whether NO_2^- was directly reduced to N_2O or NO, or if NO was the byproduct of some other transient intermediate (4). The argument was laid to rest by the late 1980's, with the isolation of NO reductases (Nor), identification of NO production from nitrite reductase (Nir), and ΔNor and ΔNir mutagenesis experiments (5–7). Other sources of bacterial NO include hydroxylamine oxidoreductase (8), and stzF in streptozocin biosynthesis (9). In addition to denitrification, plants may produce NO from nitrate reductases (10, 11), and nonenzymatically from the reaction of nitrogen dioxide with carotenoids (12), or reduction of nitrite by ascorbate (13, 14).

NO had been used in pharmacology for over a century before its significance in mammalian biology was recognized. Inhalation of amyl nitrites and ingestion of nitroglycerin were observed to produce vasodilatory effects as early as the 1850's, and became a common treatment for headaches and ischemic chest pain (15). When investigating effect of vasodilators on smooth muscle and liver tissues in the late 1970's, the pharmacologist Ferid Murad observed they caused cGMP concentrations to rise; this effect was also observed upon administering NO gas, and he suggested that NO could be the biological activator of soluble guanylyl cyclase (sGC) (16). Three years later, Robert Furchgott observed the vasodilation of rabbit aorta was dependent on the endothelium, and concluded it must release some unknown endothelial derived relaxation factor (EDRF) (17). In 1987, Louis Ignarro identified EDRF as NO after observing the same effects were caused by NO and EDRF; activation of sGC by both was inhibited by hemoglobin, this inhibition was reversed with CO, and both produced the same Soret shift in hemoglobin spectra (18). Murad, Furchgott, and Ignarro were awarded the 1998 Nobel Prize in Physiology and Medicine, which is fitting as the prize was founded with the fortune Alfred Nobel had made from the commercialization of nitroglycerin almost a century prior (15).

1.2 Mammalian Nitric Oxide Synthase

The enzyme responsible for the production of NO, nitric oxide synthase (NOS), was first isolated from rat cerebellum in 1990 (19). Three isoforms are found in animals; two are constitutively expressed and named for the tissue from which they were originally extracted: endothelial NOS (eNOS) is primarily found in vascular endothelial cells (20), and neuronal NOS (nNOS) is found in neurons (19). The third isoform, inducible NOS (iNOS), is found in

Figure 1.1: Domain architecture of mammalian and bacterial NOS

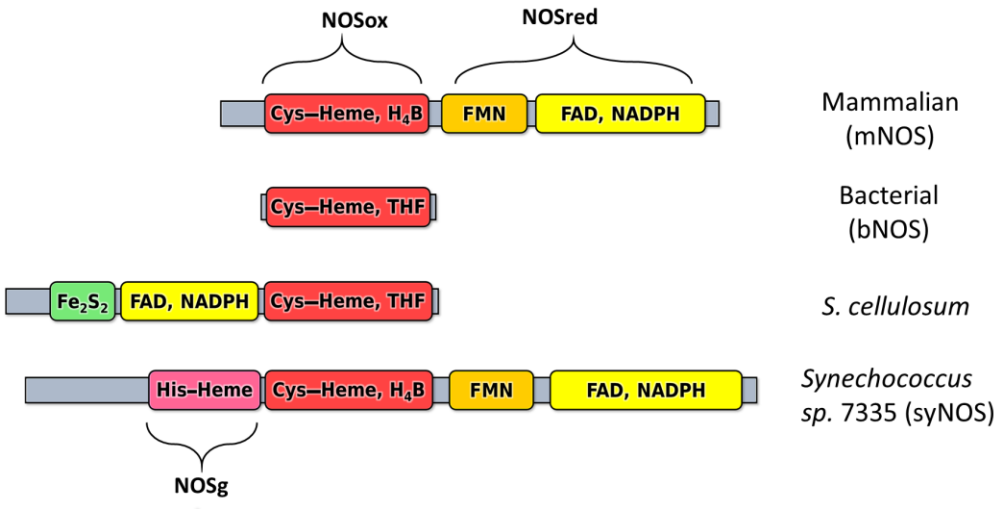

macrophages and is expressed upon induction by lipopolysaccharides of the bacterial cell wall, cytokines, or endotoxins (21). All three NOS isoforms are composed of two domains, a heme containing NOS_{ox} and a flavin binding NOS_{red}. NOS_{ox} is a member of the cytochrome P450 (CYP450) family of proteins and NOS_{red} shares similarity with cytochrome P450 reductases (CYPOR) (22, 23). NOS_{ox} and CYP450 are both heme monooxygenases, which add one atom from O_2 to substrate and convert the other atom to water, and also share a characteristic Soret at ~450 nm for the ferrous-CO species (22). Much of what is known about CYP450 has been used to investigate NOS, in particular to investigate the mechanism of substrate oxidation (24, 25). NOS_{red} and CYPOR are both diflavin reductases, composed of an FMN-binding flavodoxin-like domain (NOS_{FMN}) followed by a FAD- and NADPH-binding ferredoxin-$NADP^+$ reductase (FNR)-like domain (NOS_{FAD}) (23). NOS are active as N-terminal homodimers, and the NOS_{red} of one monomer serves to reduce the heme of the opposite NOS_{ox}. nNOS additionally contains an N-terminal PDZ sequence, which dictates its biological function by binding to postsynaptic density protein (PSD-95) which localizes nNOS to NMDA glutamate receptors (26). NOS_{ox} is an N-terminal heme-binding domain,

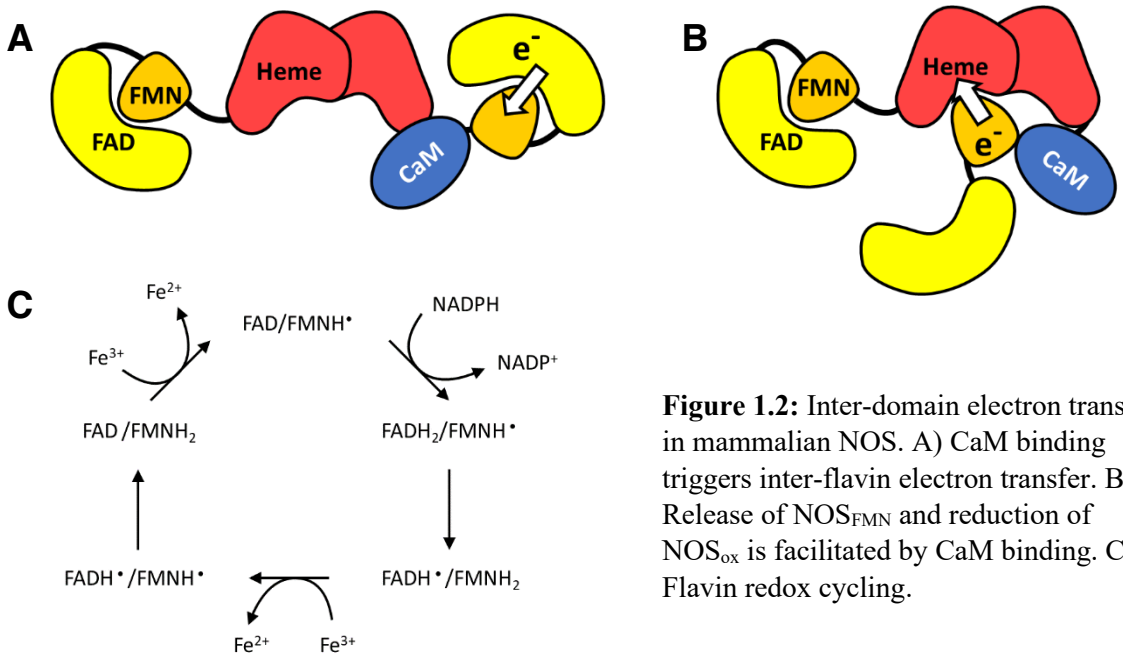

Figure 1.2: Inter-domain electron transfer in mammalian NOS. A) CaM binding triggers inter-flavin electron transfer. B) Release of NOS_{FMN} and reduction of NOS_{ox} is facilitated by CaM binding. C) Flavin redox cycling.

containing a Cys-ligated b-type heme, and is the location of dimerization. N-terminal β-loops "hook" together between dimers, bringing together four cysteine residues that coordinate to a zinc atom, which is responsible for increased dimer stability. Dimer contacts also occur at the helical T and helical lariat (27). NOS_{ox} and NOS_{red} are connected by a linker containing a calmodulin-binding sequence. Electron transfer between domains is facilitated by the binding of calmodulin to calcium (Ca^{2+}-CaM) (Fig. 1.2), which is the regulating factor in the constitutive isoforms (28, 29). In the absence of Ca^{2+}-CaM, NOS_{FMN} remains associated to NOS_{FAD}. An autoinhibitory loop found in NOS_{FMN} of eNOS and nNOS suppresses electron transfer in the absence of Ca^{2+}-CaM and dictates the calcium concentration dependence (30). This regulatory element is not found in iNOS, whose activity is controlled by its expression level and thus is independent of calcium concentration. In all isoforms, electron transfer between FAD and FMN is also facilitated by CaM binding (31). Reducing equivalents are supplied by NADPH, which reduces FAD to the hydroquinone state ($FADH_2$) and performs

the one-electron reduction of the semiquinone ($FMNH^{\bullet}$) to its hydroquinone ($FMNH_2$). *In vivo* FMN cycles between the hydroquinone and semiquinone, but only the hydroquinone has a sufficiently low enough reduction potential to reduce NOS_{ox} (Fig. 1.2C) (32). The FMN semiquinone can be reduced by $FADH_2$ or $FADH^{\bullet}$ to return to the hydroquinone state, and FAD will be re-reduced by another equivalent of NADPH (Fig. 1.2C). The NOS catalytic cycle of the constitutive isoforms is initiated upon Ca^{2+}-CaM binding. This triggers electron transfer (ET) and release of NOS_{FMN} from NOS_{FAD} (Fig. 1.2A and B). The initial resting state of NOS_{ox} is a ferric low-spin heme (Fig. 1.3 species **1**), and arginine binding at the distal site results in a high-spin heme and rise in reduction potential (from –347 mV to –235 mV for iNOS, –239 mV to –220 mV nNOS (32)). This increase in reduction potential accelerates

Figure 1.3: Activation of molecular oxygen and oxidation of L-arg to L-cit and NO

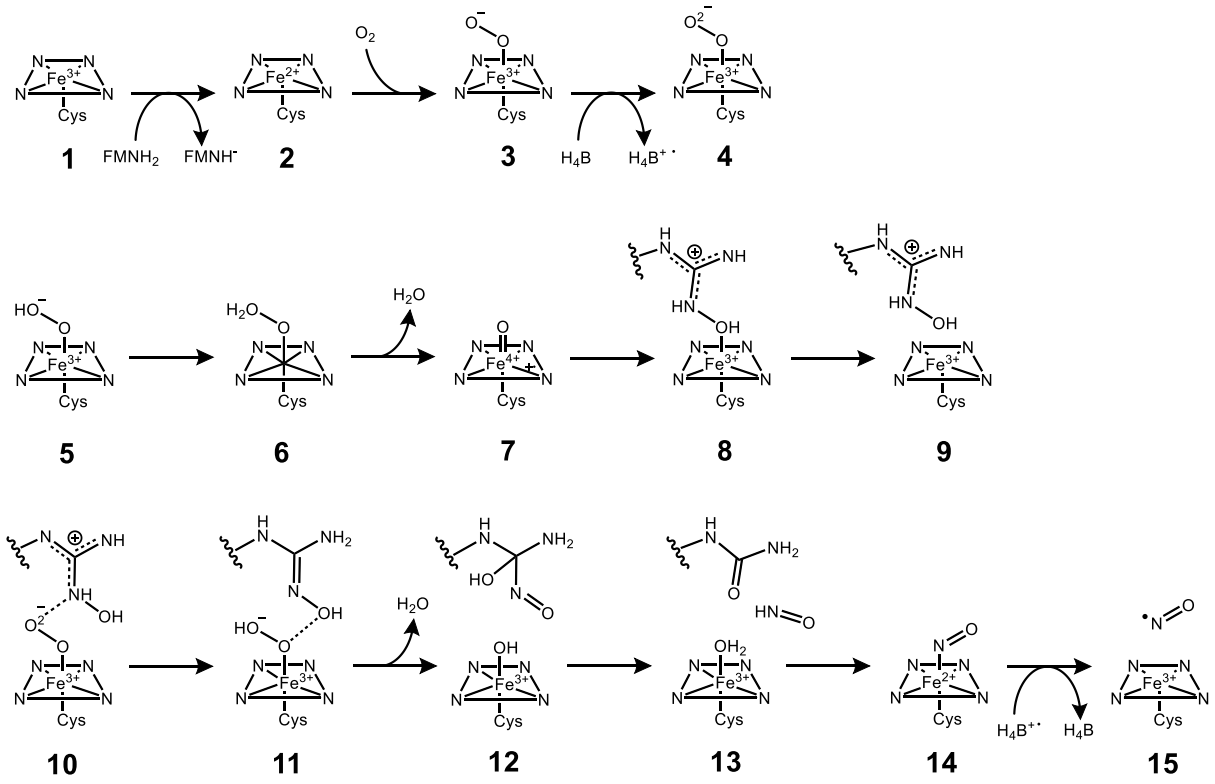

heme reduction by $FMNH_2$ (**2**) (32). In the first stage of the catalytic cycle (Fig. 1.3), the ferrous heme binds oxygen (**3**), forming the ferric-peroxo species (25). Another reducing equivalent is required to activate oxygen and prevent superoxide release, however, ET between NOS_{ox} and NOS_{red} is relatively slow. Instead, the second electron is rapidly delivered by the nearby tetrahydrobiopterin (H_4B) cofactor (33), with hydrogen bonding interaction with a heme propionate, to form the ferric-superoxo species which then becomes protonated to the ferric-dihydroperoxo state (**6**). Water is eliminated upon the heterolytic cleavage of the H_2O-O bond, resulting in the formation of the oxy-ferryl radical compound I (**7**). Compound I oxidizes L-arginine to the intermediate Nω-hydroxy-L-arginine via a radical recombination mechanism (25), returning the heme to the ferric state. The second stage of L-arginine oxidation begins much like the first, with the formation of the ferric-superoxo species, however, compound I is not the oxidant. The hydroperoxo nucleophilically attacks the imine carbon, forming a tetrahedral intermediate, and the following rearrangement releases nitroxyl (25). This nitroxyl molecule then gets oxidized by the ferric heme to produce NO, and the ferrous heme reduces the oxidized pterin ($H_4B^{+\bullet}$) (34), so that the second stage is a net one electron process.

1.3 Bacterial Nitric Oxide Synthase

The existence of NOS is not exclusive to eukaryotic organisms; the first evidence of bacterial NOS activity (bNOS) was reported in 1994 from *Nocardia* (NOS_{NOC}) (35). bNOS have been characterized structurally and biochemically, and although they share significant sequence and structural identity to $mNOS_{ox}$, no reductase domain homologous to that of mNOS has been identified. In fact, only one bNOS has been found with a covalently attached

reductase domain, however, it is quite dissimilar to $mNOS_{red}$ (Fig. 1.1). The NOS from *Sorangium cellulosum* (scNOS) contains an N-terminal reductase domain composed of a bacterioferritin-associated ferredoxin containing a 2Fe2S cluster, followed by an FNR-like domain (36). Electron transfer from FAD/NADPH to NOS_{ox} is proposed to proceed via the 2Fe2S domain, analogous to that of the three-protein system of FNR, ferredoxin, and cytochrome P450 (36).

The search for a bNOS reductase partner has been informative, yet inconclusive. The flavodoxins YkuN and YkuP have been investigated as potential *B. subtilis* NOS (bsNOS) specific reductases, and *in vitro,* both proteins have been discovered to support bsNOS catalysis and NO production (37). *In vivo*, bsNOS prepares the cell to survive exposure to hydrogen peroxide, and deletion of bsNOS results in susceptibility to H_2O_2 (38). However, deletion of the proposed bsNOS reductases, YkuN or cisJ, the latter having a high homology to mNOS, did not hinder *B. subtilis* survival (39). Instead of one specific reductase partner, bNOS proteins are proposed to use any of the many available chemical or protein-based reductants. In a search of 22 bNOS genes, none were found on the same operon with any known reductase (39). bNOS may be the evolutionary ancestors to eukaryotic NOS, which later acquired CaM binding and NOS_{red} domains (39).

Although bNOS and $mNOS_{ox}$ share significant sequence identity, there are still significant dissimilarities that affect cofactor usage and NO release. The helical T and helical lariat, which form the dimer interface in mNOS, are also present in bNOS, however, the N-terminal hook is absent (40). This allows for flexibility in pterin cofactor usage, and bNOS can use either H_4B or its larger analogue tetrahydrofolic acid (THF) (41, 42). The presence of the N-terminal hook in mNOS restricts the size of the pterin-binding pocket (27), leaving no

space for the large glutamyl p-amino benzoic acid (pABA) side chain of THF. The absence of this hook in bNOS may not be accidental; it is necessary for bNOS to accommodate the larger pterin as few bacteria are capable of H_4B synthesis. The H_4B biosynthesis pathway consists of three enzymes: GTP cyclohydrolase I (GTPCH I), 6-pyruvoyl tetrahydropterin synthase (PTS), and sepiapterin reductase (SR) (43). GTPCH I and PTS are commonly found in bacteria and are a part of the folate biosynthesis pathway; SR, however, is typically absent (44, 45). Instead, bNOS use THF which is part of the folate biosynthesis pathway and widely available in bacteria (46). In addition to pterin usage, there are small differences in the distal pocket of bNOS. Val567 is conserved in mammalian isoforms, however in bNOS, this residue is always an Ile. Mutation of Ile to Val in bsNOS resulted in accelerated NO synthesis and release, while replacing Val with Ile in iNOS slowed down these processes (47). Differences in the hydrogen-bonding network at this site were found to affect NO synthesis, and NO release was slowed by the bulkier side chain (47).

Compared to its eukaryotic counterpart, the functions of prokaryotic NOS are largely unknown and the existence of bNOS is species-dependent and not widely conserved within a genus (48). Thus, little functional information can be inferred *a priori* upon the discovery of a bNOS, whose function can range from recovery from UV damage (49), toxin biosynthesis (50), control of aerobic respiration (51), and protection from oxidative stress (51, 52). For example, exogenous and bsNOS-derived NO was observed to protect *B. subtilis* from hydrogen peroxide induced oxidative stress by increasing catalase expression (53) and inhibiting Fenton chemistry (38). The Fenton reaction, i.e., the reduction of H_2O_2 to OH^- and $OH^{\bullet}$, oxidizes ferrous iron, which is then re-reduced by free cysteine to maintain the destructive cycle (38). NO interrupts this by inhibiting the thiol reducing system Trx/TrxRed,

thus preventing ferrous iron recycling (38). The functions of bNOS are disparate and their occurrences relatively rare, but the full distribution and diversity of bNOS largely remains unexplored.

1.4 NOS in the Plant Kingdom

The search for NOS in the plant kingdom has been inconclusive, despite many observations of L-arginine-dependent NO production (54). NOS inhibitors have been reported to decrease NO production in plants, and proteins have been detected using NOS antibodies (55). However, these proteins have no sequence similarity to mNOS and have only led to false positives identifying plant NOS (56, 57). AtNOS was observed to produce NO and *in vitro* oxidize L-arg to NO in a CaM dependent manner (58). However, AtNOS has no sequence similarity to mNOS, and NOS activity was not reproduceable (57). Instead it was found to hydrolyze GTP and was renamed NO-associated protein 1 (AtNOA1) (57).

Recently, the first NOS from the plant kingdom was identified in the unicellular algae *Ostreococcus tauri* (otNOS) (59, 60). This NOS is homologous to mNOS (34-42% identical) and contains sequences for the NOS_{ox}, NOS_{FMN}, and NOS_{FAD} domains (59). otNOS oxidation of l-arg was dependent on H_4B and Ca-CaM, however it retained 70% of activity in the absence of CaM (59). The physiological role of this NOS is currently under investigation, but increased NOS activity has been observed *in vivo* during exponential growth phase and upon high intensity light irradiation (59). Very recently, NOS have also been identified in several cyanobacterial species. These cyanobacterial NOS are unlike previously studied bacterial and eukaryotic NOS; they are the first bNOS to contain a reductase domain similar to that of

mNOS and also contain an additional domain assigned to the globin family of proteins (61, 62). In addition to their novel NOS, cyanobacteria are a particularly interesting area of research due to their indispensable role in the past, present, and future of Earth's biogeochemistry.

Early Earth was an anaerobic and mildly reducing environment, with abundant hydrogen, sulfur, and carbon dioxide gases; the first microorganism had evolved and adapted to use these as reagents for synthesis. Early cyanobacteria began oxygenic photosynthesis around 2.4 billion years ago in the Paleoproterozoic era, and the accumulation of oxygen oxidized the early Earth, now called the Great Oxidation Event (GOE) (63, 64). Not only did this allow for great biological diversification and the evolution of eukaryotes, it also transformed Earth's geochemistry and mineralogy. The increased stability of metal oxides is thought to be responsible for an estimated 2,500 mineral species out of the 4,400 currently known (65).

The environmental importance of modern cyanobacteria has grown significantly since the GOE. Eutrophication, climate change, and increasing CO_2 levels have fueled the growth of toxic algal blooms globally, which have increased in size, duration, and severity since the Industrial Revolution (66, 67). These overgrowths of cyanobacteria and algae have caused death and disease in aquatic and land animals, leading to decreased biodiversity (66). The blooms release various cyanotoxins, composed of peptides, alkaloids, and lipopolysaccharides, which target the nervous and hepatic systems (66). The large accumulation of organic carbon created by the blooms in benthic zones, primarily through growth and death of the blooms, is decomposed by microbes, which consumes dissolved oxygen and creates anoxic environments that lead to the death of aquatic organisms (66).

Naturally hypoxic environments do exist, however, new hypoxic zones have been forming and the sizes of these "dead zones" are increasing (67). Although the growth of algal blooms is an active threat to the environment, cyanobacteria may also serve to save the environment through the development of biofuels. Cyanobacteria-produced biofuels have several advantages over both fossil fuels and plant-based biofuels. Production of these renewable fuels would be sustainable and non-polluting, and may even be coupled to CO_2 emissions from industrial sources (68, 69). Unlike plant-based biofuels, cyanobacteria grow faster and do not compete for arable land use or require pesticides (70). However, the low yields and high costs keeps the demand for cyanobacteria-based fuels low. Efforts to improve profit margins focus on engineering strains to optimize fuel production; heterologous metabolic pathways have been inserted into *Synechococcus* and *Synechocystis* and optimized for the production of ethylene, iso-butyraldehyde, iso-butanol and others (68). Other strategies include removal of pathways that may compete for resources used or products made, and increasing the tolerance to toxic products (70). The study of cyanobacterial NOS may facilitate the development of these optimized strains, as NO is known to participate in cyanobacterial growth and stress tolerance. NO production is correlated with *Microcystis* and *Chattonella* growth (71, 72), and low levels of exogenous NO accelerate *Microcystis* growth (72). NO is also observed to protect nitrogenase from UVB induced damage in *Spirulina* (73) and alleviate damage from aluminum accumulation in *Anabaena* (74). Cyanobacteria also contain heme nitric oxide/oxygen binding proteins (H-NOX) (75), which regulate biofilm formation, quorum sensing, colonization, and motility in bacteria (76, 77). Understanding how NOS factors into the complex roles NO plays in cyanobacteria can be exploited to engineer strains optimized for biofuel production and mitigate the spread of algal blooms.

The NOS described herein (syNOS) is found in *Synechoccocus* sp. 7335. Also referred to as *S. mexicanus* or *Coccusdissimilis mexicanus* (78), this marine organism was isolated from snail shells in Puerto Peñasco at the intertidal zone in the Gulf of California (79). This photoautotroph is capable of nitrogen fixation; however, it does not form heterocysts (79), which physically separate the incompatible nitrogen fixation and photosynthesis processes. Instead, *Synechococcus* may temporally separate the two in a light dependent manner, wherein the switch from photosynthesis to nitrogen fixation is controlled by the diurnal light/dark cycle (80). Alternatively, the switch can be growth phase dependent, where nitrogen fixation is inactive during cell division, for example (81). Little has been published on this strain of *Synechococcus* specifically, although it has taken part in numerous phylogenetic and comparative genomics studies of cyanobacteria (82, 83). Recently, it has been investigated among several cyanobacteria for their ability to photosynthesize using far-red light. During a far-red light photoacclimation (FaRLiP) process these organisms were found to synthesize chlorophyll *d* and *f*, whose Q_y bands lie just outside (706 nm) the range of photosynthetically active radiation (400 – 700 nm) (84, 85). This allows for greater flexibility in its light requirements for oxygenic photosynthesis

1.5 *Synechococcus* Nitric Oxide Synthase

Full-length syNOS is a 1468 amino acid protein with a predicted molecular weight of 166,254 Da. A BLAST search restricted to the mammalia class found 35% identity to mammalian iNOS. The first ~320 amino acids of syNOS cannot be assigned to any class of proteins, and sequence searches only return other proteins annotated as a NOS. Residues 343-459 (NOS_g) are assigned to the globin family of proteins, and do not share significant identity

with any mammalian protein, but share 31 % identity with the flavohemoglobin from *Methylacidiphilum infernorum* (Hell's Gate globin), whose function is unknown. $syNOS_{ox}$ (479-833) is slightly more similar to bNOS (~48% identity) than $mNOS_{ox}$ (~44% identity). The linker between NOS_{ox} and NOS_{red} does not contain the calmodulin-binding sequence found in the mammalian enzymes (Fig. 1.4). Although this sequence is conserved in all eukaryotic NOS, its absence from syNOS is not unexpected; no calmodulin homologue is present in the genome of *Synechococcus* sp. PCC 7335. The reductase domain (NOS_{red} residues 856-1468) is slightly more similar to CYPOR (33% identity) than $iNOS_{red}$ (30%). $syNOS_{red}$ also lacks several NOS_{red} specific regulatory elements, including the inhibitory loop, CD2A regulatory element, and phosphorylation sites.

syNOS is the first NOS to be identified in cyanobacteria and its function is unclear. Algal otNOS was shown to increase NO production upon intense light irradiance and during exponential growth (59), however, the significance of this has yet to be determined and may not be relevant to syNOS, as otNOS does not have the added globin domain. In fact, the presence of $syNOS_g$ is likely to be integral to its function in *Synechococcus*. Flavohemoglobins are efficient NO dioxygenases (NOD) composed of an N-terminal histidine ligated heme B and a C-terminal FNR-like domain (86, 87). The presence of a potential NOD attached to a NOS is perplexing, however, there are examples in biology of NOD and NOS working together. For example, in mammals α-globin is associated to eNOS and attenuates signaling by consumption of NO (88). In *S. aureus*, saNOS-derived NO is detoxified by flavohemoglobin (hmp) under fully aerobic conditions. However, under microaerobic conditions, hmp cannot bind oxygen yet saNOS remains active. NO is free to inhibit terminal cytochrome oxidases of the electron transport chain, which forces the cell to

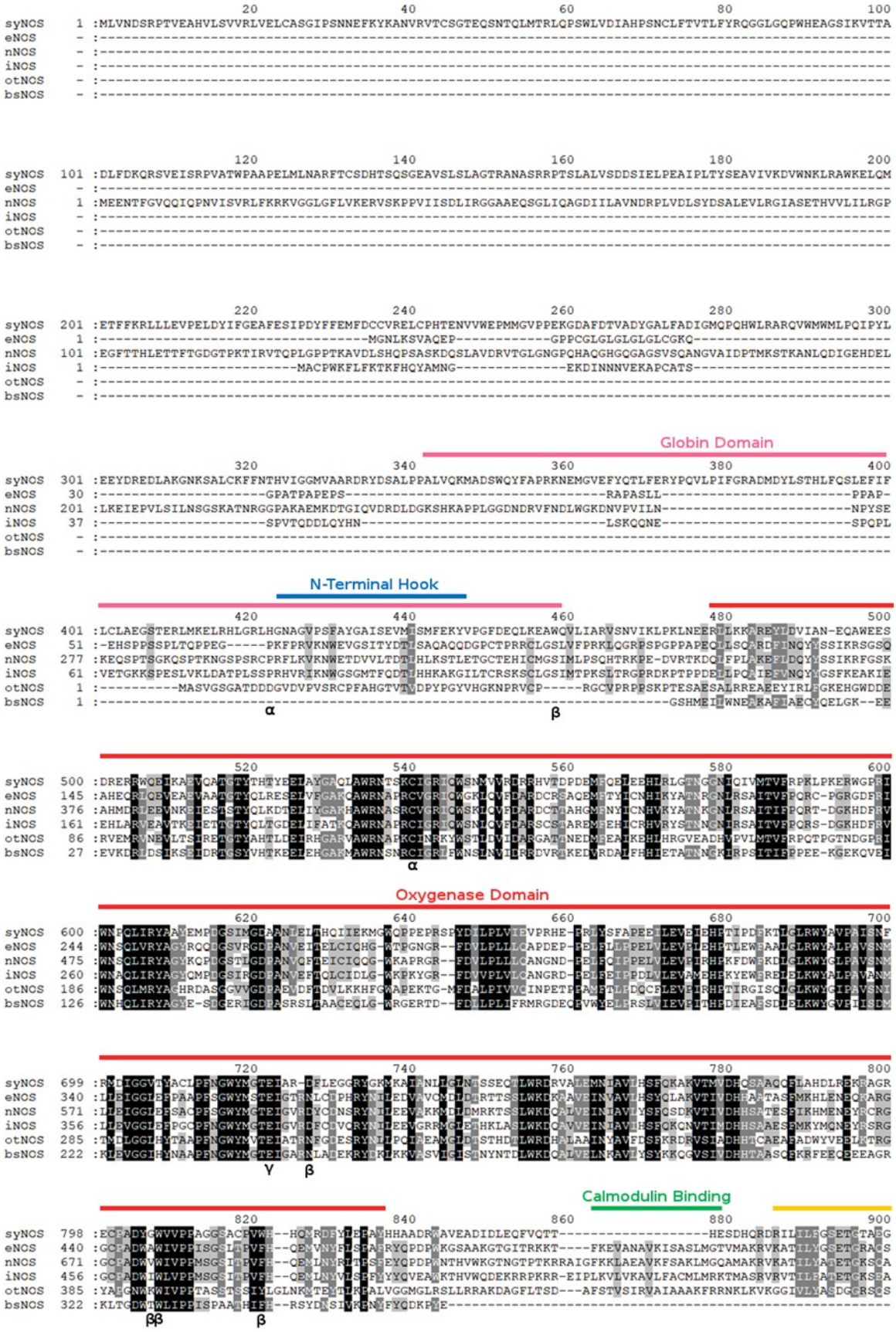
Globin Domain
N-Terminal Hook
α
β
α
Oxygenase Domain
γ
β
Calmodulin Binding
ββ
β

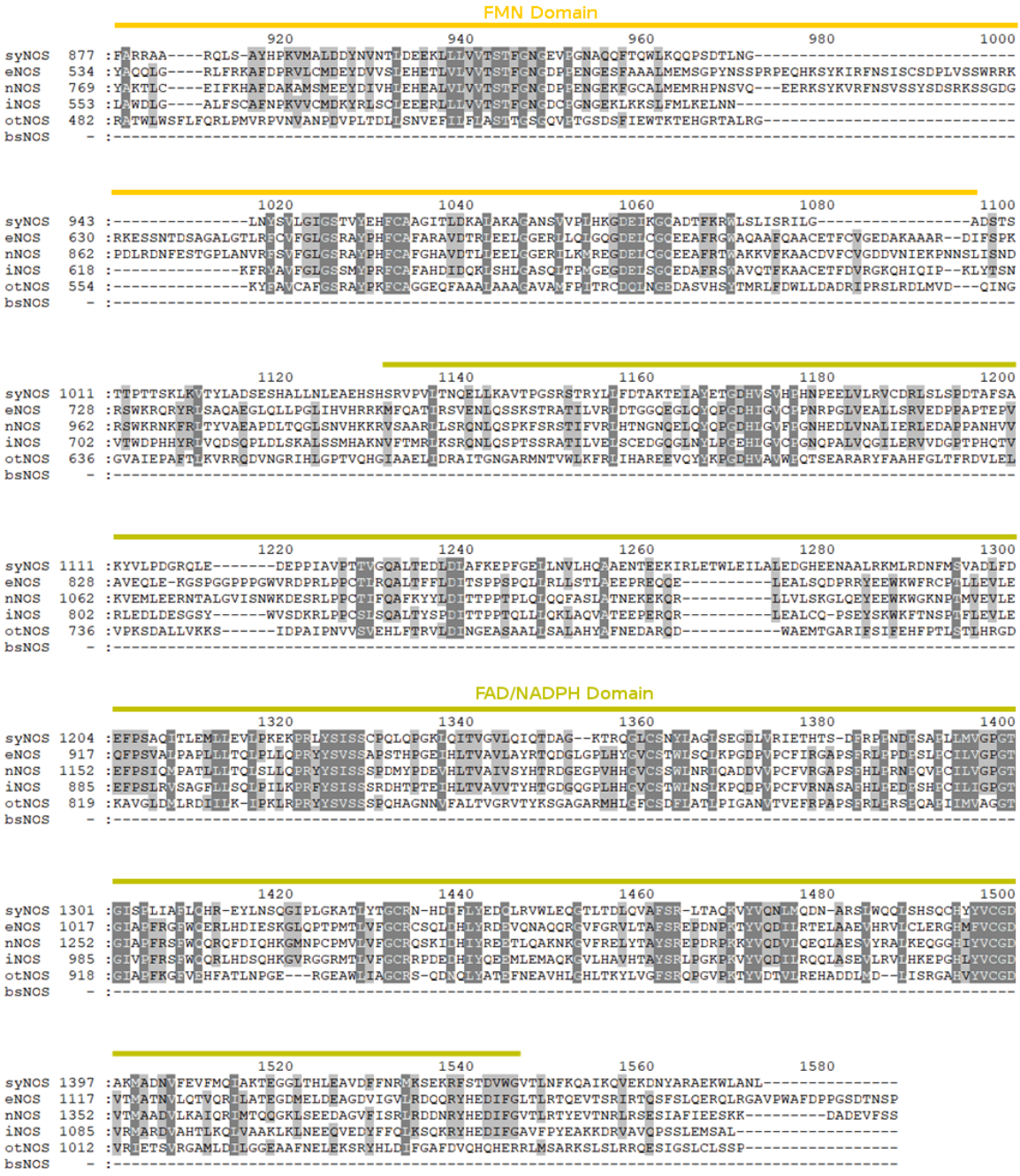

Figure 1.4: Protein sequence alignment of syNOS to other NOS proteins. The alignment was performed using ClustalX2 and visualized with GeneDoc; proximal heme binding residues (α), pterin binding residues (β), arginine coordinating glutamate (γ), *Homo sapien* endothelial NOS (eNOS), *Rattus norvegicus* neuronal NOS (nNOS), *Homo sapien* inducible NOS (iNOS), *Ostreococcus tauri* NOS (otNOS), *Bacillus subtilis* (bsNOS)

respire nitrate (51, 89).

This thesis confirms syNOS is a *bona fide* NOS. Chapter two discusses the expression, purification and spectroscopic characteristics of syNOS. Factors governing NOS activity are investigated, and NO dioxygenase functionality is identified. The potential function of syNOS in nitrogen assimilation and NO detoxification is also examined. Chapter three investigates the electron transfer between the flavin and heme domains and its potential significance to syNOS function. Crystallographic structures of NOS_{FMN} and NOS_{FAD} have been determined and are discussed.

1.6 References

1. Hughes, M. N. (2008) Chemistry of Nitric Oxide and Related Species. in *Methods in Enzymology*, pp. 3–19, 436, 3–19
2. Smith, W. D. A. (1972) A history of nitrous oxide and oxygen anaesthesia part ia: The discovery of nitrous oxide and of oxygen. *Br. J. Anaesth.* 44, 297–304
3. Environmental Protection Agency (1999) Nitrogen oxides (NOx), why and how they are controlled. *Epa-456/F-99-006R*. EPA 456/F-99-006R
4. Ye, R. W., Averill, B. A., and Tiedje, J. M. (1994) Denitrification: Production and consumption of nitric oxide. *Appl. Environ. Microbiol.* 60, 1053–1058
5. Carr, G. J., and Ferguson, S. J. (1990) The nitric oxide reductase of Paracoccus denitrificans. *Biochem. J.* 269, 423–429
6. Braun, C., and Zumft, W. G. (1991) Marker exchange of the structural genes for nitric oxide reductase blocks the denitrification pathway of Pseudomonas stutzeri at nitric oxide. *J. Biol. Chem.* 266, 22785–22788
7. Firestone, M. K., Firestone, R. B., and Tiedje, J. M. (1979) Nitric oxide as an intermediate in denitrification: Evidence from nitrogen-13 isotope exchange. *Biochem. Biophys. Res. Commun.* 91, 10–16
8. Caranto, J. D., and Lancaster, K. M. (2017) Nitric oxide is an obligate bacterial nitrification intermediate produced by hydroxylamine oxidoreductase. *Proc. Natl. Acad. Sci.* 114, 8217–8222
9. He, H. Y., Henderson, A. C., Du, Y. L., and Ryan, K. S. (2019) Two-Enzyme Pathway Links l-Arginine to Nitric Oxide in N-Nitroso Biosynthesis. *J. Am. Chem. Soc.* 141, 4026–4033
10. Rockel, P., Strube, F., Rockel, A., Wildt, J., and Kaiser, W. M. (2002) Regulation of nitric oxide (NO) production by plant nitrate reductase in vivo and in vitro. *J. Exp. Bot.* 53, 103–110
11. Dean, J. V, and Harper, J. E. (1988) The Conversion of Nitrite to Nitrogen Oxide(s) by the Constitutive NAD(P)H-Nitrate Reductase Enzyme from Soybean. *Plant Physiol.* 88, 389–395
12. Cooney, R. V, Harwood, P. J., Custer, L. J., and Franke, A. A. (1994) Light-mediated conversion of nitrogen dioxide to nitric oxide by carotenoids. *Environ. Health Perspect.* 102, 460–462
13. Bethke, P. C., Badger, M. R., and Jones, R. L. (2004) Apoplastic Synthesis of Nitric Oxide by Plant Tissues. *Plant Cell*. 16, 332–341
14. Yamasaki, H. (2000) Nitrite-dependent nitric oxide production pathway: Implications for involvement of active nitrogen spicies in photoinhibition in vivo. in *Philosophical Transactions of the Royal Society B: Biological Sciences*, pp. 1477–1488, 355, 1477–

1488

15. Marsh, N., and Marsh, A. (2000) A short history of nitroglycerine and nitric oxide in pharmacology and physiology. *Clin. Exp. Pharmacol. Physiol.* 27, 313–319

16. Katsuki, S., Arnold, W., Mittal, C., and Murad, F. (1977) Stimulation of guanylate cyclase by sodium nitroprusside, nitroglycerin and nitric oxide in various tissue preparations and comparison to the effects of sodium azide and hydroxylamine. *J. Cyclic Nucleotide Res.* 3, 23–35

17. Zawadski, J. V., Furchgott, R. F., and Cherry, P. (1980) The obligatory role of endothelial cells in the relaxation of arterial smooth muscle by substance. *Nature*

18. Ignarro, L. J., Byrns, R. E., Buga, G. M., and Wood, K. S. (1987) Endothelium-derived relaxing factor from pulmonary artery and vein possesses pharmacologic and chemical properties identical to those of nitric oxide radical. *Circ. Res.* 61, 866–879

19. Bredt, D. S., and Snyder, S. H. (1990) Isolation of nitric oxide synthetase, a calmodulin-requiring enzyme. *Proc. Natl. Acad. Sci. U. S. A.* 87, 682–685

20. Palmer, R. M. J., and Moncada, S. (1989) A novel citrulline-forming enzyme implicated in the formation of nitric oxide by vascular endothelial cells. *Biochem. Biophys. Res. Commun.* 158, 348–352

21. MacMicking, J., Xie, Q.-W., and Nathan, C. (2002) NITRIC OXIDE AND MACROPHAGE FUNCTION. *Annu. Rev. Immunol.* 15, 323–350

22. White, K. a, and Marletta, M. a (1992) Nitric oxide synthase is a cytochrome P-450 type hemoprotein. *Biochemistry*. 31, 6627–6631

23. Iyanagi, T., Xia, C., and Kim, J. J. P. (2012) NADPH-cytochrome P450 oxidoreductase: Prototypic member of the diflavin reductase family. *Arch. Biochem. Biophys.* 528, 72–89

24. Abu-Soud, H. M., Gachhui, R., Raushel, F. M., and Stuehr, D. J. (1997) The ferrous-dioxy complex of neuronal nitric oxide synthase. *J. Biol. Chem.* 272, 17349–17353

25. Santolini, J. (2011) The molecular mechanism of mammalian NO-synthases: a story of electrons and protons. *J. Inorg. Biochem.* 105, 127–41

26. Brenman, J. E., Chao, D. S., Gee, S. H., McGee, A. W., Craven, S. E., Santillano, D. R., Wu, Z., Huang, F., Xia, H., Peters, M. F., Froehner, S. C., and Bredt, D. S. (1996) Interaction of nitric oxide synthase with the postsynaptic density protein PSD-95 and α1-syntrophin mediated by PDZ domains. *Cell*. 84, 757–767

27. Crane, B. R., Arvai, a S., Ghosh, D. K., Wu, C., Getzoff, E. D., Stuehr, D. J., and Tainer, J. a (1998) Structure of nitric oxide synthase oxygenase dimer with pterin and substrate. *Science*. 279, 2121–2126

28. Salerno, J. C., Harris, D. E., Irizarry, K., Patelf, B., Morales, A. J., Smith, S. M. E., Martasek, P., Roman, L. J., Masters, B. S. S., Jones, C. L., Weissman, B. A., Lane, P., Liu, Q., and Gross, S. S. (1997) An autoinhibitory control element defines calcium-

regulated isoforms of nitric oxide synthase. *J. Biol. Chem.* 272, 29769–29777

29. Daff, S. (2003) Calmodulin-dependent regulation of mammalian nitric oxide synthase. *Biochem. Soc. Trans.* 31, 502–5

30. Garcin, E. D., Bruns, C. M., Lloyd, S. J., Hosfield, D. J., Tiso, M., Gachhui, R., Stuehr, D. J., Tainer, J. a., and Getzoff, E. D. (2004) Structural basis for isozyme-specific regulation of electron transfer in nitric-oxide synthase. *J. Biol. Chem.* 279, 37918–37927

31. Matsuda, H., and Iyanagi, T. (1999) Calmodulin activates intramolecular electron transfer between the two flavins of neuronal nitric oxide synthase flavin domain. *Biochim. Biophys. Acta - Gen. Subj.* 1473, 345–355

32. Presta, A., Weber-Main, A. M., Stankovich, M. T., and Stuehr, D. J. (1998) Comparative effects of substrates and pterin cofactor on the heme midpoint potential in inducible and neuronal nitric oxide synthases. *J. Am. Chem. Soc.* 120, 9460–9465

33. Tejero, J., and Stuehr, D. (2013) Tetrahydrobiopterin in nitric oxide synthase. *IUBMB Life*. 65, 358–365

34. Ramasamy, S., Haque, M. M., Gangoda, M., and Stuehr, D. J. (2016) Tetrahydrobiopterin redox cycling in nitric oxide synthase: evidence supports a through-heme electron delivery. *FEBS J.* 283, 4491–4501

35. Chen, Y. J., and Rosazza, J. P. N. (1994) A Bacterial, Nitric Oxide Synthase from a Nocardia Species. *Biochem. Biophys. Res. Commun.* 203, 1251–1258

36. Agapie, T., Suseno, S., Woodward, J. J., Stoll, S., Britt, R. D., and Marletta, M. a (2009) NO formation by a catalytically self-sufficient bacterial nitric oxide synthase from Sorangium cellulosum. *Proc. Natl. Acad. Sci. U. S. A.* 106, 16221–16226

37. Wang, Z.-Q., Lawson, R. J., Buddha, M. R., Wei, C.-C., Crane, B. R., Munro, A. W., and Stuehr, D. J. (2007) Bacterial flavodoxins support nitric oxide production by Bacillus subtilis nitric-oxide synthase. *J. Biol. Chem.* 282, 2196–2202

38. Gusarov, I., and Nudler, E. (2005) NO-mediated cytoprotection: instant adaptation to oxidative stress in bacteria. *Proc. Natl. Acad. Sci. U. S. A.* 102, 13855–13860

39. Gusarov, I., Starodubtseva, M., Wang, Z. Q., McQuade, L., Lippard, S. J., Stuehr, D. J., and Nudler, E. (2008) Bacterial nitric-oxide synthases operate without a dedicated redox partner. *J. Biol. Chem.* 283, 13140–13147

40. Crane, B. R., Sudhamsu, J., and Patel, B. a (2010) Bacterial nitric oxide synthases. *Annu. Rev. Biochem.* 79, 445–70

41. Adak, S., Bilwes, A. M., Panda, K., Hosfield, D., Aulak, K. S., McDonald, J. F., Tainer, J. a, Getzoff, E. D., Crane, B. R., and Stuehr, D. J. (2002) Cloning, expression, and characterization of a nitric oxide synthase protein from Deinococcus radiodurans. *Proc. Natl. Acad. Sci. U. S. A.* 99, 107–112

42. Adak, S., Aulak, K. S., and Stuehr, D. J. (2002) Direct Evidence for Nitric Oxide

Production by a Nitric-oxide Synthase-like Protein from Bacillus subtilis* Downloaded from. *J. Biol. Chem.* 277, 16167–16171

43. Thöny, B., Auerbach, G., and Blau, N. (2000) Tetrahydrobiopterin biosynthesis, regeneration and functions. *Biochem. J.* 347 Pt 1, 1–16

44. Yamamoto, K., Kataoka, E., Miyamoto, N., Furukawa, K., Ohsuye, K., and Yabuta, M. (2003) Genetic engineering of Escherichia coli for production of tetrahydrobiopterin. *Metab. Eng.* 5, 246–254

45. Wang, H., Yang, B., Hao, G., Feng, Y., Chen, H., Feng, L., Zhao, J., Zhang, H., Chen, Y. Q., Wang, L., and Chen, W. (2011) Biochemical characterization of the tetrahydrobiopterin synthesis pathway in the oleaginous fungus Mortierella alpina. *Microbiology*. 157, 3059–3070

46. Reece, S. Y., Woodward, J. J., and Marletta, M. A. (2009) Synthesis of nitric oxide by the NOS-like protein from Deinococcus radiodurans: A direct role for tetrahydrofolate. *Biochemistry*. 48, 5483–5491

47. Wang, Z. Q., Wei, C. C., Sharma, M., Pant, K., Crane, B. R., and Stuehr, D. J. (2004) A Conserved Val to Ile Switch near the Heme Pocket of Animal and Bacterial Nitric-oxide Synthases Helps Determine Their Distinct Catalytic Profiles. *J. Biol. Chem.* 279, 19018–19025

48. Sudhamsu, J., and Crane, B. R. (2009) Bacterial nitric oxide synthases: what are they good for? *Trends Microbiol.* 17, 212–8

49. Patel, B. a, Moreau, M., Widom, J., Chen, H., Yin, L., Hua, Y., and Crane, B. R. (2009) Endogenous nitric oxide regulates the recovery of the radiation-resistant bacterium Deinococcus radiodurans from exposure to UV light. *Proc. Natl. Acad. Sci. U. S. A.* 106, 18183–8

50. Kers, J. A., Wach, M. J., Krasnoff, S. U., Widom, J., Cameron, K. D., Dukhalid, R. A., Gibson, D. M., Crane, B. R., and Loria, R. (2004) Nitration of a peptide phytotoxin by bacterial nitric oxide synthase. *Nature*. 429, 79–82

51. Kinkel, T. L., Ramos-Montañez, S., Pando, J. M., Tadeo, D. V., Strom, E. N., Libby, S. J., and Fang, F. C. (2016) An essential role for bacterial nitric oxide synthase in Staphylococcus aureus electron transfer and colonization. *Nat. Microbiol.* 2, 1–7

52. Mogen, A. B., Carroll, R. K., James, K. L., Lima, G., Silva, D., Culver, J. A., Petucci, C., Shaw, L. N., and Rice, K. C. (2017) Staphylococcus aureus nitric oxide synthase (saNOS) modulates aerobic respiratory metabolism and cell physiology. *Mol. Microbiol.* 105, 139–157

53. Moore, C. M., Nakano, M. M., Wang, T., Ye, R. W., and Helmann, J. D. (2004) Response of Bacillus subtilis to nitric oxide and the nitrosating agent sodium nitroprusside. *J. Bacteriol.* 186, 4655–4664

54. Moreau, M., Lindermayr, C., Durner, J., and Klessig, D. F. (2010) NO synthesis and signaling in plants - where do we stand? *Physiol. Plant.* 138, 372–383

55. Butt, Y. K. C., Lum, J. H. K., and Lo, S. C. L. (2003) Proteomic identification of plant proteins probed by mammalian nitric oxide synthase antibodies. *Planta*. 216, 762–71

56. Tischner, R., Galli, M., Heimer, Y. M., Bielefeld, S., Okamoto, M., Mack, A., and Crawford, N. M. (2007) Interference with the citrulline-based nitric oxide synthase assay by argininosuccinate lyase activity in Arabidopsis extracts. *FEBS J.* 274, 4238–4245

57. Moreau, M., Gyu, I. L., Wang, Y., Crane, B. R., and Klessig, D. F. (2008) AtNOS/AtNOA1 is a functional Arabidopsis thaliana cGTPase and not a nitric-oxide synthase. *J. Biol. Chem.* 283, 32957–32967

58. Guo, F. Q., Okamoto, M., and Crawford, N. M. (2003) Identification of a plant nitric oxide synthase gene involved in hormonal signaling. *Science (80-.).* 302, 100–103

59. Foresi, N., Correa-Aragunde, N., Parisi, G., Caló, G., Salerno, G., and Lamattina, L. (2010) Characterization of a nitric oxide synthase from the plant kingdom: NO generation from the green alga Ostreococcus tauri is light irradiance and growth phase dependent. *Plant Cell*. 22, 3816–3830

60. Weisslocker-Schaetzel, M., André, F., Touazi, N., Foresi, N., Lembrouk, M., Dorlet, P., Frelet-Barrand, A., Lamattina, L., and Santolini, J. (2017) The NOS-like protein from the microalgae Ostreococcus tauri is a genuine and ultrafast NO-producing enzyme. *Plant Sci.* 265, 100–111

61. Picciano, A. L., and Crane, B. R. (2019) A nitric oxide synthase-like protein from Synechococcus produces NO/NO 3 - from L-arginine and NAPDH in a tetrahydrobiopterin- and Ca 2+ -dependent manner . *J. Biol. Chem.* 294, jbc.RA119.008399

62. Correa-Aragunde, N., Foresi, N., Del Castello, F., and Lamattina, L. (2018) A singular nitric oxide synthase with a globin domain found in Synechococcus PCC 7335 mobilizes N from arginine to nitrate. *Sci. Rep.* 8, 12505

63. Sánchez-Baracaldo, P., and Cardona, T. (2019) On the origin of oxygenic photosynthesis and Cyanobacteria. *New Phytol.* 10.1111/nph.16249

64. Lyons, T. W., Reinhard, C. T., and Planavsky, N. J. (2014) The rise of oxygen in Earth's early ocean and atmosphere. *Nature*. 506, 307–15

65. Hazen, R. M., Papineau, D., Bleeker, W., Downs, R. T., Ferry, J. M., McCoy, T. J., Sverjensky, D. A., and Yang, H. (2008) Mineral evolution. *Am. Mineral.* 93, 1693–1720

66. Huisman, J., Codd, G. A., Paerl, H. W., Ibelings, B. W., Verspagen, J. M. H., and Visser, P. M. (2018) Cyanobacterial blooms. *Nat. Rev. Microbiol.* 16, 471–483

67. Diaz, R. J., and Rosenberg, R. (2008) Spreading dead zones and consequences for marine ecosystems. *Science (80-.).* 321, 926–929

68. Wijffels, R. H., Kruse, O., and Hellingwerf, K. J. (2013) Potential of industrial biotechnology with cyanobacteria and eukaryotic microalgae. *Curr. Opin. Biotechnol.*

24, 405–13

69. Quintana, N., Van Der Kooy, F., Van De Rhee, M. D., Voshol, G. P., and Verpoorte, R. (2011) Renewable energy from Cyanobacteria: Energy production optimization by metabolic pathway engineering. *Appl. Microbiol. Biotechnol.* 91, 471–490

70. Nozzi, N. E., Oliver, J. W. K., and Atsumi, S. (2013) Cyanobacteria as a Platform for Biofuel Production. *Front. Bioeng. Biotechnol.* lipid, 1–6

71. Kim, D., Yamaguchi, K., and Oda, T. (2006) Nitric oxide synthase-like enzyme mediated nitric oxide generation by harmful red tide phytoplankton, Chattonella marina. *J. Plankton Res.* 28, 613–620

72. Tang, X., Chen, J., Wang, W. H., Liu, T. W., Zhang, J., Gao, Y. H., Pei, Z. M., and Zheng, H. L. (2011) The changes of nitric oxide production during the growth of Microcystis aerugrinosa. *Environ. Pollut.* 159, 3784–3792

73. Xue, L., Li, S., Zhang, B., Shi, X., and Chang, S. (2011) Counteractive action of nitric oxide on the decrease of nitrogenase activity induced by enhanced ultraviolet-B radiation in cyanobacterium. *Curr. Microbiol.* 62, 1253–1259

74. Tiwari, S., Verma, N., Singh, V. P., and Prasad, S. M. (2019) Nitric oxide ameliorates aluminium toxicity in Anabaena PCC 7120: Regulation of aluminium accumulation, exopolysaccharides secretion, photosynthesis and oxidative stress markers. *Environ. Exp. Bot.* 161, 218–227

75. Tsai, A. L., Berka, V., Martin, F., Ma, X., Van Den Akker, F., Fabian, M., and Olson, J. S. (2010) Is nostoc H-NOX a no sensor or redox switch? *Biochemistry*. 49, 6587–6599

76. Plate, L., and Marletta, M. A. (2013) Nitric oxide-sensing H-NOX proteins govern bacterial communal behavior. *Trends Biochem. Sci.* 38, 566–575

77. Nisbett, L. M., and Boon, E. M. (2016) Nitric Oxide Regulation of H-NOX Signaling Pathways in Bacteria. *Biochemistry*. 55, 4873–4884

78. Walter, J. M., Coutinho, F. H., Dutilh, B. E., Swings, J., Thompson, F. L., and Thompson, C. C. (2017) Ecogenomics and taxonomy of Cyanobacteria phylum. *Front. Microbiol.* 10.3389/fmicb.2017.02132

79. Rippka, R., Deruelles, J., Waterbury, J. B., Herdman, M., and Stanier, R. Y. (1979) Generic Assignments, Strain Histories and Properties of Pure Cultures of Cyanobacteria. *J. Gen. Microbiol.* 111, 1–61

80. Khamees, H. S., Gallon, J. R., and Chaplin, A. E. (1987) The pattern of acetylene reduction by cyanobacteria grown under alternating light and darkness. *Br. Phycol. J.* 22, 55–60

81. León, C., Kumazawa, S., and Mitsui, A. (1986) Cyclic appearance of aerobic nitrogenase activity during synchronous growth of unicellular cyanobacteria. *Curr. Microbiol.* 13, 149–153

82. Uyeda, J. C., Harmon, L. J., and Blank, C. E. (2016) A comprehensive study of cyanobacterial morphological and ecological evolutionary dynamics through deep geologic time. *PLoS One*. 11, 1–32

83. Coutinho, F., Tschoeke, D. A., Thompson, F., and Thompson, C. (2016) Comparative genomics of Synechococcus and proposal of the new genus Parasynechococcus. *PeerJ*. 10.7717/peerj.1522

84. Gan, F., and Bryant, D. A. (2015) Adaptive and acclimative responses of cyanobacteria to far-red light. *Environ. Microbiol.* 17, 3450–3465

85. Herrera-Salgado, P., Leyva-Castillo, L. E., Ríos-Castro, E., and Gómez-Lojero, C. (2018) Complementary chromatic and far-red photoacclimations in Synechococcus ATCC 29403 (PCC 7335). I: The phycobilisomes, a proteomic approach. *Photosynth. Res.* 138, 39–56

86. Forrester, M. T., and Foster, M. W. (2012) Protection from nitrosative stress: A central role for microbial flavohemoglobin. *Free Radic. Biol. Med.* 52, 1620–1633

87. Bonamore, A., and Boffi, A. (2008) Flavohemoglobin: Structure and reactivity. *IUBMB Life*. 60, 19–28

88. Lechauve, C., Butcher, J. T., Freiwan, A., Biwer, L. A., Keith, J. M., Good, M. E., Ackerman, H., Tillman, H. S., Kiger, L., Isakson, B. E., and Weiss, M. J. (2018) Endothelial cell α-globin and its molecular chaperone α-hemoglobin-stabilizing protein regulate arteriolar contractility. *J. Clin. Invest.* 128, 5073–5082

89. James, K. L., Mogen, A. B., Brandwein, J. N., Orsini, S. S., Ridder, M. J., Markiewicz, M. A., Bose, J. L., and Rice, K. C. (2019) Interplay of Nitric Oxide Synthase (NOS) and SrrAB in modulation of staphylococcus aureus metabolism and virulence. *Infect. Immun.* 87, 570–588

CHAPTER TWO

A nitric oxide synthase-like protein from *Synechococcus* produces NO/NO_3^- from L-arginine and NAPDH in a tetrahydrobiopterin- and Ca^{2+}-dependent manner

Picciano, A. L. and Crane, B. R.

Published in the Journal of Biological Chemistry, July 2019

2.1 Abstract

Nitric oxide synthase (NOS) proteins are heme-based monooxygenase enzymes that convert L-arginine (L-arg) to L-citrulline (L-cit) and nitric oxide (NO), which is a key signaling molecule and cytotoxic agent in mammals. Bacteria also contain NOS proteins, but the purpose for NO production within these organisms, where understood, differs considerably compared to that of mammals. For example, a NOS protein found in the marine cyanobacteria *Synechococcus* sp. PCC 7335 (syNOS) has recently been proposed to function in nitrogen assimilation from L-arg. SyNOS retains the oxygenase (NOS_{ox}) and reductase (NOS_{red}) domains also found in mammalian NOS enzymes (mNOS), but also contains an N-terminal globin domain (NOS_g) homologous to bacterial flavohemoglobin proteins. Herein we show that syNOS functions as a dimer and produces NO from L-arg and NADPH in a tetrahydrobiopterin (H_4B)-dependent manner at levels commensurate with other bacterial NOS proteins, but does not require Ca^{2+}-calmodulin, which regulates reduction of NOS_{ox} by NOS_{red} in mammalian NOSs. Unlike other bacterial NOSs, syNOS cannot function with tetrahydrofolate and requires high levels of Ca^{2+} (> 200 μM) for activation. NOS_g converts NO to NO_3^- in the presence of O_2 and NADPH; however, NOS_g conveys no advantage to *E. coli* strains against nitrosative stress, even in a mutant devoid of NO-protective flavohemoglobin. We also find that syNOS does not have NOS activity in *E. coli* (due to the absence of H_4B) and that the recombinant protein does not confer advantage to growth on L-arg as a nitrogen source.

2.2 Introduction

Nitric oxide (NO) is a gaseous free radical involved in numerous biological processes; it is an intermediate in the denitrification pathway (1), a precursor to protein post-translational modification via s-nitrosylation (2), and is the activator of soluble guanylate cyclase in animals or H-NOX proteins in bacteria (3, 4). In mammals, NO is the product of arginine oxidation by nitric oxide synthases (NOS) (5, 6). The three mammalian isoforms, endothelial (eNOS), neuronal (nNOS), and inducible (iNOS) (6–8), share a heme-containing oxygenase domain (NOS_{ox}) and a C-terminal reductase domain (NOS_{red}). NOS_{red}, which functions to reduce NOS_{ox} using NADPH, is composed of an FMN binding domain and a ferredoxin-$NADP^+$-reductase (FNR)-like domain. NOSs function as N-terminal homodimers, whereby the NOS_{red} of one subunit reduces the NOS_{ox} of the opposite subunit (9). Electron transfer is activated by Ca^{2+}-loaded calmodulin (CaM) (10) that binds at a conserved sequence between NOS_{ox} and NOS_{red}, and is also facilitated by the essential cofactor tetrahydrobiopterin (H_4B) that acts to supply electrons to the NOS heme for oxygen activation (11). Each of the mammalian NOS isoforms play key roles in many biological processes, such as vasoconstriction, immune response, and neuronal plasticity (12–14), and are also involved in several pathologies, including tumorigenesis, septic shock, and cerebral ischaemia (15–18).

Although NOS is ubiquitous in the animal kingdom, it is infrequently found in bacteria. The occurrence and purpose of bacterial NOS is highly species-dependent, ranging from recovery from UV damage (drNOS) (19), signaling biofilm formation (siliNOS) (20), protection from oxidative stress (bsNOS) (21), aiding pathogen virulence (baNOS) (22), and controlling oxygen-based respiration (saNOS) (23, 24). Although their heme domain structure and catalytic mechanisms are similar to that of mammalian NOS, most bacterial NOSs lack a

dedicated reductase domain, instead relying on promiscuous cellular reductases (25, 26). One NOS found in *Sorangium cellulosum* has an N-terminal reductase domain containing a 2Fe-2S cluster and ferredoxin-like FAD and NADPH domain, dissimilar to mammalian NOS_{red} (27). No bacterial NOS with a covalently attached FMN/FNR reductase domain has been biochemically characterized thus far.

NOSs are also found in photosynthetic organisms. A mammalian NOS homolog was characterized from the algae *Ostreococcus tauri* (otNOS) (28), which is intriguing because NOS has not yet been identified in higher plants, despite NO having an undisputed role in plant signaling (29). Recently, a mammalian-like NOS with a C-terminal P-450 reductase domain was identified in the photosynthetic diazotroph *Synechococcus* sp. PCC 7335 (syNOS) (30). SyNOS is the first prokaryotic NOS to contain a mammalian NOS_{red} homolog; in addition, syNOS contains a somewhat unusual globin domain (NOS_g) N-terminal to NOS_{ox}, as well as a 342 residue N-terminal region of unknown properties (Fig. 2.S1). The syNOS-harboring *Synechococcus* strain was shown to produce NO in an arginine (L-arg) dependent manner and this activity was inhibited by known NOS inhibitors (30). Based on genetic experiments in *Synechococcus* and heterologous expression experiments in *E. coli*, syNOS was proposed to function in nitrogen utilization from L-arg (30). Specifically, this model asserts that syNOS first converts L-arg to NO with NOS_{ox}, and then from NO to NO_3^- with NOS_g. Nitrate would then be assimilated back into reduced forms of nitrogen. Herein we report the first recombinant expression, purification, and biochemical characterization of syNOS. The enzyme indeed acts as a bona fide NO synthase and also has strong NO dioxygenase (NOD) activity; however, it cannot utilize the general folate cofactor tetrahydrofolate as do other bacterial NOSs and instead requires tetrahydrobiopterin, like mammalian NOS. Although activation does not depend on

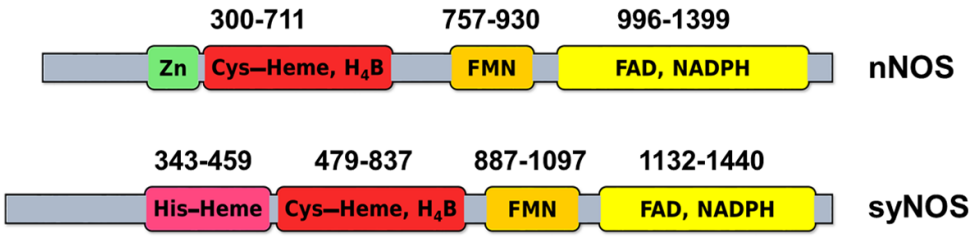

Figure 2.1: Domain map of nNOS and syNOS. The flavin and heme domains typical of nNOS are also present in syNOS, however the zinc ligating cysteines (Cys327 and Cys332 in nNOS) are absent from syNOS. Instead syNOS also contains a globin domain not found in typical NOSs.

CaM, it does strongly rely on Ca^{2+}. Importantly, syNOS does not appear to aid in nitrogen utilization from L-arg when recombinantly expressed in *E. coli* and also has minimal impact on NO detoxification.

2.3 Results

2.3.1 Expression, Purification and Oligomeric State of syNOS

Full-length syNOS (residues 1-1468) was co-expressed with the chaperonin GroEL/ES in *E. coli* BL21 DE3 cells; excess chaperonin was necessary to produce consistently well-folded and active enzyme. The yield (approximately 3 mg per liter of culture) and activity were very similar when the protein was expressed from two different vectors (pET28a or pCW-LIC). Affinity chromatography with ADP-sepharose targeting the reductase domain was more effective as a first purification step than with Ni-NTA resin targeting the His_6-tag. On size exclusion chromatography (SEC) syNOS eluted in two major peaks presumably corresponding to monomer and dimer (and a minor amount of aggregate) (Fig. 2.2A). Non-reducing SDS-PAGE of the trailing peak produced one band corresponding to the syNOS monomer at approximately 166 kDa whereas the second leading peak produced two bands, representing the

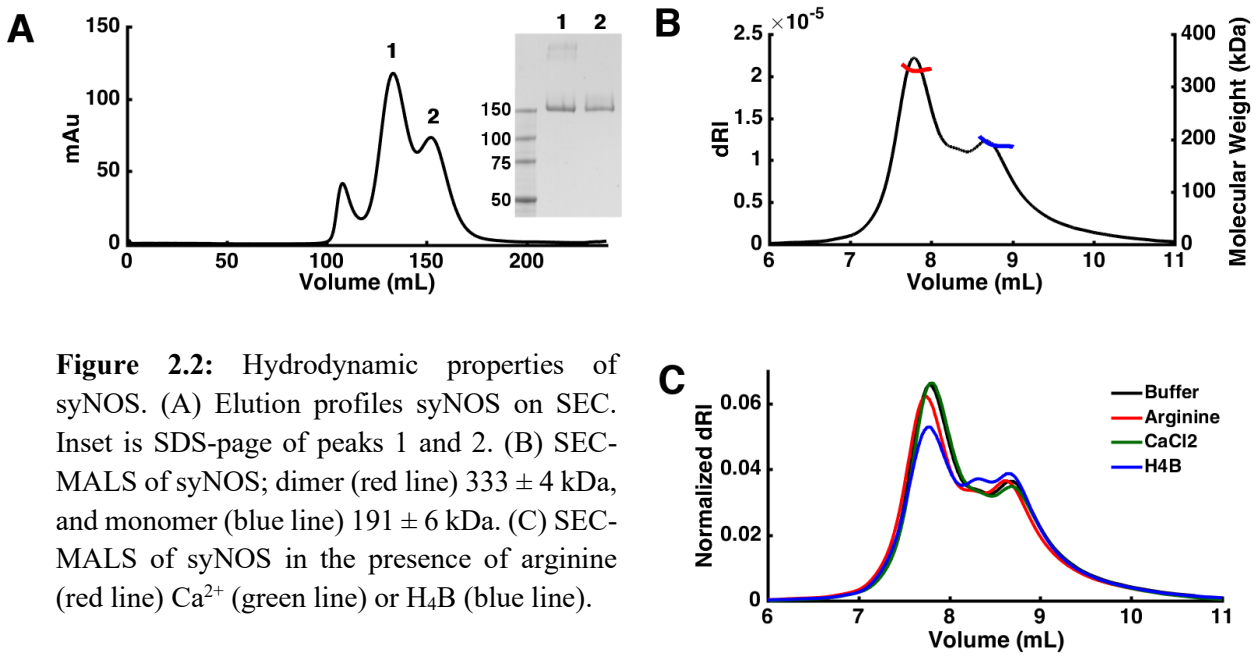

Figure 2.2: Hydrodynamic properties of syNOS. (A) Elution profiles syNOS on SEC. Inset is SDS-page of peaks 1 and 2. (B) SEC-MALS of syNOS; dimer (red line) 333 ± 4 kDa, and monomer (blue line) 191 ± 6 kDa. (C) SEC-MALS of syNOS in the presence of arginine (red line) Ca^{2+} (green line) or H_4B (blue line).

monomer and the syNOS dimer (Fig. 2.2A inset). SEC coupled with multiangle light scattering (SEC-MALS) confirmed formation of a syNOS dimer and its sensitivity to factors known to influence NOS dimerization (Fig. 2.2B and C). The measured molecular weight of the first peak in the elution trace, 333 ± 4 kDa, equates to that of a syNOS dimer and the second peak, 191 ± 6 kDa, corresponds to the monomer. A small peak was also observed at intermediate mass between those of the dimer and monomer. The sample does not appear to suffer from contamination or degradation, and thus this third peak may represent a third syNOS species in rapid oligomeric exchange. The addition of substrate or calcium did not significantly affect the population of dimer, however, H_4B modestly decreased the amount of dimer.

In order to isolate contributions from the two independent heme domains, variant proteins that removed key heme binding ligands were also expressed and purified in the same manner as the wild-type enzyme. The NOS_{ox} proximal cysteine (Cys539) was identified by alignment to NOS sequences (Fig. 2.S1) and was substituted for alanine (C539A). The NOS_g

ligating histidine was identified as His422 with sequence alignments to globins of known structure (Fig. 2.S2) and was also substituted for alanine (H422A) in a separate variant. Heme content of the WT and each variant, measured with the pyridine hemochrome assay, indicated that the mutations substantially reduced heme binding in the targeted domains: syNOS 1.00 ± 0.10 μM heme per μM protein, H422A 0.39 ± 0.08, and C539A 0.72 ± 0.07 (Table 2.S2). A syNOS variant with both heme ligand substitutions (H422A, C539A), bound very little heme (Table 2.S2, Fig. 2.S4). The sum of the heme content in the H422A and C539A variants approximately equaled that of the wild-type, therefore 39% of the syNOS Soret was attributed to the NOS_{ox} heme. The concentration of NOS_{ox} bound heme and the Soret intensity at 415 nm were used to calculate an extinction coefficient for quantifying active protein in subsequent assays.

2.3.2 Spectroscopic Properties

Purified syNOS has a Soret band at 415 nm, which is red-shifted compared to the ferric heme absorption of typical globins (~405 nm) and the high-spin thiol-ligated ferric heme of NOS_{ox} (~397 nm) (Fig. 2.3A). The Soret for the globin heme (the C539A variant) is observed at 413 nm (Fig. 2.3C), similar to a flavohemoglobin from *M. tuberculosis* (414 nm) (31, 32), and the NOS_{ox} heme Soret at 417 nm (Fig. 2.3B) is more similar that of the NOS protein from *S. cellulosum* (416 nm) (27). Broad α-bands characteristic of ferric globin-hemes are observed around 540 nm and 580 nm in all three proteins. A single band at ~550 nm, expected for a NOS-type heme, is not prominent in H422A, perhaps due to remaining globin heme and protonation or dissociation of the NOS_{ox} proximal cysteine to form an inactive P420 state (33, 34). After reduction with dithionite the Soret shifts to 425 nm and peaks at 530 and 560 nm are observed

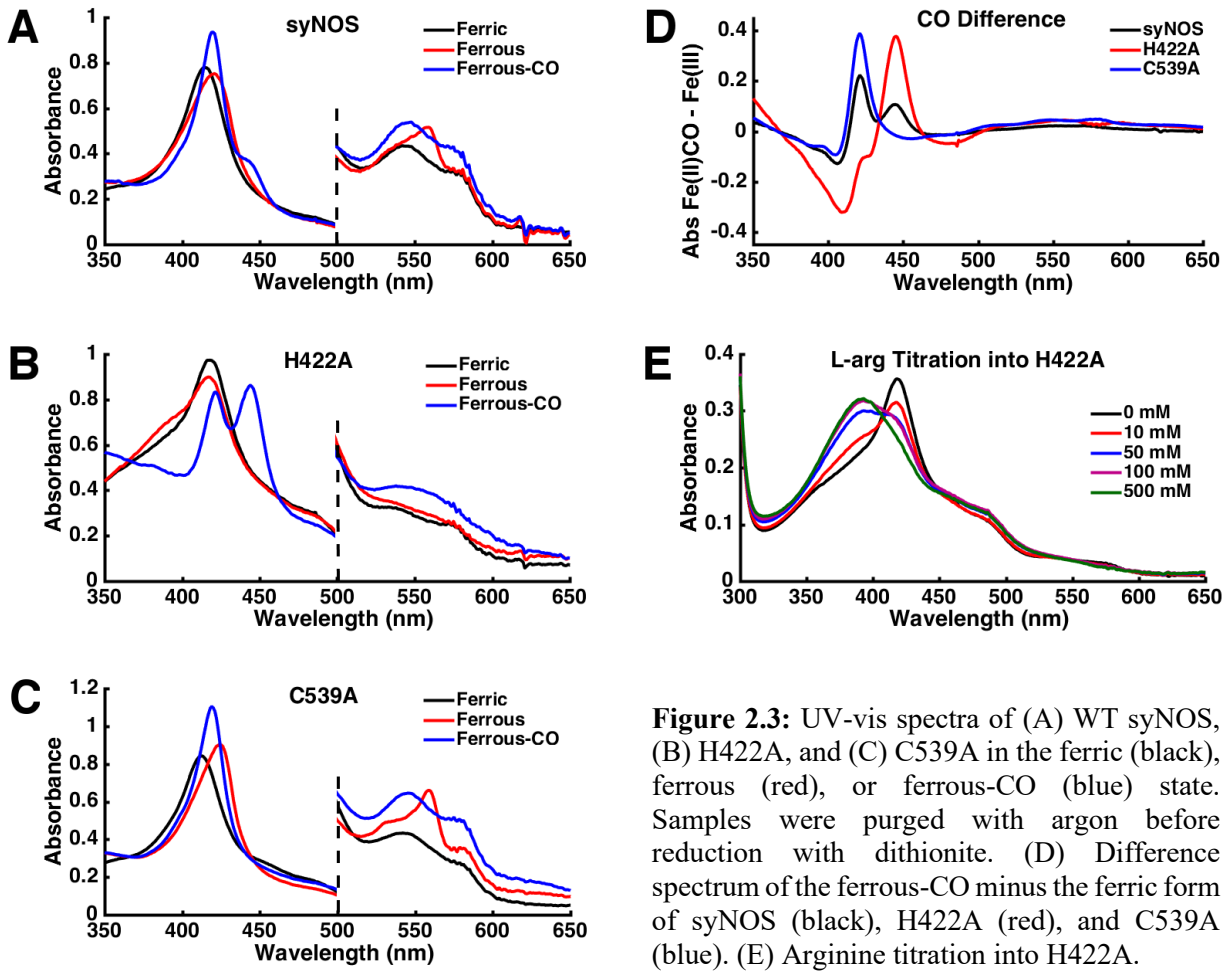

Figure 2.3: UV-vis spectra of (A) WT syNOS, (B) H422A, and (C) C539A in the ferric (black), ferrous (red), or ferrous-CO (blue) state. Samples were purged with argon before reduction with dithionite. (D) Difference spectrum of the ferrous-CO minus the ferric form of syNOS (black), H422A (red), and C539A (blue). (E) Arginine titration into H422A.

for syNOS and C539A; this is similar to spectra of hexacoordinate neuroglobin, known to oxidize NO to nitrate (35, 36). These peaks are not observed for H422A, indicating there is little globin heme bound in this variant. NOSs are thiolate-ligated P450-type heme proteins with a characteristic ferrous-CO Soret band at ~450 nm (37). For wild-type syNOS, this species was observed as a shoulder at 444 nm corresponding to the NOS_{ox} heme and another intense absorbance at 420 nm corresponding to the ferrous-CO NOS_g heme; however, the NOS_{ox} heme in the P420 state may also contribute to the intensity at 420 nm. As expected, H422A exhibits greater P450 Soret intensity at 444 nm compared to WT-syNOS, however there is still significant absorbance at 420 nm, most likely caused by the inactive P420 species. The ferrous

CO-complex of C539A has no Soret peak at 444 nm and only a band from NOS_g is observed. These spectral features are evident in the Fe(II)CO - Fe(III) difference spectra (Fig. 2.3D).

Mammalian and bacterial NOSs primarily contain five-coordinate low-spin hemes that exhibit a shift to high-spin (Soret band at ~390 nm) upon binding L-Arg; such a Soret shift was difficult to observe in wild-type syNOS. However, H422A undergoes a blue shift to ~391 nm upon addition of excess L-arg (Fig. 2.3E). A large amount of L-arg (500 mM) is required for complete conversion. This far exceeds the observed Michaelis constant for L-arg (101 ± 12 μM, Fig. 2.S3A) but may reflect the fact that without the globin domain the protein is destabilized (the activity drops by a factor of 8, see Table 2.1) and the NOS heme at least partially converts to the P420 state. Large amounts of L-arg may stabilize the protein fold and heme center in a non-specific manner so that a substrate-induced transition to a high-spin state can be observed. No Soret shift is observed when L-arg is added to the NOS_{ox} heme-deficient C539A variant.

2.3.3 Recombinant syNOS produces nitric oxide from L-arginine.

NO production by full-length syNOS was first measured through the detection of its oxidized products, nitrate and nitrite, with the Griess assay. The specific activity of syNOS was 35.7 ± 5 nmol/min/mg (Table 2.1), approximately half that of the nNOS control 64.0 ± 2 nmol/min/mg, which is low compared to literature values (100 to 400 nmol/min/mg (37)). The syNOS C539A variant had very little measurable activity, and the activity of syNOS H422A was attenuated by about a factor of eight compared to wild-type, in keeping with the results above (Table 2.1). The loss of NOS activity due to the globin substitution H422A likely reflects a general destabilization of the full-length protein when the globin domain is disrupted.

syNOS activity requires L-arginine, H_4B, calcium, and NADPH (Table 2.1). Unlike

analogous mammalian NOS, syNOS activity was independent of Ca^{2+}-calmodulin (bovine), perhaps not surprisingly given that the calmodulin binding site of mNOS is not conserved in syNOS (Fig. 2.S1) and *Synechococcus* does not contain an obvious homolog of calmodulin. Remarkably, syNOS is substantially activated by calcium (>10-fold); in fact, activity was reduced in the presence of calmodulin, presumably due to competition for calcium. However, the apparent Michaelis constant for Ca^{2+} activation is 228 ± 9 μM (Fig. 2.S3), which may indicate that Ca^{2+} serves as a proxy for another physiological factor that activates the enzyme at lower concentration. syNOS cofactor utilization also differs from other bacterial NOSs in that syNOS cannot substitute tetrahydrofolate (THF) for H_4B. The NOS inhibitors L-NNA and L-NAA, which mimic the substrate L-arg, completely inhibited syNOS. This is in keeping with previous observations that L-NAME inhibits syNOS *in vivo* (30) as L-NAME requires hydrolysis to L-NNA (typically by cellular esterases) for inhibition of NOS (38).

L-citrulline, the byproduct of L-arg based NO production, was detected as the product of the syNOS reaction with analytical HPLC (Fig. 2.4). After derivatization with the fluorophore ortho-phthaldialdehyde (OPA), samples were applied to a reverse-phase column,

Table 2.1: Specific activity of syNOS, performed using the Griess assay to measure NO_2^- + NO_3^-. Citrulline was quantified with HPLC when indicated with an asterisk (*). ND, no product detected.

Ca^{2+}-CaM	Ca^{2+}	Ca^{2+}-CaM		Ca^{2+}	Ca^{2+}	Ca^{2+}
Pterin	H_4B	H_4B	H_4B	THF	H_4B	H_4B
Inhibitor					L-NNA	L-NAA
syNOS	36 ± 5, 34 ± 9*	14.8 ± 1.0	ND	ND	ND	ND
nNOS	1.0 ± 0.2	64 ± 2				
H422A	4.6 ± 0.8					
C539A	0.5 ± 0.2					

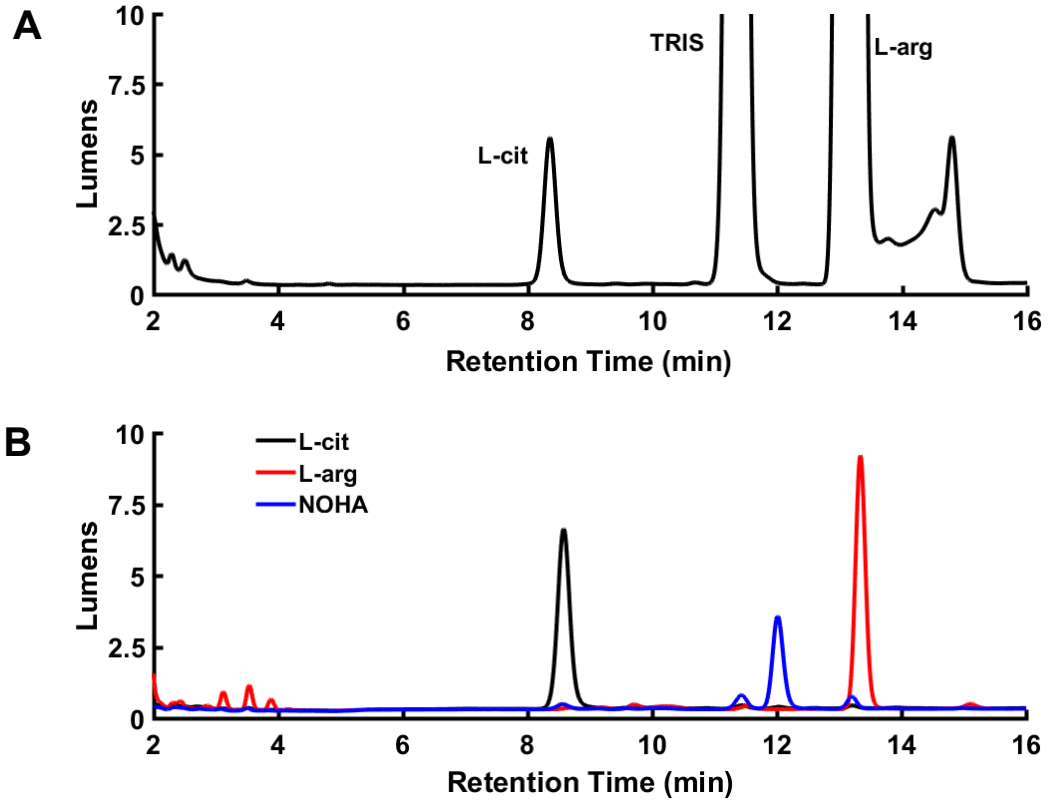

Figure 2.4: syNOS produces L-citrulline from L-arginine. (A) HPLC trace of syNOS products. (B) HPLC trace of L-citrulline (black line), L-arginine (red line), and N-hydroxy-L-arginine (blue line) standards.

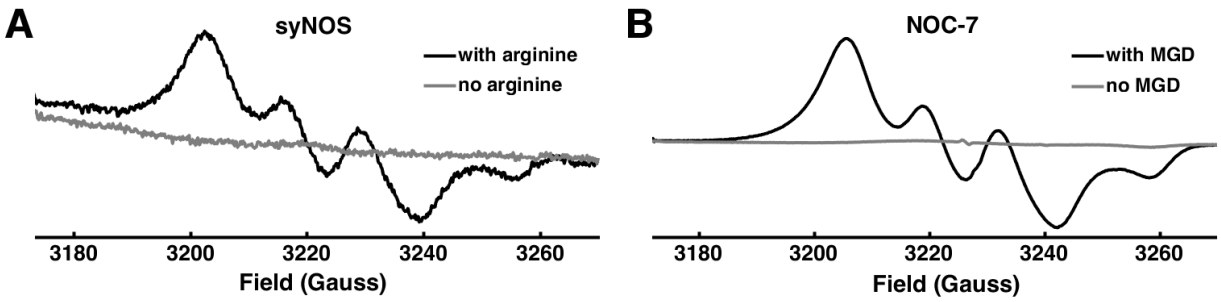

Figure 2.5: NO production by syNOS. Continuous-wave ESR of the NO complex of spin-trap Fe-MGD for (A) syNOS with (black line) and without (grey line) arginine. (B) NO donor NOC-7 with (black line) and without (grey line)

and L-citrulline (8.58 min) was resolved from substrate L-arg (13.34 min). The amount of citrulline detected by HPLC was roughly equivalent to the amount of NO_2^- + NO_3^- measured by Griess, 0.95: 1.

To directly detect NO production from syNOS, NO was chelated by the spin-trap Fe^{2+}-MGD and detected by continuous-wave ESR spectroscopy (Fig. 2.5). The NO releasing small molecule NOC-7 was used as a positive control. syNOS produced an NO signal identical to that of NOC-7. Moreover, addition of the spin trap reacted with nearly all of the product NO and prevented conversion to NO_2^- or NO_3^- (Table 2.S1).

2.3.4 NOS_{ox} and NOS_g are both directly reduced by NOS_{red}

In mammalian NOS, NOS_{ox} is reduced by NOS_{red} and NADPH. To evaluate whether $syNOS_{red}$ can reduce $syNOS_{ox}$ and $syNOS_g$ independent of each other, the $syNOS_{ox}$ and $syNOS_g$ domains (residues 475-795 and residues 337-469, respectively) were cloned and expressed in isolation and then tested for their ability to accept electrons from NOS_{red} (residues 856–1468). In the case of NOS_{ox}, the reduction experiment was carried out in the presence of CO to trap the reduced heme as a characteristic thiolate-ligated Fe(II)-CO (Soret band at 444 nm). In the

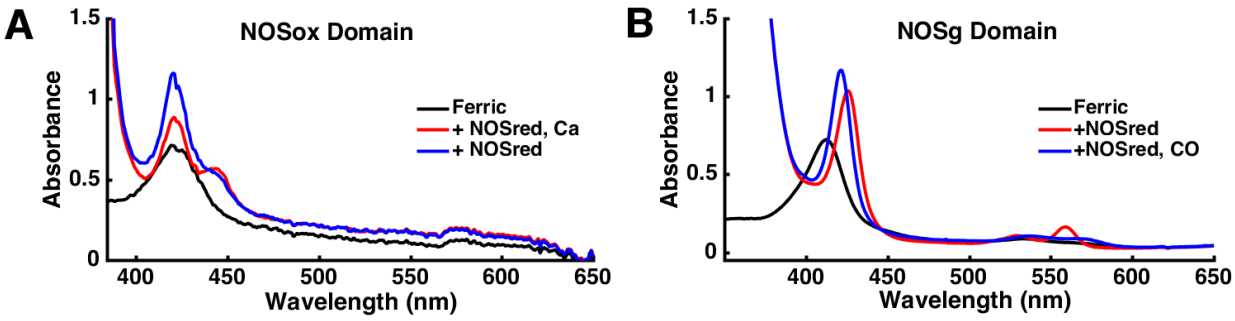

Figure 2.6. UV-vis spectrum of (A) NOS_{ox} in the presence of NOS_{red}, NADPH, and CO with or without calcium ion (Ca^{2+}), (B) NOS_g in the presence NOS_{red} and NADPH with or without CO. Samples with NADPH were measured under anaerobic conditions.

presence of NADPH, NOS_{red} produced some reduction of NOS_{ox} as indicated by a small Soret shift to 444 nm (Fig. 2.6A). However, Ca^{2+} addition substantially increased the reduced form relative to the inactive P420 form. Thus, either Ca^{2+} facilitates NOS_{ox} reduction by NOS_{red}, or Ca^{2+} attenuates the formation of the inactive P420 species through some means of NOS_{ox} stabilization.

Likewise, $syNOS_{red}$ and NADPH directly reduce $syNOS_g$, as indicated by the Soret shift to 426 nm and α-bands at 530 and 560 nm (Fig. 2.6B). The reductase domains of flavoHbs usually contain binding sites for FAD and NADH, but not FMN (39). Thus, either the FAD-containing FNR domain, or the flavodoxin-like FMN module of $syNOS_{red}$ could directly reduce NOS_g.

3.5 syNOS globin oxidizes NO to Nitrate

Upon assay of syNOS with the Griess reaction it was found that the enzyme produces primarily nitrate with little to no nitrite formed, despite nitrite being the initial product of NO oxidation by air. Because related flavohemoglobins detoxify NO to nitrate, $syNOS_g$ may function as a NO dioxygenase (NOD). Thus, we investigated the ability of NO generated by NOC-7 to be oxidized by syNOS (Table 2.2). NO was oxidized primarily to nitrate (74%) by syNOS in an NADPH dependent manner during the time course of the experiment (NOS activity was stopped after 30 min, which equates to approximately three NOC-7 half-lives). removal of the ligating cysteine from NOS_{ox} (C539A) did not decrease nitrate production, confirming NO dioxygenation by the globin heme. In contrast, removal of the proximal histidine from NOS_g did reduce NO_3^- production, but not completely. The H422A variant produced more nitrate than nonenzymatic oxidation by air, suggesting that the NOS_{ox} domain

Table 2.2: NO dioxygenation by syNOS (0.5 μM), H422A (1 μM), and C539A (0.5 μM). Samples were incubated for 30 min in the presence of the NO donor NOC-7 before heat denaturing. Percent NO oxidized to NO_2^- + NO_3^- was measured by the Griess assay. The rate constants for NOD activity were measured with an NO electrode. The rate constants were averages of at least nine measurements and a Q test was used to remove outliers. Student's t-test indicated a significant difference between the rate constants of syNOS and H422A ($p < 0.001$) and between H422A and C539A ($p < 0.001$), but no significant difference between syNOS and C539A ($p > 0.7$). ND, not determined.

	Griess Method		NO oxidation rate constant
	% NO_2^-	% NO_3^-	(s^{-1} nanomole $heme^{-1}$)
syNOS	25.6 ± 0.6	74 ± 2	0.6 ± 0.2
H422A	44.6 ± 1.6	55 ± 3	0.11 ± 0.05
C539A	29.0 ± 1.6	71 ± 7	1.0 ± 0.6
no NADPH	76 ± 3	23 ± 3	ND

also oxidizes NO to nitrate, as has been found for mNOS (40).

The rate constants for dioxygenation by syNOS and variants were measured with an NO-specific electrode (Table 2.2). NOC-7 derived NO produced a measurable current on the order of microamperes. Upon addition of syNOS, the NO signal decayed rapidly under first order kinetics. Consistent with results from the Griess assay, the rate constant for NO oxidation by the C539A variant (0.6 ± 0.4 s^{-1} nanomole $heme^{-1}$) is approximately equal to that of WT-syNOS (0.6 ± 0.3 s^{-1} $nmole^{-1}$), and the rate constant of the H422A variant is far less than either (0.10 ± 0.06 s^{-1} $nmole^{-1}$). These results reveal that not only is NOS_g an efficient NOD, but confirm that NOS_{red} directly reduces both the NOS_{ox} and NOS_g heme cofactors.

2.3.6 Activity of syNOS in *E. coli* cells.

It was previously reported that syNOS enabled *E. coli* to use L-arg as its sole nitrogen source, and that expression of syNOS increased cell density when growing on L-arg, compared

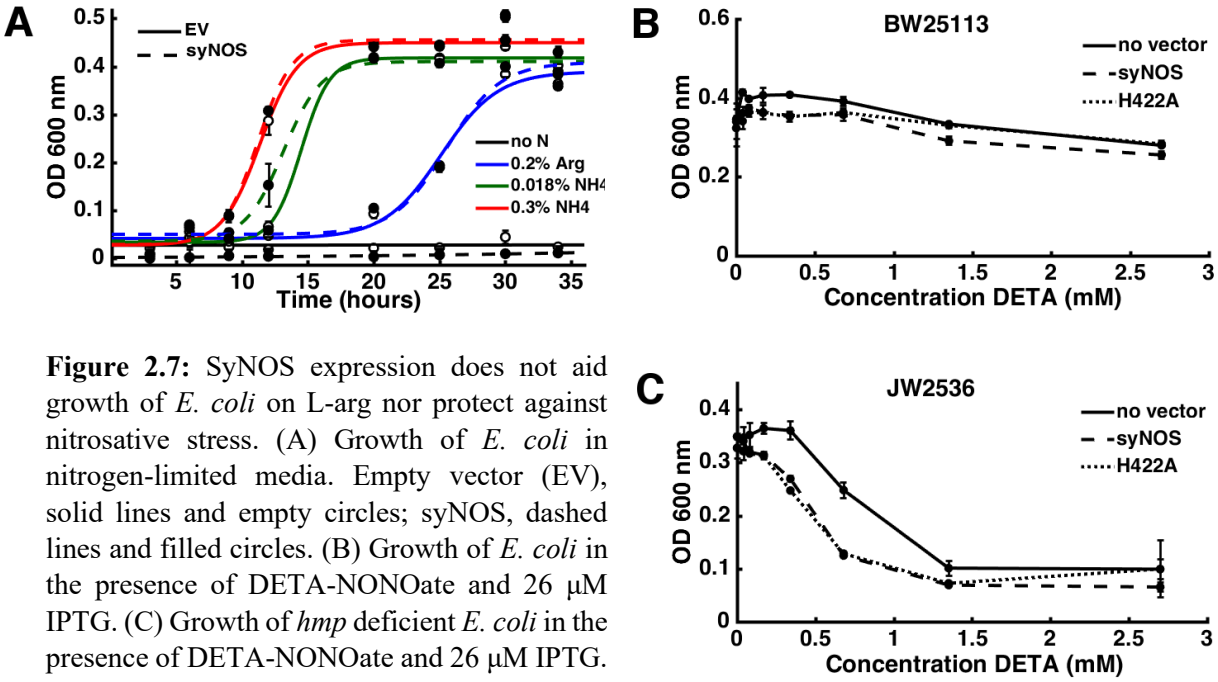

Figure 2.7: SyNOS expression does not aid growth of *E. coli* on L-arg nor protect against nitrosative stress. (A) Growth of *E. coli* in nitrogen-limited media. Empty vector (EV), solid lines and empty circles; syNOS, dashed lines and filled circles. (B) Growth of *E. coli* in the presence of DETA-NONOate and 26 μM IPTG. (C) Growth of *hmp* deficient *E. coli* in the presence of DETA-NONOate and 26 μM IPTG.

to an empty vector (EV) control (30). Under our conditions this benefit of syNOS was not observed; instead we found that syNOS expression conferred no significant advantage for growth on L-arg compared to the EV control (Fig. 2.7A). Given that syNOS requires H_4B for NO production from L-arg, and *E. coli* does not make H_4B (41), it is unclear how expression of syNOS would increase conversion of L-arg to more oxidized forms of nitrogen, such as nitrate.

Although syNOS should not be active as a NOS when recombinantly expressed in *E. coli*, it should retain NOD activity, which may mitigate the effects of nitrosative stress. To test the ability of recombinant syNOS to protect *E. coli* against NO, syNOS and the NOD deficient variant H422A were expressed from the tac promoter (pCW-LIC) in a WT *E. coli* strain BW25113, as well as the flavohemoglobin deficient strain JW2536. The absence of the flavohemoglobin gene (Δ*hmp*) renders *E. coli* more sensitive to NO (42), and the addition of a NOD should, in theory, allow growth at higher NO concentrations. However, this was not observed (Fig 6B and C). The Δ*hmp* strain is more sensitive to nitrosative stress induced by

addition of DETA-NONOate than the WT, but the added expression of syNOS actually increased sensitivity to NO. Additionally, the growth of cells containing the NOD deficient H422A construct was indistinguishable from those containing wild-type syNOS. Thus, syNOS cannot complement a *hmp* mutant of *E. coli*, indicating that its NOD activity in this context is low.

2.4 Discussion

Full length syNOS proved to be a challenging protein to express recombinantly in *E. coli*. Although soluble protein with heme and flavin cofactors bound could be produced under several conditions, many attempts at purification produced protein with little or no synthase activity. Furthermore, active and inactive syNOS share the same spectroscopic characteristics and elute similarly on SEC. Co-expression with the chaperonin GroEL/ES was essential to consistently produce active protein. *E. coli* encodes GroEL/ES and several other chaperones in its genome; however, their basal level of expression was insufficient to reliably correct syNOS misfolding.

Biochemical and spectroscopic results confirm syNOS is a genuine NOS and NOD. The NOS_{ox} ferrous-carbonmonoxy species is observed at 444 nm, as expected of a P450 type heme. In the absence of the NOS_{ox} heme, nitric oxide is not produced and in the absence of the NOS_{g} heme the amount of NO dioxygenation is attenuated. syNOS shares the same substrate, products, and activating cofactors expected of a mammalian NOS, however, there are several unusual facets of syNOS enzymology.

A feature that distinguishes syNOS from animal NOSs is the absence of the calmodulin-binding sequence and auto-inhibitory loop. All three mammalian NOS isoforms require Ca^{2+}-

CaM, and in eNOS and nNOS the calcium concentration dependence is dictated by the presence of an auto-inhibitory loop in the FMN domain (43, 44). Although syNOS does not bind mammalian calmodulin (and no protein in its genome has significant similarity to calmodulin), the addition of calcium increases NO turnover tenfold. Moreover, NOS_{ox} reduction by NOS_{red} is substantially enhanced by Ca^{2+} and thus Ca^{2+} alone may be playing a similar role in syNOS as Ca^{2+}-CaM does in mNOS. No other NOS has been reported to be activated by calcium independent of calmodulin. The Swiss Institute for Bioinformatics ScanProsite tool was used to search for possible EF-hand calcium binding motifs (Prosite accession numbers PS50222, PS00018) in syNOS, but no such sites were identified. It is possible that calcium may have a structural role, perhaps at the dimer interface, similar to zinc in mammalian NOS (45, 46), or at inter-domain contacts to facilitate electron transfer to the NOS_{ox} heme. However, the measured activation constant for calcium was high, 228 ± 9 μM, far exceeding biological concentration ranges (hundreds of nanomolar to 10 micromolar (47, 48)). The mechanism of calcium binding and activation of syNOS is currently unknown; additional cofactors or proteins may be required for efficient calcium use, or Ca^{2+} may serve as a proxy for another factor *in vivo*.

Cofactor utilization also differentiates syNOS from other bacterial NOSs. All bacteria produce THF, but few produce H_4B, which differs from THF in its dihydroxypropyl side chain. All bacterial NOSs characterized to date can utilize both cofactors, and thus the preference of syNOS for H_4B over THF confers with its mammalian-like NOS domain architecture. Genome analysis suggests that *Synechococcus* sp. PCC 7335 can produce H_4B. The H_4B biosynthetic pathway requires GTP cyclohydrolase I (GTPCH I), 6-pyruvoyl tetrahydropterin synthase (PTS), and sepiapterin reductase (SR) (49, 50). Both GTPCH and PTS are found in the genome

of *Synechococcus* sp. PCC 7335 and are highly homologous to the mammalian enzymes (>50% identity), however no gene in *Synechococcus* is annotated as a SR. SR belongs to the short-chain dehydrogenase/reductase (SDR) family of oxidoreductases, a large family of proteins found in all kingdoms of life (51). *Synechococcus* encodes many genes belonging to the SDR family. Although none share high sequence similarity (greater than 30% identity) with mammalian SR, one gene annotated as an SDR (CDS YP_002711555.1) is immediately adjacent to a gene encoding GTPCH I. Additionally, of the fifteen photosynthetic prokaryotes containing gene sequences highly similar to syNOS (greater than 60% identity) fourteen also encode an SDR adjacent to a GTPCH I. Thus, it is highly likely that *Synechococcus* has the enzymatic machinery to produce H_4B.

Mammalian NOSs cannot use THF because an N-terminal □-extension, known as the N-terminal hook, occludes the long THF p-aminobenzoyl-glutamate side chain (52). In syNOS, this region is replaced by a short linker (18 residues) to the globin domain. This raises questions concerning not only the manner of selective H_4B binding, but also the manner of $syNOS_{ox}$ dimer formation and coupling to NOS_g. The NOS_{ox} motifs located at the dimer interface in other NOS, the helical lariat and helical T (52), are conserved in syNOS however, the close proximity of NOS_g suggests it could also play a role in stabilizing the NOS_{ox} subunit, as well as the NOS_{ox} dimer. In support of a tight coupling between NOS_{ox} and NOS_g, the H422A substitution in NOS_g appears to also affect the stability of NOS_{ox} and/or its affinity for L-arg.

In addition to structural implications, the NOS_g domain adds a layer of complexity to syNOS chemistry and physiology. Sequence alignments assign this domain to the globin superfamily of proteins. In particular, flavoHbs catalyze reduction of nitrite to nitric oxide and reduction of nitric oxide to nitrous oxide (53), but most commonly carry out the oxidation of

NO to nitrate (39, 54). syNOS catalyzes the oxidation of NO to nitrate and this activity depends on a functional globin domain. Removal of the NOS_{ox} heme (the C539A variant) did not hinder NO oxidation, however, the NOS_{ox} domain was also capable of NO dioxygenation because nitrate production was still observed in the absence of the NOS_g heme (H422A). NO dioxygenase activity by NOS enzymes has precedent; mammalian NOSs are also capable of NO dioxygenation, and chimeras composed of $iNOS_{ox}$ and $nNOS_{red}$ exhibit increased NOD activity (40). By producing chimeras that coupled the fast heme reduction (k_r) of nNOS with the slow NO dissociation (k_d) of iNOS, as well as the addition of a V346I substitution that further slowed the NO release (55), NO dioxygenation by mNOS was substantially accelerated (40). Note that in syNOS the equivalent position of V346 in the distal heme pocket contains Ile natively, typical of bacterial NOS. The NO dioxygenase activity of syNOS has two implications; i) syNOS is the first NOS whose final product can be nitrate and not NO, and ii) the reductase domain of syNOS can reduce both the NOS_{ox} and NOS_g directly. It is also worth noting that the spin trap compound intercepted nearly all NO from syNOS before it could be oxidized to NO_3^- by NOS_g. Thus, NOD activity in syNOS is independent from NOS activity, with any NO produced by NOS_{ox} released to the solution before reaction with NOS_g.

Our biochemical results confirm that syNOS oxidizes L-arg to nitrate (30); however, we are unable to replicate the finding that syNOS allows *E. coli* to use L-arg as the sole nitrogen source. The growth of *E. coli* transformed with empty vector is indistinguishable from that transformed with syNOS. Both strains are capable of growth on L-arg which is not surprising given that *E. coli* already contains the arginine succinyl transferase pathway (AST) to derive reduced nitrogen from arginine (56, 57). Although *Synechococcus* does not contain the AST pathway, it does contain alternate L-arg salvage pathways, that rely on enzymes such as

arginase and deaminating L-amino acid oxidases (58, 59)). Furthermore, syNOS is not expected to be active in *E. coli* as the third enzyme in the H_4B biosynthesis pathway, sepiapterin reductase, is absent from its genome (41) and syNOS cannot substitute H_4B with THF. The proposed role of syNOS in nitrogen assimilation is somewhat questionable given the environmental conditions in which the cyanobacteria are found. *Synechococcus* sp. PCC 7335 is a marine organism, where the concentrations of dissolved nitrates (tens of micromolar (60–62)) far exceeds that of arginine in (tens of nanomolar (63–65)). Additionally, this organism is capable of nitrogen fixation (66–68). It is unclear what biochemical merits result from expending reducing power (NADPH) to oxidize L-arg to nitrate, only to then reductively assimilate nitrate back to ammonia.

Owing to the lack of H_4B, $syNOS_{ox}$ should be inactive in *E. coli*. However, $syNOS_g$ and $syNOS_{red}$ do not depend on specialized cofactors and thus syNOS may function as an NO dioxygenase in *E. coli.* However, the flavohemoglobin deficient strain (JW2536) containing syNOS is actually more susceptible to damage by NO than compared to the untransformed control. If syNOS was functioning as a flavoHb we would expect the opposite. Thus, either the protein does not exhibit NOD activity in *E. coli* because of interfering cellular factors, or it has other additional activities that are detrimental to growth that overcome any benefit of NO oxidation to nitrate.

The dual functionality of syNOS as both a NOS and a NOD is mysterious. As syNOS is actively expressed in growing cyanobacteria (30) some regulatory mechanism or "on/off switch" may be necessary to control NO production. NOS_g may participate in such a function. Globin-based regulation of NOS has precedent in animals; eNOS binds to and stabilizes α-globin at the myoendothelial junction so that α-globin can regulate NO signaling by oxidizing

NO to nitrate (69). Additionally, *in vitro* experiments found full-length eNOS was able to reduce α-globin to the active ferrous state at a faster rate than the methemoglobin reductase cytochrome B5 reductase (69).

In *S. aureus*, NOS is proposed to play a role in the transition from aerobic respiration to nitrate respiration under microaerobic conditions (23). This control is mediated by the combined action of NOS and flavoHb; at high oxygen concentrations NOS-derived NO is detoxified by flavoHb, whereas under microaerobic conditions flavoHb cannot bind oxygen as substrate and NO is free to inhibit cytochrome oxidase, thus inhibiting oxygen reduction and favoring nitrate respiration. Although syNOS would genetically link NOS and NOD activity for such a purpose, the NOS-containing *Synechococcus* species does not respire nitrate (as it lacks ccNIR and associated *nrf* genes). Finally, a feature of syNOS activity that may provide clues as to its biological function is its reliance on calcium, which is well-known to be a tightly regulated signaling molecule in cyanobacteria (47, 70). Interestingly, Ca^{2+} is used in cyanobacteria as a signal to convey changes in nitrogen utilization. Increased levels of calcium in *Synechoccocus elongatus* accompany acclimation to nitrogen starvation (71), and in *Anabaena* sp. PCC 7120 elevated calcium levels are necessary for heterocyst differentiation (72). Thus, syNOS may be poised to respond to these signals. The high Ca^{2+} threshold that we observe in our assays is not without note but may be a consequence of the *ex vivo* conditions.

In conclusion, we demonstrate that syNOS has both NOS and NOD activities. The protein represents a bacterial NOS enzyme with properties closely related to its mNOS counterparts, especially with respect to reductase coupling and cofactor utilization. However, the NOS function is not activated by Ca^{2+}-CaM and instead appears to require only Ca^{2+} for activity. The enzyme's reliance on H_4B calls into question any NOS activity when

recombinantly expressed in *E. coli*, and likewise the protein is unable to aid a flavoHb null strain in tolerating nitrosative stress. The properties of syNOS in the context of *Synechococcus* metabolism suggest that it is unlikely to be solely involved in nitrogen utilization from arginine. That said, the coupling of NOS and NOD activity in a single protein indicates a genetic link between these respective activities that is beneficial to cyanobacteria.

2.5 References

1. Zumft, W. G. (1997) Cell biology and molecular basis of denitrification. *Microbiol. Mol. Biol. Rev.* 61, 533–616
2. Gusarov, I., and Nudler, E. (2018) Protein S-Nitrosylation: Enzymatically Controlled, but Intrinsically Unstable, Post-translational Modification. *Mol. Cell*. 69, 351–353
3. Plate, L., and Marletta, M. A. (2013) Nitric oxide-sensing H-NOX proteins govern bacterial communal behavior. *Trends Biochem. Sci.* 38, 566–575
4. Denninger, J. W., and Marletta, M. A. (1999) Guanylate cyclase and the ·NO/cGMP signaling pathway. *Biochim. Biophys. Acta - Bioenerg.* 1411, 334–350
5. Knowles, R., Palacios, M., Palmer, R., and Moncada, S. (1989) Formation of nitric oxide from L-arginine in the central nervous system: a transduction mechanism for stimulation of the soluble guanylate cyclase. *Proc. Natl. Acad. Sci.* 86, 5159–5162
6. Palmer, R. M. J., and Moncada, S. (1989) A novel citrulline-forming enzyme implicated in the formation of nitric oxide by vascular endothelial cells. *Biochem. Biophys. Res. Commun.* 158, 348–352
7. Bredt, D. S., and Snyder, S. H. (1990) Isolation of nitric oxide synthetase, a calmodulin-requiring enzyme. *Proc. Natl. Acad. Sci. U. S. A.* 87, 682–685
8. Yui, Y., Hattori, R., Kosuga, K., Eizawa, H., Hiki, K., Ohkawa, S., Ohnishi, K., Terao, S., and Kawai, C. (1991) Calmodulin-independent nitric oxide synthase from rat polymorphonuclear neutrophils. *J Biol Chem*. 266, 3369–3371
9. Siddhanta, U., Presta, A., Fan, B., Wolan, D., Rousseau, D. L., and Stuehr, D. J. (1998) Domain Swapping in Inducible Nitric-oxide Synthase. *J. Biol. Chem.* 273, 18950–18958
10. Daff, S. (2003) Calmodulin-dependent regulation of mammalian nitric oxide synthase. *Biochem. Soc. Trans.* 31, 502–5
11. Tejero, J., and Stuehr, D. (2013) Tetrahydrobiopterin in nitric oxide synthase. *IUBMB Life*. 65, 358–365
12. Bogdan, C. (2001) Nitric oxide and the immune response. *Nat. Immunol.* 2, 907–916
13. Chachlaki, K., Garthwaite, J., and Prevot, V. (2017) The gentle art of saying NO: How nitric oxide gets things done in the hypothalamus. *Nat. Rev. Endocrinol.* 13, 521–535
14. Ignarro, L. J. (2002) Nitric oxide as a unique signaling molecule in the vascular system: A historical overview. *J. Physiol. Pharmacol.* 53, 503–514
15. Hobbs, A. J., Higgs, A., and Moncada, S. (1999) Inhibition of nitric oxide synthase as a potential therapeutic target. *Annu. Rev. Pharmacol. Toxicol.* 39, 191–220
16. Vanini, F., Kashfi, K., and Nath, N. (2015) The dual role of iNOS in cancer. *Redox Biol.* 6, 334–343
17. Connelly, L., Madhani, M., and Hobbs, A. J. (2005) Resistance to endotoxic shock in endothelial nitric-oxide synthase (eNOS) knock-out mice: A pro-inflammatory role for eNOS-derived no in vivo. *J. Biol. Chem.* 280, 10040–10046
18. Choudhari, S. K., Chaudhary, M., Bagde, S., Gadbail, A. R., and Joshi, V. (2013) Nitric oxide and cancer : a review. *World J. Surg. Oncol.* 11, 1
19. Patel, B. a, Moreau, M., Widom, J., Chen, H., Yin, L., Hua, Y., and Crane, B. R. (2009) Endogenous nitric oxide regulates the recovery of the radiation-resistant bacterium Deinococcus radiodurans from exposure to UV light. *Proc. Natl. Acad. Sci.*

U. S. A. 106, 18183–8
20. Rao, M., Smith, B. C., and Marletta, A. (2015) Nitric Oxide Mediates Biofilm Formation and Symbiosis in Silicibacter. *MBio*. 6, 1–10
21. Gusarov, I., and Nudler, E. (2005) NO-mediated cytoprotection: instant adaptation to oxidative stress in bacteria. *Proc. Natl. Acad. Sci. U. S. A.* 102, 13855–13860
22. Shatalin, K., Gusarov, I., Avetissova, E., Shatalina, Y., McQuade, L. E., Lippard, S. J., and Nudler, E. (2008) Bacillus anthracis-derived nitric oxide is essential for pathogen virulence and survival in macrophages. *Proc. Natl. Acad. Sci. U. S. A.* 105, 1009–13
23. Kinkel, T. L., Ramos-Montañez, S., Pando, J. M., Tadeo, D. V., Strom, E. N., Libby, S. J., and Fang, F. C. (2016) An essential role for bacterial nitric oxide synthase in Staphylococcus aureus electron transfer and colonization. *Nat. Microbiol.* 2, 1–7
24. Chaudhari, S. S., Kim, M., Lei, S., Razvi, F., Alqarzaee, A. A., Hutfless, E. H., Powers, R., Zimmerman, M. C., Fey, P. D., and Thomas, V. C. (2017) Nitrite Derived from Endogenous Bacterial Nitric Oxide Synthase Activity Promotes Aerobic Respiration. *MBio*. 8, 1–16
25. Crane, B. R., Sudhamsu, J., and Patel, B. a (2010) Bacterial nitric oxide synthases. *Annu. Rev. Biochem.* 79, 445–70
26. Gusarov, I., Starodubtseva, M., Wang, Z. Q., McQuade, L., Lippard, S. J., Stuehr, D. J., and Nudler, E. (2008) Bacterial nitric-oxide synthases operate without a dedicated redox partner. *J. Biol. Chem.* 283, 13140–13147
27. Agapie, T., Suseno, S., Woodward, J. J., Stoll, S., Britt, R. D., and Marletta, M. a (2009) NO formation by a catalytically self-sufficient bacterial nitric oxide synthase from Sorangium cellulosum. *Proc. Natl. Acad. Sci. U. S. A.* 106, 16221–16226
28. Foresi, N., Correa-Aragunde, N., Parisi, G., Caló, G., Salerno, G., and Lamattina, L. (2010) Characterization of a nitric oxide synthase from the plant kingdom: NO generation from the green alga Ostreococcus tauri is light irradiance and growth phase dependent. *Plant Cell*. 22, 3816–3830
29. Domingos, P., Prado, A. M., Wong, A., Gehring, C., and Feijo, J. A. (2015) Nitric oxide: A multitasked signaling gas in plants. *Mol. Plant*. 8, 506–520
30. Correa-Aragunde, N., Foresi, N., Del Castello, F., and Lamattina, L. (2018) A singular nitric oxide synthase with a globin domain found in Synechococcus PCC 7335 mobilizes N from arginine to nitrate. *Sci. Rep.* 8, 12505
31. Gupta, S., Pawaria, S., Lu, C., Yeh, S. R., and Dikshit, K. L. (2011) Novel flavohemoglobins of mycobacteria. *IUBMB Life*. 63, 337–345
32. Gupta, S., Pawaria, S., Lu, C., Hade, M. D., Singh, C., Yeh, S. R., and Dikshit, K. L. (2012) An unconventional hexacoordinated flavohemoglobin from Mycobacterium tuberculosis. *J. Biol. Chem.* 287, 16435–16446
33. Sabat, J., Stuehr, D. J., Yeh, S. R., and Rousseau, D. L. (2009) Characterization of the proximal ligand in the P420 form of inducible nitric oxide synthase. *J. Am. Chem. Soc.* 131, 12186–12192
34. Perera, R., Sono, M., Sigman, J. A., Pfister, T. D., Lu, Y., and Dawson, J. H. (2003) Neutral thiol as a proximal ligand to ferrous heme iron: implications for heme proteins that lose cysteine thiolate ligation on reduction. *Proc. Natl. Acad. Sci. USA*. 100, 3641–3646
35. Kakar, S., Hoffman, F. G., Storz, J. F., Fabian, M., and Hargrove, M. S. (2010) Structure and reactivity of hexacoordinate hemoglobins. *Biophys. Chem.* 152, 1–14

36. Brunori, M., Giuffre, A., Nienhaus, K., Nienhaus, G. U., Scandurra, F. M., and Vallone, B. (2005) Neuroglobin, nitric oxide, and oxygen: Functional pathways and conformational changes. *Proc. Natl. Acad. Sci.* 102, 8483–8488
37. Stuehr, D. J., and Ikeda-Saito, M. (1992) Spectral characterization of brain and macrophage nitric oxide synthases: Cytochrome P-450-like hemeproteins that contain a flavin semiquinone radical. *J. Biol. Chem.* 267, 20547–20550
38. Pfeiffer, S., Leopold, E., Schmidt, K., Brunner, F., and Mayer, B. (1996) Inhibition of nitric oxide synthesis by NG * nitro-L-arginine methyl ester (L-NAME): requirement for bioactivation to the free acid ,. *Br. J. Pharmacol.* 118, 1433–1440
39. Bonamore, A., and Boffi, A. (2008) Flavohemoglobin: Structure and reactivity. *IUBMB Life*. 60, 19–28
40. Wang, Z. Q., Haque, M. M., Binder, K., Sharma, M., Wei, C. C., and Stuehr, D. J. (2016) Engineering nitric oxide synthase chimeras to function as NO dioxygenases. *J. Inorg. Biochem.* 158, 122–130
41. Yamamoto, K., Kataoka, E., Miyamoto, N., Furukawa, K., Ohsuye, K., and Yabuta, M. (2003) Genetic engineering of Escherichia coli for production of tetrahydrobiopterin. *Metab. Eng.* 5, 246–254
42. Membrillo-Hernández, J., Coopamah, M. D., Anjum, M. F., Stevanin, T. M., Kelly, A., Hughes, M. N., and Poole, R. K. (1999) The flavohemoglobin of Escherichia coli confers resistance to a nitrosating agent, a “nitric oxide releaser,” and paraquat and is essential for transcriptional responses to oxidative stress. *J. Biol. Chem.* 274, 748–754
43. Salerno, J. C., Harris, D. E., Irizarry, K., Patelf, B., Morales, A. J., Smith, S. M. E., Martasek, P., Roman, L. J., Masters, B. S. S., Jones, C. L., Weissman, B. A., Lane, P., Liu, Q., and Gross, S. S. (1997) An autoinhibitory control element defines calcium-regulated isoforms of nitric oxide synthase. *J. Biol. Chem.* 272, 29769–29777
44. Daff, S., Sagami, I., and Shimizu, T. (1999) The 42-amino acid insert in the FMN domain of neuronal nitric-oxide synthase exerts control over Ca2+/calmodulin-dependent electron transfer. *J. Biol. Chem.* 274, 30589–30595
45. Li, H., Raman, C. S., Glaser, C. B., Blasko, E., Young, T. A., Parkinson, J. F., Whitlow, M., and Poulos, T. L. (1999) Crystal structures of zinc-free and -bound heme domain of human inducible nitric-oxide synthase. *J. Biol. Chem.* 274, 21276–21284
46. Raman, C. S., Li, H., Martásek, P., Král, V., Masters, B. S. S., and Poulos, T. L. (1998) Crystal structure of constitutive endothelial nitric oxide synthase: A paradigm for pterin function involving a novel metal center. *Cell*. 95, 939–950
47. Domínguez, D. C., Guragain, M., and Patrauchan, M. (2015) Calcium binding proteins and calcium signaling in prokaryotes. *Cell Calcium*. 57, 151–165
48. Clapham, D. (2007) Calcium Signaling. *Cell*. 10.1515/pjvs-2015-0054
49. Wang, H., Yang, B., Hao, G., Feng, Y., Chen, H., Feng, L., Zhao, J., Zhang, H., Chen, Y. Q., Wang, L., and Chen, W. (2011) Biochemical characterization of the tetrahydrobiopterin synthesis pathway in the oleaginous fungus Mortierella alpina. *Microbiology*. 157, 3059–3070
50. Thöny, B., Auerbach, G., and Blau, N. (2000) Tetrahydrobiopterin biosynthesis, regeneration and functions. *Biochem. J.* 347 Pt 1, 1–16
51. Fujimoto, K., Hara, M., Yamada, H., Sakurai, M., Inaba, A., Tomomura, A., and Katoh, S. (2001) Role of the conserved Ser-Tyr-Lys triad of the SDR family in sepiapterin reductase. *Chem. Biol. Interact.* 130–132, 825–832

52. Crane, B. R., Arvai, a S., Ghosh, D. K., Wu, C., Getzoff, E. D., Stuehr, D. J., and Tainer, J. a (1998) Structure of nitric oxide synthase oxygenase dimer with pterin and substrate. *Science*. 279, 2121–2126
53. Kim, S. O., Orii, Y., Lloyd, D., Hughes, M. N., Poole, R. K., and Kim, S. O. (1999) Anoxic function for the Escherichia coli flavohaemoglobin (Hmp): reversible binding of nitric oxide and reduction to nitrous oxide. *FEBS Lett.* 445, 389–394
54. Gardner, P. R., Gardner, A. M., Martin, L. a., and Salzman, A. L. (1998) Nitric oxide dioxygenase: an enzymic function for flavohemoglobin. *Proc. Natl. Acad. Sci. U. S. A.* 95, 10378–10383
55. Wang, Z. Q., Wei, C. C., Sharma, M., Pant, K., Crane, B. R., and Stuehr, D. J. (2004) A Conserved Val to Ile Switch near the Heme Pocket of Animal and Bacterial Nitric-oxide Synthases Helps Determine Their Distinct Catalytic Profiles. *J. Biol. Chem.* 279, 19018–19025
56. Schneider, B. L., Kiupakis, A. K., and Reitzer, L. J. (1998) Arginine Catabolism and the Arginine Succinyltransferase Pathway in Escherichia coli. *J. Bacteriol.* 180, 4278–4286
57. Reitzer, L. (2005) Catabolism of Amino Acids and Related Compounds. *EcoSal Plus*. 10.1128/ecosalplus.3.4.7
58. Schriek, S., Rückert, C., Staiger, D., Pistorius, E. K., and Michel, K. P. (2007) Bioinformatic evaluation of L-arginine catabolic pathways in 24 cyanobacteria and transcriptional analysis of genes encoding enzymes of L-arginine catabolism in the cyanobacterium Synechocystis sp. PCC 6803. *BMC Genomics*. 10.1186/1471-2164-8-437
59. Gau, A. E., Heindl, A., Nodop, A., Kahmann, U., and Pistorius, E. K. (2007) L-amino acid oxidases with specificity for basic L-amino acids in cyanobacteria. *Zeitschrift fur Naturforsch. - Sect. C J. Biosci.* 62, 273–284
60. Patey, M. D., Rijkenberg, M. J. A., Statham, P. J., Stinchcombe, M. C., Achterberg, E. P., and Mowlem, M. (2008) Determination of nitrate and phosphate in seawater at nanomolar concentrations. *TrAC - Trends Anal. Chem.* 27, 169–182
61. Masami Watanabe, Jun Ohtsu, A. O. (2000) Daily Variations in Nutrient Concentrations of Seawater at 321 m Depth in Toyama Bay, Japan Sea. *J. Oceanogr.*
62. Hansell, D. A., and Follows, M. J. (2008) Nitrogen in the Atlantic Ocean. in *Nitrogen in the Marine Environment*, pp. 597–630, 10.1016/B978-0-12-372522-6.00013-X
63. Clark, M. E., Jackson, G. A., and North, W. J. (1972) Dissolved Free Amino Acids in Southern California Coastal Waters. *Limnol. Oceanogr.* [online] http://citeseerx.ist.psu.edu/viewdoc/download?doi=10.1.1.497.1957&rep=rep1&type=pdf (Accessed October 1, 2018)
64. Kaiser, K., and Benner, R. (2009) Biochemical composition and size distribution of organic matter at the Pacific and Atlantic time-series stations. *Mar. Chem.* 113, 63–77
65. Hubberten, U., Lara, R. J., and Kattner, G. (1994) Amino acid composition of seawater and dissolved humic substances in the Greenland Sea. *Mar. Chem.* 45, 121–128
66. Rippka, R., and Waterbury, J. B. (1977) The synthesis of nitrogenase by non-heterocystous cyanobacteria. *FEMS Microbiol. Lett.* 2, 83–86
67. Shih, P. M., Wu, D., Latifi, A., Axen, S. D., Fewer, D. P., Talla, E., Calteau, A., Cai, F., Tandeau de Marsac, N., Rippka, R., Herdman, M., Sivonen, K., Coursin, T., Laurent, T., Goodwin, L., Nolan, M., Davenport, K. W., Han, C. S., Rubin, E. M.,

Eisen, J. a, Woyke, T., Gugger, M., and Kerfeld, C. a (2013) Improving the coverage of the cyanobacterial phylum using diversity-driven genome sequencing. *Proc. Natl. Acad. Sci. U. S. A.* 110, 1053–8

68. Rippka, R., Deruelles, J., Waterbury, J. B., Herdman, M., and Stanier, R. Y. (1979) Generic Assignments, Strain Histories and Properties of Pure Cultures of Cyanobacteria. *J. Gen. Microbiol.* 111, 1–61
69. Lechauve, C., Butcher, J. T., Freiwan, A., Biwer, L. A., Keith, J. M., Good, M. E., Ackerman, H., Tillman, H. S., Kiger, L., Isakson, B. E., and Weiss, M. J. (2018) Endothelial cell α-globin and its molecular chaperone α-hemoglobin-stabilizing protein regulate arteriolar contractility. *J. Clin. Invest.* 128, 5073–5082
70. Walter, J., Lynch, F., Battchikova, N., Aro, E. M., and Gollan, P. J. (2016) Calcium impacts carbon and nitrogen balance in the filamentous cyanobacterium Anabaena sp. PCC 7120. *J. Exp. Bot.* 67, 3997–4008
71. Leganés, F., Forchhammer, K., and Fernández-Piñas, F. (2009) Role of calcium in acclimation of the cyanobacterium Synechococcus elongatus PCC 7942 to nitrogen starvation. *Microbiology*. 155, 25–34
72. Zhao, Y., Shi, Y., Zhao, W., Huang, X., Wang, D., Brown, N., Brand, J., and Zhao, J. (2005) CcbP, a calcium-binding protein from Anabaena sp. PCC 7120, provides evidence that calcium ions regulate heterocyst differentiation. *P Natl Acad Sci-Biol*. 102, 5744–5748

2.6 Supplemental Information

	nmol NO_2^- + NO_3^-
syNOS	
+ Fe-MGD	1.0 ± 1.0
- Fe-MGD	35 ± 4
NOC – 7	78 ± 2

Table 2.S1: NO_2^- + NO_3^- production from syNOS measured by the Griess assay, in the presence or absence of the spin-trap Fe-MGD.

	Hemin & δ-ala	δ-ala
syNOS	1.00 ± 0.10	0.77 ± 0.10
C539A	0.72 ± 0.07	0.42 ± 0.02
H422A	0.39 ± 0.08	0.20 ± 0.03
H422A/C539A	0.10 ± 0.02	0.036 ± 0.009

Table 2.S2: Heme incorporation (μM heme per μM protein) of syNOS constructs expressed in the presence of excess hemin and δ-ala, or just δ-ala.

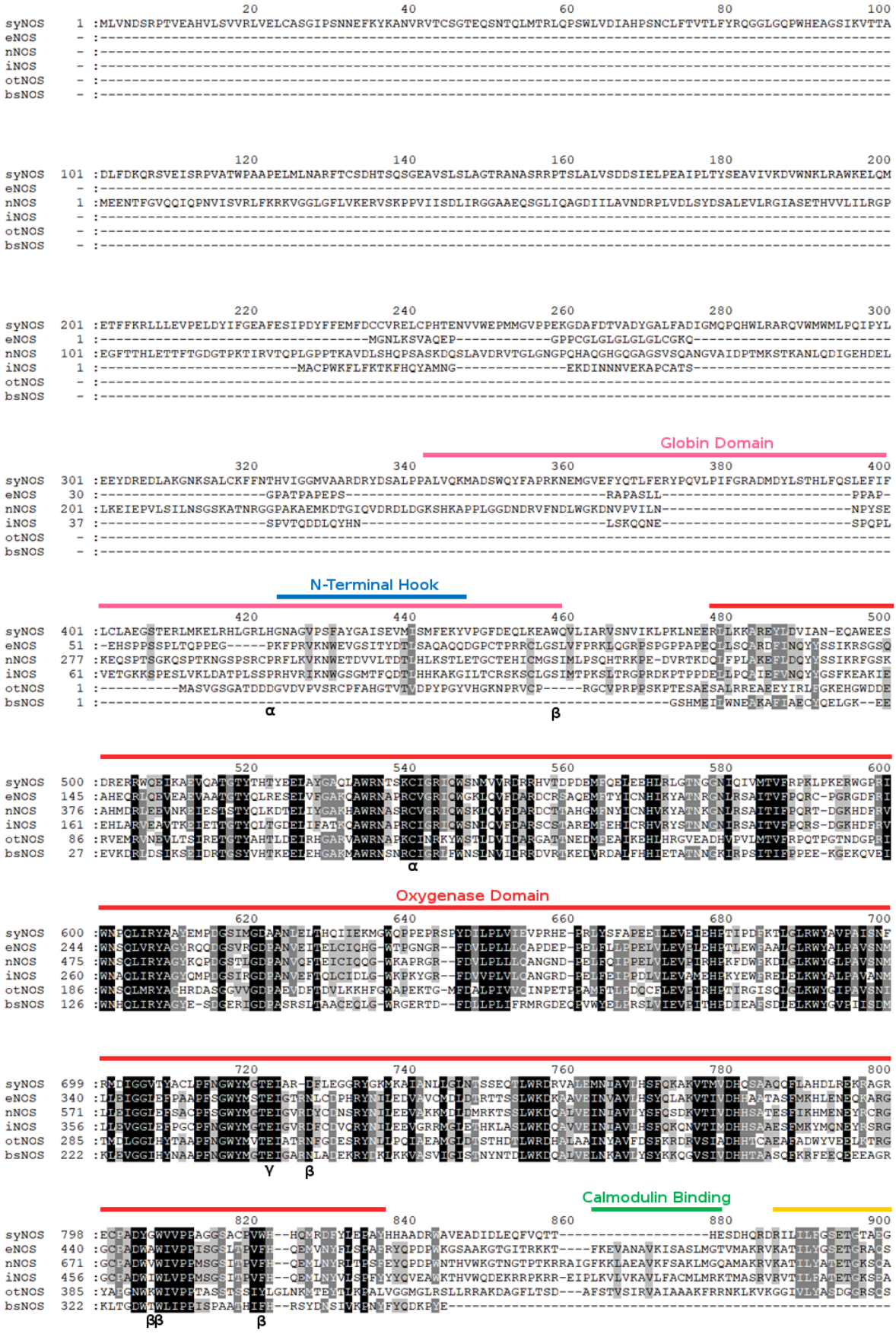
Globin Domain
N-Terminal Hook
α
β
α
Oxygenase Domain
γ
β
Calmodulin Binding
ββ
β

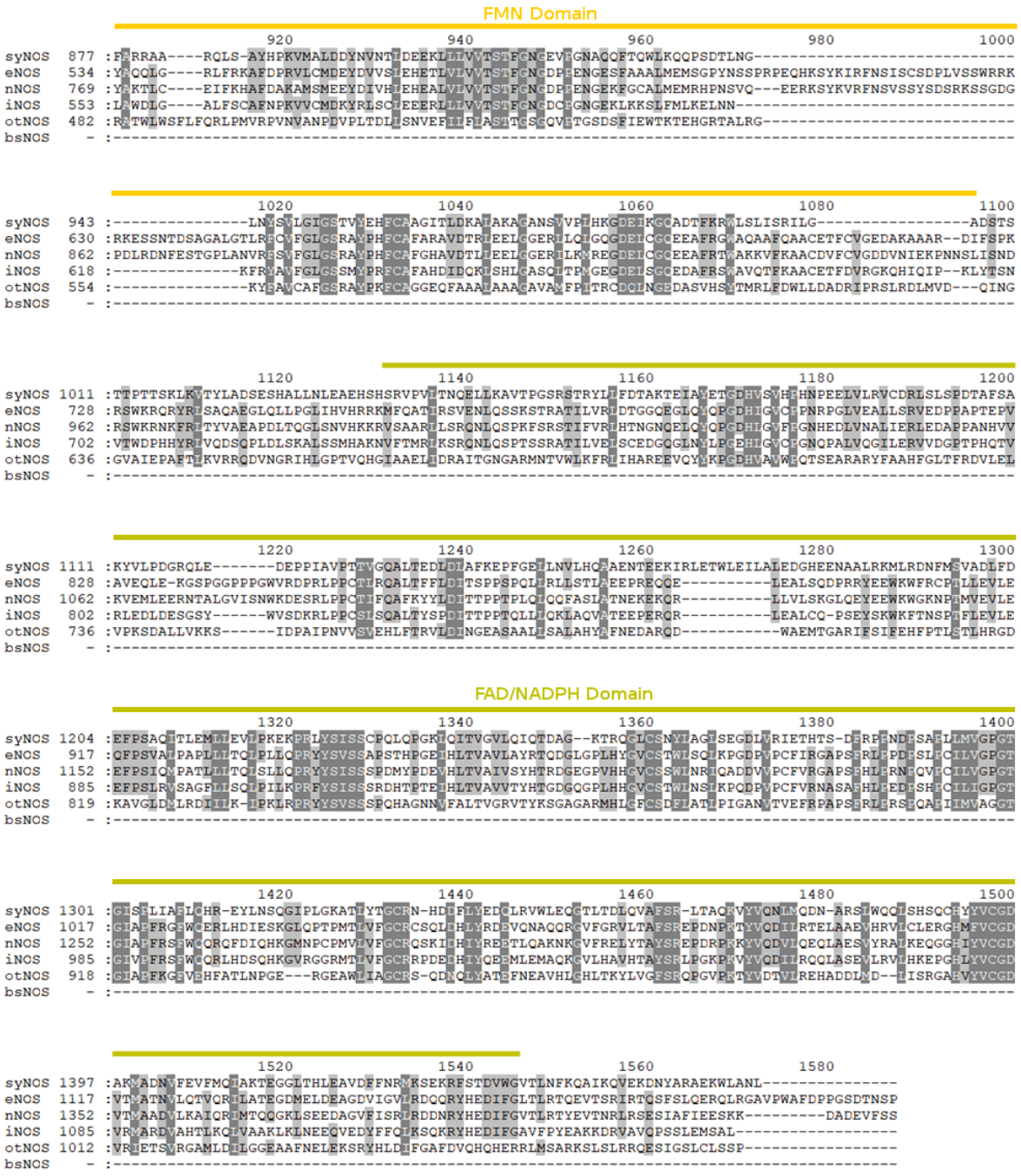

Figure 2.S1: Protein sequence alignment of syNOS to other NOS proteins. The alignment was performed using ClustalX2 and visualized with GeneDoc; proximal heme binding residues (α), pterin binding residues (β), arginine coordinating glutamate (γ), *Homo sapien* endothelial NOS (eNOS), *Rattus norvegicus* neuronal NOS (nNOS), *Homo sapien* inducible NOS (iNOS), *Ostreococcus tauri* NOS (otNOS), *Bacillus subtilis* (bsNOS).

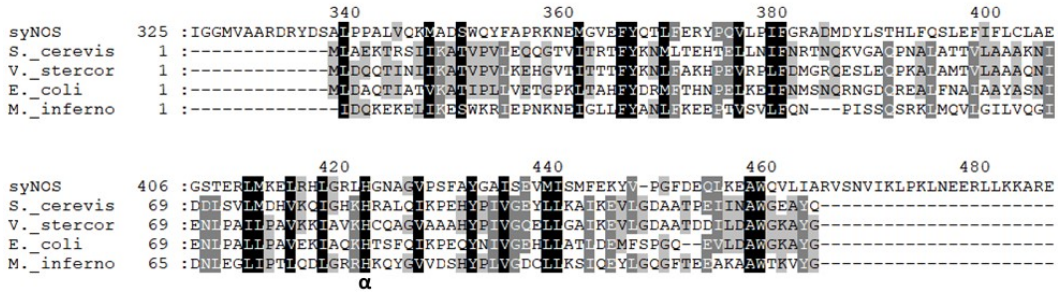

Figure 2.S2: Protein sequence alignment of syNOS$_g$ to other globins and flavohemoglobins of known structures (*Saccharomyces cerevisiae* 4G1V, *Vitreoscilla stercoraria* 1VHB, *Escherichia coli* 1GVH, *Methylokorus infernorum* 3UBC). The alignment was performed using ClustalX2 and visualized with GeneDoc; proximal heme binding residue (α).

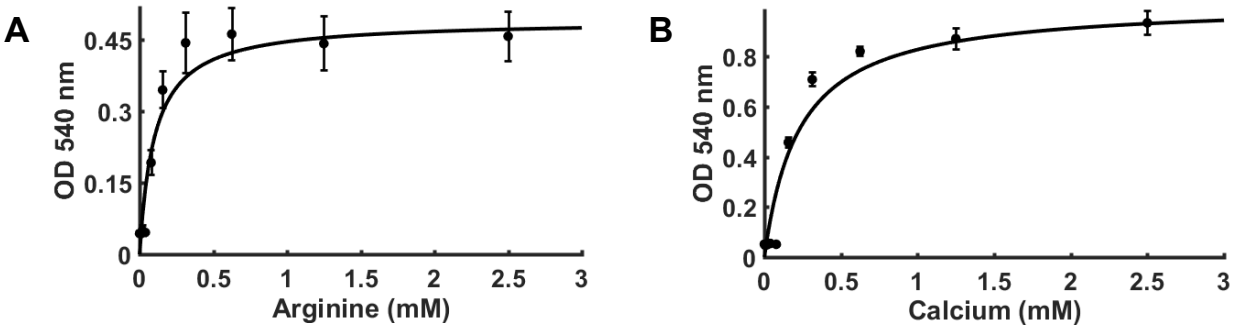

Figure 2.S3: Michaelis-Menten plots for syNOS activity as a function of L-arg concentration (A) and calcium concentration (B). K_M values for arginine and calcium were calculated to be 101 ± 12 μM and 228 ± 9 μM, respectively.

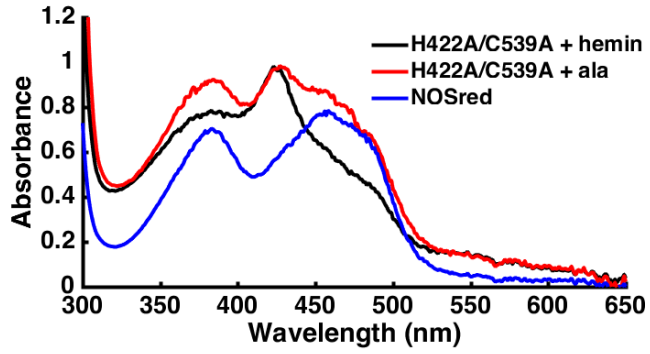

Figure 2.S4: UV-vis spectra of the syNOS variant H422A/C539A compared to the syNOS reductase domain reveals little heme is bound when the proximal heme ligands are changed to alanine.

CHAPTER THREE

Crystal structures of the syNOS FMN and FAD domains and their electron-transfer reactions with NOS_{ox} and NOS_g

3.1 Abstract

Nitric oxide synthases (NOS) is a member of the cytochrome P450 family of monooxygenases and oxidizes L-arginine (L-arg) to nitric oxide (NO) and L-citrulline (L-cit) in animals and bacteria. The eukaryotic enzymes are composed of a catalytic heme domain (NOS_{ox}) with an attached flavin-containing reductase domain (NOS_{red}), and while the NOS_{ox} domain is conserved in bacteria, there is no corresponding NOS_{red}, and NOS_{ox} is instead reduced by nonspecific reductases. Recently a NOS from the nitrogen-fixing cyanobacteria *Synechococcus* sp. 7335 (syNOS) was identified to contain a NOS_{ox} domain with an attached NOS_{red} homologous to mNOS, and an additional globin-like domain (NOS_g). syNOS oxidizes L-arg to NO, but rapidly oxidizes it to nitrate by NOS_g. Here we report rate constants for heme reduction and have found that NOS_g reduction is ~20x faster than NOS_{ox}. The truncated NOS_{FAD} domain reduces NOS_g at the same rate as NOS_{red}, suggesting NOS_g reduction is analogous to flavohemoglobins and not NOS. The structures of isolated NOS_{FMN} and NOS_{FAD} domains have been elucidated with X-ray crystallography, and reveal structural conservation with mNOS.

3.2 Introduction

Nitric oxide synthase (NOS) are heme monooxygenase enzymes that catalyze the oxidation of L-arginine to L-citrulline and nitric oxide. NOS are found in all mammals and are involved in controlling vasodilation (endothelial NOS (1)), immune response (inducible NOS (2)), and neuronal plasticity (neuronal NOS (3)). The architecture of these NOS enzymes is highly conserved; they are comprised of an N-terminal oxygenase domain (NOS_{ox}) and a C-terminal reductase domain (NOS_{red}). NOS_{ox} contains a heme cofactor responsible for catalysis, and NOS_{red} contains an FMN binding flavodoxin-like domain followed by an FAD & NADPH binding FNR-like domain (4, 5). The crystal structures of truncated NOS_{ox} and NOS_{red} have been determined (6–8), however there is no full-length structure of any NOS at atomic resolution, although low-resolution structures (> 20 Å) have been obtained using negative-stain electron microscopy (9, 10) and cryo-EM (11, 12).

NOS are also found in prokaryotic organisms, and their functions are diverse and species dependent. This includes protection from oxidative stress (*B. subtilis* NOS (13)), recovery from UV damage (*D. radiodurans* NOS (14)), and control of aerobic respiration (*S. aureus* NOS (15)). Although bacterial NOS share significant similarity to the NOS_{ox} domain of mammals, they do not have an attached reductase domain. The dedicated reductase domain of mammalian NOS is integral to the function and control of mNOS activity and the lack of such a domain in bacteria has led to an extensive search for its reductase partner. *In vitro*, the flavodoxin YkuN is capable of bsNOS reduction and NO production (16), and chimeras of bsNOS and YkuN have been used as a tool to investigate bacterial NOS inhibitors (17). However, *in vivo* single deletions of YkuN and other proposed reductases did not decrease bsNOS activity (18). It is currently proposed that bNOS do not use one specific

reductase, but instead are reduced by any of the many cellular reductases present. The first bacterial NOS with a dedicated reductase domain was identified in *Sorangium cellulosum* (scNOS) (19). However, this reductase domain contains an N-terminal FNR-like domain and an iron-sulfur cluster, and is very dissimilar from the C-terminal, FNR and flavodoxin of mammalian NOS_{red} (19).

Recently, a NOS from the diazotrophic cyanobacteria *Synechococcus* sp. 7335 (syNOS) has been found to have a covalently attached reductase domain homologous to that of mNOSs (20, 21). Although $syNOS_{red}$ is 35% identical to mNOS, there are striking dissimilarities. In particular, absences of a calmodulin binding domain, a NOS_{FMN} inhibitory loop, connecting domain loop (CD2A), and C-terminal phosphorylation sites from the syNOS sequence suggest the regulation of electron transfer in syNOS may diverge from that of mNOS. In fact, it has already been established that syNOS activation is independent of Ca^{2+}-calmodulin, and instead requires calcium alone (21). The mechanism of this calcium activation is unknown, and the structural characterization of syNOS will aid in the investigation of its regulation and catalysis.

Another question concerns the manner of $syNOS_g$ reduction. It has been established that $syNOS_g$ is reduced by $syNOS_{red}$ independent of the $syNOS_{ox}$ heme (21). How this reduction occurs is unknown and has little precedent in NOS enzymology. $eNOS_{red}$ has been demonstrated to rapidly reduce α-globin, a suppressor of vascular NO signalling, *in vitro* (22). α-globin is natively reduced by the methemoglobin reductase, cytochrome B5 reductase (23, 24), but how happens reduction happens by eNOS, through use of FAD or FMN, has not been investigated. Rather the family of flavohemoglobins (flavoHb) may serve to model $syNOS_g$ reduction. In flavoHb the globin domain is attached to a C-terminal FNR-like domain, and the

heme is reduced by either the FAD hydroquinone or semiquinone (25). It remains to be seen if $syNOS_g$ is reduced by the FMN hydroquinone analogous to $mNOS_{ox}$ reduction, or by FAD in a flavoHb-like fashion.

Here, we have demonstrated that the truncated $syNOS_{FAD}$ domain reduces $syNOS_g$ directly. This is the first example of a NOS_{red} using an FAD to heme reduction mechanism natively. The rate constants for inter-protein reduction were measured and reveal that electron transfer is orders of magnitude more rapid for $syNOS_g$ compared to $syNOS_{ox}$. The first structures of bacterial NOS_{FMN} and NOS_{FAD} domains are also elucidated using x-ray crystallography. The $syNOS_{FMN}$ structure is very similar to that of the mammalian $nNOS_{FMN}$ structure. $syNOS_{FAD}$ differs from that of nNOS in the connecting domain, the α-helical sub-domain between the FMN and FAD binding domains, but the FAD and NADPH domains are conserved. $syNOS_{FAD}$ is quite dissimilar from *E. coli* hmp and has a large RMSD, 8.87 Å, and when the $syNOS_g$ to $syNOS_{FAD}$ domain interaction is modeled based on hmp structures, there are no extensive clashes that would preclude an analogous association model.

3.3 Results

3.3.1 Spectroscopic characterization of syNOS flavin domains

The truncated $syNOS_{FMN}$ (residues 856-1027), $syNOS_{FAD}$ (residues 1027-1468), and $syNOS_{red}$ (856-1468) domains were recombinantly expressed in *E. coli* and purified. Unlike full-length syNOS and its truncated heme domains, the flavin domains do not require co-expression with excess GroEL/ES, and cofactors are fully incorporated upon purification. UV-vis spectra of $syNOS_{red}$ and the truncated domains are similar to that of the mammalian enzyme. Two major peaks are observed in the visible region with a small shoulder at a shorter

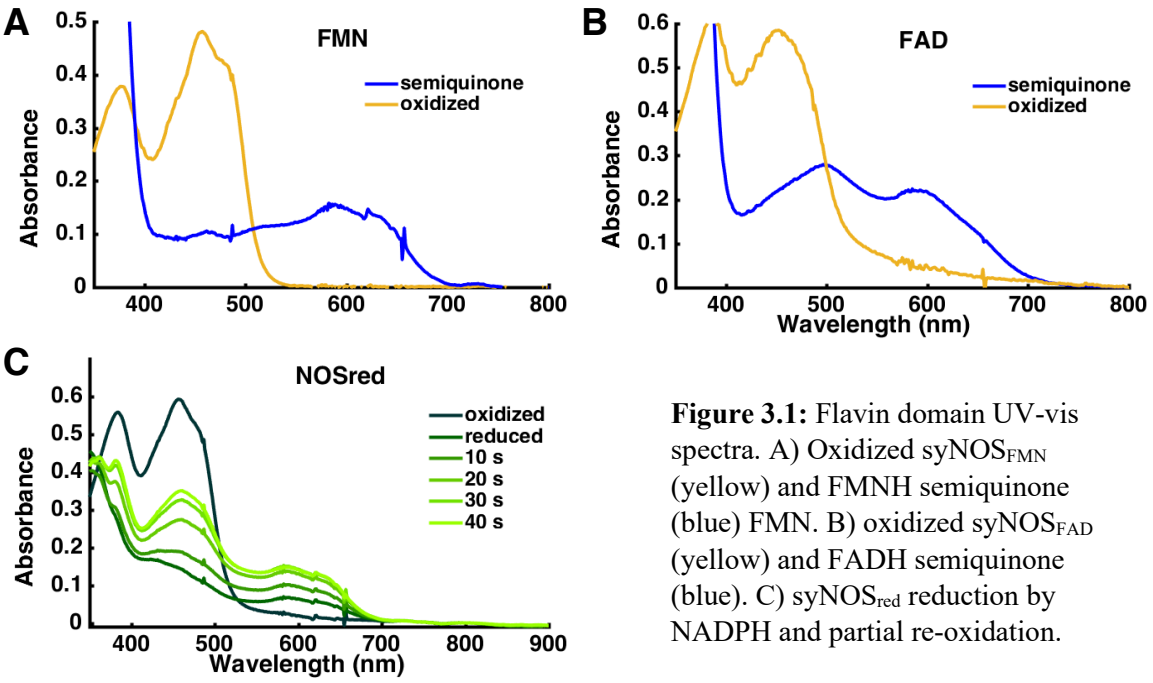

Figure 3.1: Flavin domain UV-vis spectra. A) Oxidized syNOS$_{FMN}$ (yellow) and FMNH semiquinone (blue) FMN. B) oxidized syNOS$_{FAD}$ (yellow) and FADH semiquinone (blue). C) syNOS$_{red}$ reduction by NADPH and partial re-oxidation.

wavelength in the syNOS$_{FMN}$ and syNOS$_{red}$ truncations, but these peaks were less defined in syNOS$_{FAD}$ (Fig. 3.1B). Both flavins form neutral semiquinones upon one electron reduction through photoreduction with deazariboflavin and EDTA under anaerobic conditions, the syNOS$_{FMN}$ maxima at 462 nm, 517 nm 625 nm 727nm, and syNOS$_{FAD}$ maxima at 498 nm and 590 nm. The semiquinone and hydroquinone of syNOS$_{FAD}$ are air sensitive, fully oxidizing in minutes, while the syNOS$_{FMN}$ semiquinone is air stable for hours. Formation of a stable di-semiquinone has been reported for the mammalian enzyme (26, 27), however this species is transient in syNOS$_{red}$ and cannot be isolated using similar methods. Instead $FAD^{2+}/FMNH^{\bullet}$ accumulates, and there is no significant intensity at 498 nm that would indicate the presence of the $FADH^{\bullet}$ semiquinone. This behavior can be seen in Fig 3.1C, during the reduction and re-oxidation of syNOS$_{red}$; this method yields the most semiquinone, yet no di-semiquinone can be detected using UV-vis or ESR. This may indicate differences between the rates of syNOS$_{red}$ and mNOS$_{red}$ inter-flavin electron transfer.

3.3.2 Rates of $syNOS_g$ and $syNOS_{ox}$ reduction by $syNOS_{red}$

As discussed in Chapter Two, the rate of NO oxidation by $syNOS_g$ far exceeds the rate of NO production by $syNOS_{ox}$; to determine whether this difference correlates with the rate of electron transfer to either heme, flavin to heme electron-transfer rate constants were measured by UV-Vis spectroscopy in the absence of either the $syNOS_{ox}$ heme (the C539A variant), or the $syNOS_g$ heme (the H422A variant). Anaerobic samples of H422A bubbled with CO were monitored at 417 nm for the oxidized heme, and at 444 nm for the reduced CO-bound P450 species. The rise at 444 nm was fit to a mono-exponential equation and the decay at 417 nm was fit to a bi-exponential equation because formation of the inactive P420 state caused the absorbance to increase at 420 nm. This species is formed by the dissociation of the NOS_{ox} proximal cysteine upon iron reduction and CO binding (28), and while this can be reversed by incubation with pterin and substrate (29), it only slightly attenuates the amount of P420 in syNOS. The calculated rate constant of $syNOS_{ox}$ reduction depends on the observed wavelength; the rate constant at 417 nm is faster than that at 444 nm (Table 3.1) but in theory they are expected to agree. This discrepancy is likely caused by the formation of significant amounts of P420, results in oxidized heme consumption by two pathways. The rate constants measured at 417 nm are the most accurate measure of electron transfer rates and will be referred to hereafter. The rate constant for $syNOS_{ox}$ reduction (0.0048 s^{-1}) agrees with that of eNOS in the presence of Ca^{2+}-CaM, L-arg, and H_4B (0.005 s^{-1} (30)), which it shares the highest identity with compared to other $mNOS_{ox}$. Rate constants were also calculated under conditions known to accelerate mNOS electron transfer; binding of substrate L-arg and the conversion to the high spin state causes the reduction potential of mNOS to increase (from -

347 mV to -235 mV for iNOS (31)). The addition of L-arg does accelerate syNOS reduction, by about a factor of three (0.013 s^{-1}.) A key factor for syNOS activation is Ca^{2+} and how it participates in NO activity is not yet understood. A convenient explanation may propose that Ca^{2+} could replace the activation of electron transfer by Ca^{2+}-CaM in mNOS. The effect of Ca^{2+} on $syNOS_{ox}$ reduction was investigated with the H422A variant. However, the rate constant for $syNOS_{ox}$ reduction was unchanged in the presence of Ca^{2+}, and the addition of both Ca^{2+} and L-arg was no faster than L-arg alone.

The reduction rate constants of C539A and $syNOS_g$ with $syNOS_{red}$ were monitored using the decay of the oxidize heme (413 nm) and growth of reduced heme (425nm and 560 nm). Traces were fit to mono-exponential equations to extract rate constants. In C539A the rate constant for $syNOS_g$ reduction (0.28 ± 0.06 s^{-1}) far exceeds the reduction of $syNOS_{ox}$. Interestingly, $syNOS_g$ reduction appears to be accelerated in the presence of Ca^{2+} (0.54 ± 0.18 s^{-1}); although the standard deviation is large, the difference is statistically significant ($p <$

Table 3.1: Rate constants for heme reduction. All units are s^{-1} unless specified otherwise. Values with an asterisk (*, k_{obs}) are under pseudo first order conditions for which NADPH is in excess. Reduction was monitored at 417 nm and 444 nm (in parentheses) for H422A. The globin heme, C539A and $syNOS_g$, was recorded at 413 nm, 426 nm, and 560 nm. NOS_g was reduced by 3 molar equivalents of $syNOS_{red}$ or $syNOS_{FAD}$.

	None	**+ L-arg**	**+ Ca^{2+}**	**+ L-arg/Ca^{2+}**
H422A	$4.7 \pm 0.9 \times 10^{-3}$ ($4.8 \pm 0.9 \times 10^{-3}$)	$13.4 \pm 3 \times 10^{-3}$ ($9.3 \pm 2.5 \times 10^{-3}$)	$4.8 \pm 1.6 \times 10^{-3}$ ($4.6 \pm 1.1 \times 10^{-3}$)	$13.1 \pm 3 \times 10^{-3}$ ($8.8 \pm 1.5 \times 10^{-3}$)
C539A	0.28 ± 0.06		$0.54 \pm 0.18 \times 10^{-3}$	
$syNOS_g$ + $syNOS_{red}$	$2.6 \pm 1.4 \times 10^{4}$ M^{-1} s^{-1} 0.16 ± 0.04*			
$syNOS_g$ + $syNOS_{FAD}$	0.112 ± 0.014*			

0.05). The rate constants for $syNOS_g$ reduction and NO dioxygenation, although rapid, are slow compared to other NOD enzymes (*E.coli* hmp 150 s^{-1} (32)). The relative sluggishness of $syNOS_g$ may reflect its role as an NO signalling on/off switch, rather than for dedicated nitrate production. The observed rate differences may also be a result of *in vitro* conditions, especially considering the low $syNOS_{ox}$ activity, however recombinant C539A and truncated $syNOS_g$ are far less unstable than $syNOS_{ox}$ and the H422A constructs. Although the rate of electron transfer to $syNOS_g$ is faster than to $syNOS_{ox}$, these rate constants were measured in the absence of the competing heme group, whose presence could influence the respective reactions. In addition, mNOS are required to dimerize for activity so that the NOS_{red} of one monomer reduces the NOS_{ox} of the other; although syNOS also dimerizes, it is very likely that subunits replete with heme (approximately ~30% of recombinant syNOS, see Chapter 2) may associate with heme-less monomers, which may also be a factor in its slow reduction.

3.3.3 $syNOS_{FAD}$ Directly Reduces $syNOS_g$

Observations in Chapter Two strongly suggest that reduction of $syNOS_g$ and $syNOS_{ox}$ occur independently, via direct electron transport from $syNOS_{red}$. The question remains which

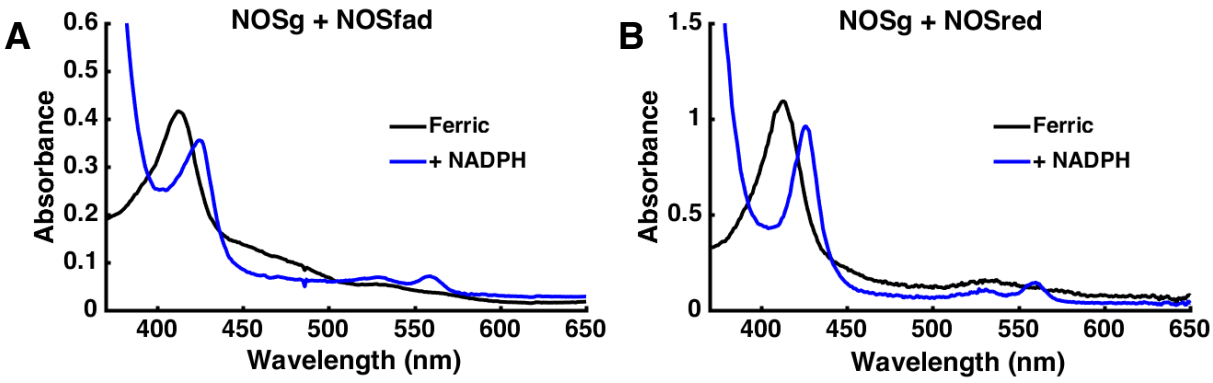

Figure 3.2 $syNOS_g$ reduction by A) three molar equivalents of $syNOS_{FAD}$ or B) three molar equivalents of $syNOS_{red}$.

flavoprotein domain of $syNOS_{red}$ reduces $syNOS_g$. In mNOSs the NOS_{FMN} contacts the NOS_{ox} domain, and only the FMN hydroquinone (-314 mV (33)) is sufficient to reduce NOS_{ox} (-263 to -248 mV (31). In traditional flavoHbs, reduction is mediated through a single FNR-like domain and both the FAD semiquinone and hydroquinone reduce the globin heme (25), so it is necessary to investigate if $syNOS_g$ reduction proceeds in a flavoHb-like or NOS-like pathway. The acting flavin was investigated by comparing the reduction of $syNOS_g$ by $syNOS_{red}$ to that with $syNOS_{FAD}$. Not only is $syNOS_{red}$ capable of rapid $syNOS_g$ reduction, $syNOS_{FAD}$ also reduces $syNOS_g$. The pseudo first-order reduction rate constant is the same under both conditions (Table 3.1), which strongly indicates $syNOS_g$ is reduced directly by $syNOS_{FAD}$ and not $syNOS_{FMN}$.

3.3.4 Crystal Structures of $syNOS_{FMN}$ and $syNOS_{FAD}$

The full-length crystal structure of syNOS would be invaluable to the investigation of calcium binding and $syNOS_g$ – $syNOS_{FAD}$ interactions. Although the structure of full-length mNOS has evaded characterization for decades, we have attempted to grow crystals of the full-length syNOS. This was unsuccessful and only yielded small, non-crystalline protein aggregates (Fig 3.S1). Many structures of mammalian and bacterial NOS_{ox} have been determined, however $syNOS_{ox}$ also resists crystallization. $syNOS_g$ also has not yet been crystallized, and instead forms small aggregates similar to the full-length.

Initial attempts to crystallize the full reductase domain yielded no crystals until two months after constructing the screen. A small cluster of needles was observed, and after optimization thick, needle-like crystals radiating from a central point were grown (Fig. 3.S2A). X-ray diffraction of this crystal was collected at the Cornell High Energy Synchrotron

Source (CHESS) line F1 with the Quantum 270 CCD detector. However, after indexing and scaling with HKL2000, and phasing and refining with Phenix, the crystals were found to include only the $syNOS_{FMN}$ domain (Fig. 3.S3B) produced by degradation of the full domain while in the crystallization drop. The smaller domain was expressed, purified & screened, and found to crystallize within days, forming small clusters of thin needles (Fig. 3.S2C). Clearly the slow degradation was a boon to $syNOS_{FMN}$ crystal formation. The final structure was determined using molecular replacement with the iNOS FMN domain (PDB ID:3HR4), and encompasses residues 860 -1005, at a final resolution of 1.84 Å. The FMN cofactor is well

Table 3.2: X-ray diffraction data collection and refinement statistics

	$syNOS_{FMN}$	$syNOS_{FAD}$
Space group	$P2_12_12_1$	$P12_11$
a, b, c (Å)	39.13, 55.18, 56.94	72.88, 63.02, 102.68
α, β, γ (°)	α = β = γ = 90.00	90.00, 93.86, 90.00
Resolution Range (Å)	1.85 – 50.00	1.85-102.44
Total observations	156897	577563
Unique Reflections		78776
Completeness (%)		99.4
<I/σ(I)>		11.9
Rmerge	0.072	0.154
Refinement Statistics		
Resolution Range (Å)	1.84 – 39.6	1.70 – 47.6
Number of reflections	11066	91824
Rwork	0.1804	0.1959
Rfree	0.2217	0.2326
Ramachandran outliers (%)	0.0	0.40
Ramachandran favored (%)	98.6	98.54
Rms bond length (Å)	0.008	0.0167
Rms bond angle (°)	1.08	1.152
Rotamer outliers (%)	0.8	1.57

defined in the electron density.

The syNOS$_{FAD}$ domain was also crystallized, and appeared as very thin plates radiating from a central point (Fig. 3.S3A). After further optimization, much wider, thin plates were formed (Fig. 3.S3B). X-ray diffraction was collected using the Northeastern

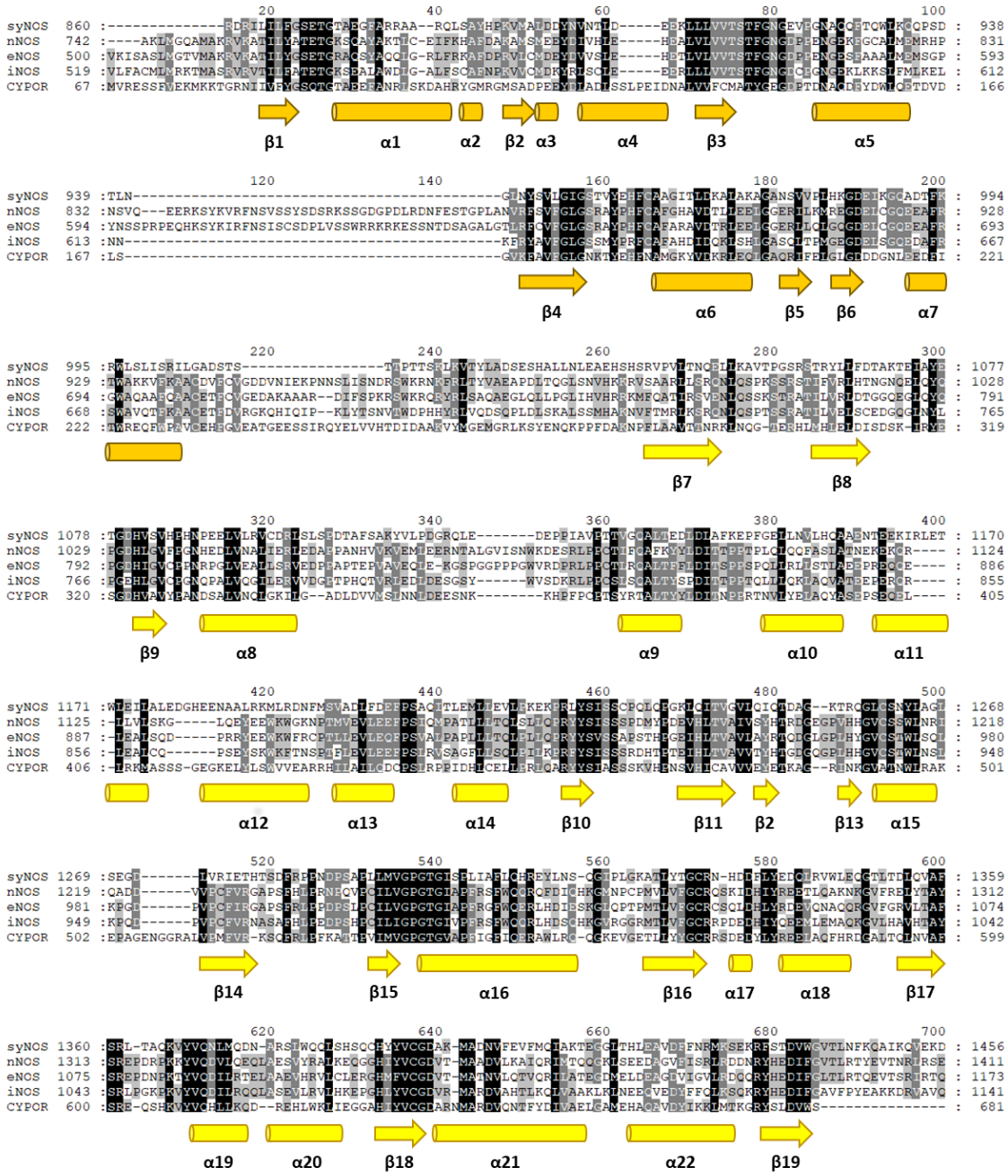

Figure 3.3: Alignment of syNOS$_{FMN}$ and syNOS$_{FAD}$ sequences to mNOS$_{red}$ and CYPOR.

Collaborative Access Team (NE-CAT) facility at the Advanced Photon Source with an ADSC Quantum 315 CCD detector. The structure was determined using molecular replacement with the $nNOS_{FAD}$ structure (PDB ID: 1TLL), and includes residues 1041 to 1447, at 1.7 Å resolution. There was significant flavin density, but no NADPH density; this was not unexpected as no NADPH was added to the crystallization condition.

The $syNOS_{FAD}$ and $syNOS_{FMN}$ structures were determined independently and to position them relative to one another they were aligned using the structure of $nNOS_{red}$ from *Rattus norvegicus* (1TLL) (Fig. 3.4). The $syNOS_{FMN}$ structure agrees well with the $nNOS_{FMN}$ of 1TLL, with 1.18 Å RMSD (Fig. 3.5A). The FAD and NADPH binding domains of $syNOS_{FAD}$ align well with 1TLL, RMSD 1.57 Å (Fig, 3.5B), however helices in the $syNOS_{FAD}$ connecting domain are significantly displaced (Fig. 3.5C), either by translation or rotation of helices 8-14 relative to mNOS, with RMSD 3.59 Å. The $syNOS_{FAD}$ structure

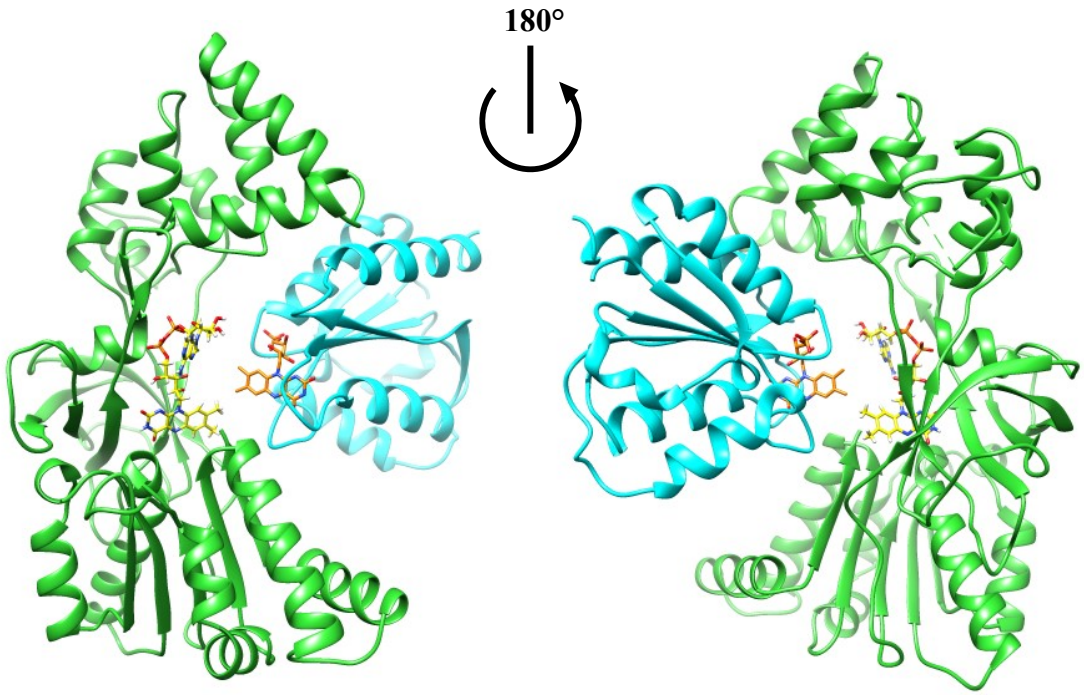

Figure 3.4: Structure of $syNOS_{FMN}$ (blue) and $syNOS_{FAD}$ (green) docked using 1TLL

begins at residue 1041, and is missing about 30 residues of the hinge region between syNOS FMN and FAD domains. The corresponding area in 1TLL forms a three-strand beta-sheet with the beta finger containing the CD2A regulatory element, residues 1059-1076. In syNOS

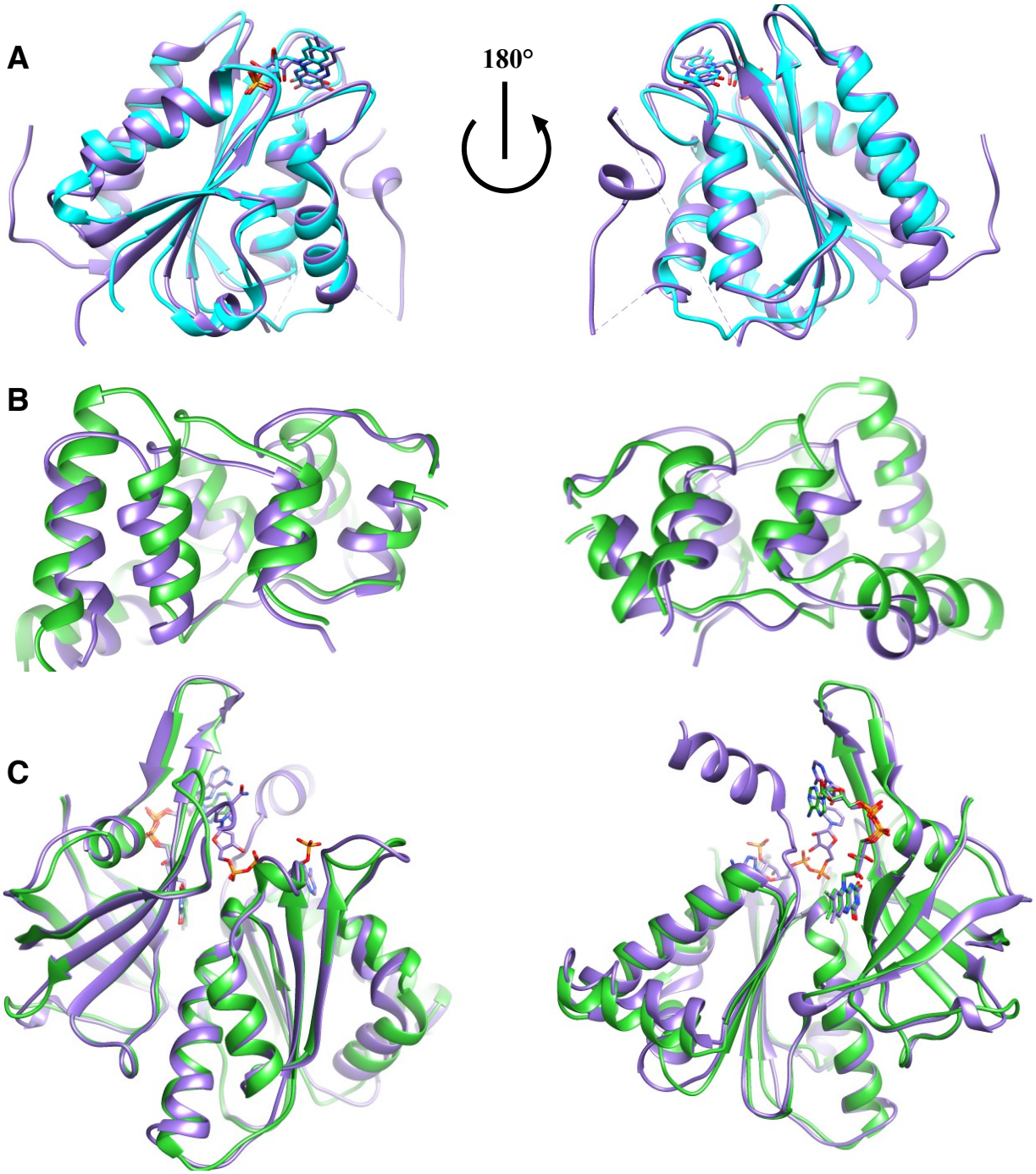

Figure 3.5: Structures of $syNOS_{FMN}$ (blue) and $syNOS_{FAD}$ (green) aligned to $nNOS_{red}$ (purple, PDB ID:1TLL)

this region could not be built into any density. When comparing 1TLL to the $nNOS_{FAD}$ domain crystalized alone (1F20), the helices in the connecting domain are also displaced. The FMN domain of nNOS and syNOS may form contacts that restricts the motion of the beta finger and alter the tertiary structure of the connecting domain. The $syNOS_{FAD}$ domain structure ends at residue 1440, 26 residues short of the C-terminus; this is the C-terminal tail in 1TLL and represses electron transfer. Perhaps the absence of $syNOS_{FMN}$ allowed more movement of this helix. The structure of the isolated $nNOS_{FAD}$ domain (1F20) also lacks density for the C-terminal tail, more evidence that the FMN domain may form contacts that restrict C-terminal tail movement in the crystal structure.

The conformations of the flavin cofactors are mostly the same between 1TLL and syNOS. The syNOS FMN isoalloxazine ring is slightly displaced compared to $nNOS_{red}$ but the di-phosphate moiety is in the same position as 1TLL. The FAD isoalloxazine ring and phosphate backbone are in the same position, however the adenine ring is displaced by Ile1249. This residue is Tyr1197 in 1TLL, and is positioned to form pi-stacking interactions with the adenine of FAD. This tyrosine is conserved in mNOS, whereas the isoleucine is conserved in syNOS homologues. The FMN isoalloxazine ring is flanked by Tyr955 and Phe958, consistent with mammalian NOS. However, the FAD-shielding residue Phe1395 in nNOS is Trp1440 in syNOS. This residue regulates reduction by NADPH and must rotate away from the isoalloxazine of FAD before it can be reduced.

One roadblock in studying the full $syNOS_{red}$ domain is its tendency to spontaneously degrade, which has also been documented for the mammalian isoforms (34). When $syNOS_{red}$ is purified there is no obvious contaminating bands that could be a protease, yet it is consistently cleaved in a matter of weeks to months, the rate being affected by crystallization

condition. One mechanism by which proteins may spontaneously degrade is through aspartate and asparagine side chain nucleophilic attack on the peptide backbone carbonyl (35, 36). This forms a succinimide intermediate and can result in either isomerization or peptide bond cleavage. The kinetics of this are on the order of days and depend on the residue immediately following said Asp or Asn, for example DG > DS > DA and NG > NS > NA > NL (35). There are three possible locations for degradation to occur in the linker between $syNOS_{FMN}$ and $syNOS_{FAD}$; D1007 is followed by serine, D1025 followed by serine, and N1033 followed by leucine. The corresponding positions for D1007 and N1033 in nNOS are both found in alpha helices, while D1025 is random coil. This D1025 is the most promising site for peptide bond cleavage, however the syNOS linker region could not be built into any density and is significantly shorter than the mammalian, so its structure may differ.

3.3.4 Homology modeling $syNOS_g$ - $syNOS_{FAD}$ interactions

The crystal structure of $syNOS_{FMN}$ and $syNOS_{FAD}$ are invaluable not only because they are the first bacterial NOS_{red} structures, but they may also yield information concerning possible $syNOS_{FAD}$ and $syNOS_g$ interactions. To explore this, a homology model of $syNOS_g$ (residues 337-464) was built using SWISS-MODEL and Hell's Gate globin I (PDB ID: 3S1I, 31% identity) for the template. $syNOS_g$ and $syNOS_{FAD}$ were oriented relative to each other using the structure of *E. coli* hmp (PDB ID:1GVH) (Fig. 3.6A), as Hell's Gate globin I does not have an FAD-binding domain; $syNOS_{FAD}$ deviates from hmp by 8.87 Å and syNOSg deviates by 5.2 Å (Fig. 3.6). The $syNOS_{FAD}$ connecting domain does not overlap with the docked $syNOS_g$, but there are severe clashes in a few areas (Fig. 3.6B). The major clash between the peptide backbone of $syNOS_g$ and $syNOS_{FAD}$ is between α14 and β10. Although

these clashes are identified in the docked model, it is likely that they may not exist in the actual structure. The $syNOS_{FAD}$ domain has fewer and less severe backbone and sidechain clashes than $nNOS_{red}$ when it is aligned to flavohemoglobin. This is because the $syNOS_{FAD}$ connecting domain is significantly displaced compared to $nNOS_{red}$. Overall, this model of the

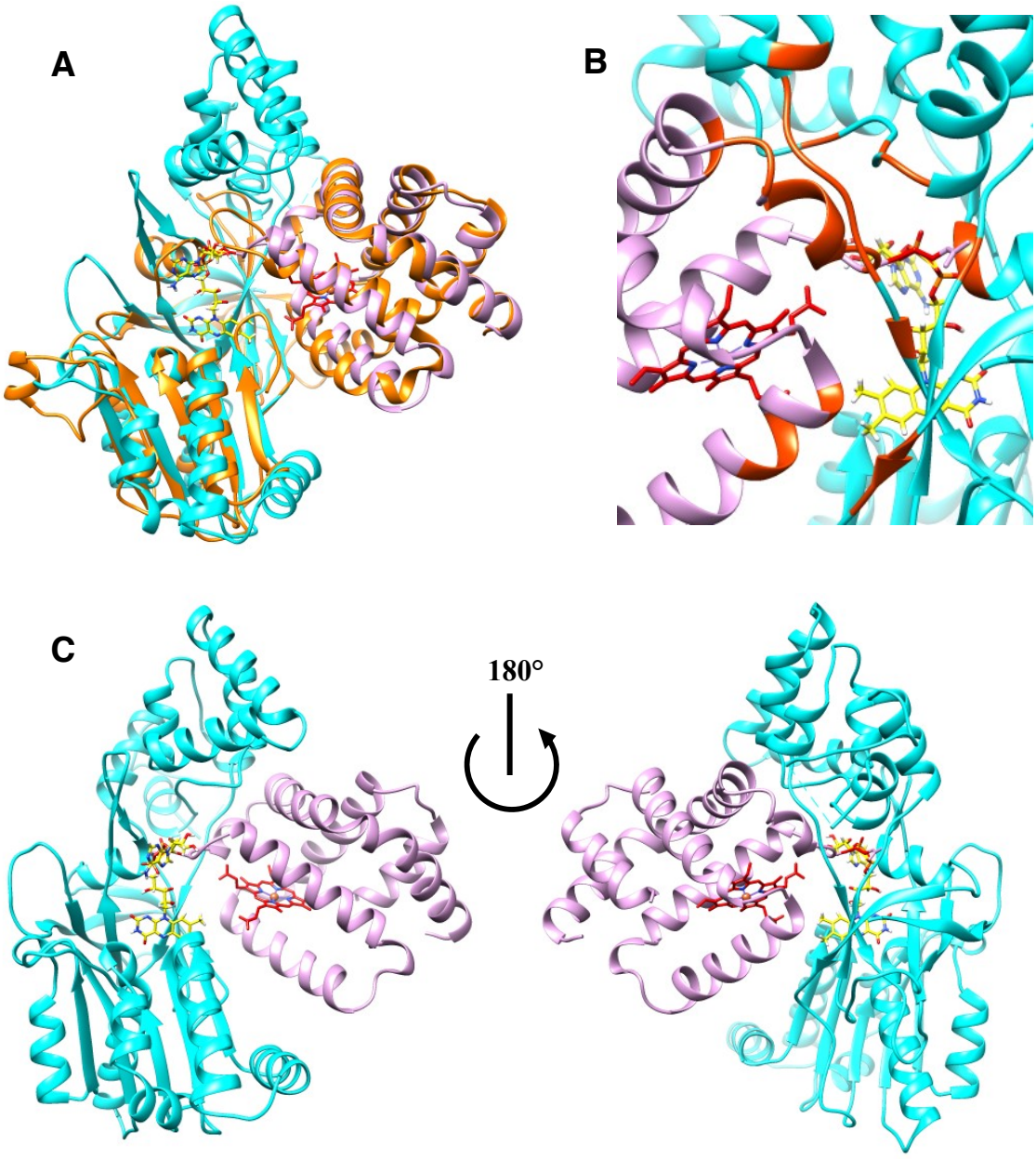

Figure 3.6: $syNOS_g$ docked to $syNOS_{FAD}$. A) Homology model of $syNOS_g$ (pink) docked with $syNOS_{FAD}$ (blue) by alignment to 1GVH (orange). B) clashes (orange) between $syNOS_g$ and $syNOS_{FAD}$. C) $syNOS_g$ docked to $syNOS_{FAD}$

$syNOS_{FAD}$ and $syNOS_g$ interface is consistent with an FAD to heme ET mechanism.

3.4 Discussion

Diflavin reductases have evolved from fusing FMN-containing flavodoxins and FAD-containing FNR modules, which have separate evolutionary pathways (37). These reductases are widespread and participate in many diverse enzymatic systems; in particular, cytochrome P450 oxidoreductase (CYPOR), sulfite reductase, methionine synthase reductase (MSR), and $mNOS_{red}$ have been thoroughly investigated and numerous full and partial structures have been obtained. Although the structure of $mNOS_{red}$ is similar to other diflavin reductases, it has a number of structural features which tightly regulate electron transfer that are absent from the other reductases. Upon Ca^{2+}-CaM binding to mNOS, inter-flavin electron transfer is accelerated by alleviating inhibition by the C-terminal tail (38), and the displacement of the autoinhibitory loop (39) "unlocks" $mNOS_{FMN}$ from $mNOS_{FAD,}$ transitioning from a "closed" to an "open" conformation. This conformational switching is common in diflavin reductases, where the closed conformation allows for inter-flavin electron transfer, and the open conformation reduces its target protein (40, 41), however the FMN and FAD modules are not "locked" into the closed position as in mNOS. $syNOS_{ox}$ reduction is expected to proceed in the same manner, with $syNOS_{FMN}$ transitioning from the closed to open conformation, but it is not expected to be locked in the closed conformation as it is missing the structural elements to do so.

In FNR-like proteins, a large aromatic residue is positioned to pi-stack with the FAD isoalloxazine ring, the identity of which affects the affinity and specificity for NADPH (42) and the efficiency of $NADP^+$ release (43, 44). The conformation of this residue must be

rotated to allow for the nicotinamide moiety to allow ET. In syNOS and CYPOR this residue is a tryptophan while in mNOS and flavoHb it is a phenylalanine. Single mutations of nNOS Phe1395 found that it was essential for repressing electron transfer from NADPH to the flavins in the absence of Ca^{2+}-CaM (44, 45). The polarity of the residue at this position may stabilize the FAD semiquinone or affect the alignment of FAD to FMN (44, 45), both of which affect interflavin electron transfer. Mutations to the tryptophan of MSR found increased inter-flavin reduction rates and decreased amounts of disemiquinone formation (46, 47). The identity of this FAD-stacking residue may factor into why the syNOS disemiquinone is difficult to isolate; in addition to the absence of regulatory elements, this may accelerate inter-flavin ET.

$syNOS_{FAD}$ is capable of rapid $syNOS_g$ reduction, but the conformation and structure of this interaction is unknown. There is limited information about NOS-globin electron transfer; *in vitro* $eNOS_{red}$ is reported to reduce α globin faster than its native reductant, the cytochrome B5/cytochrome B5 reductase system (CB5/CB5red) (22). However, the details of electron transfer between $eNOS_{red}$ and α-globin have not been investigated. A better model is flavoHb; although sequence similarity with $syNOS_g$ is very low (18% identical, Fig. 3.S4) this system is well studied structurally and biochemically. During globin reduction, no large structural movement is necessary in flavoHb as the FNR and globin remain associated (48). Highly conserved areas between $syNOS_{FAD}$ and flavoHbs are mostly in the FAD and NADPH binding sequences, β16, β18, β19, & α16, but overall $syNOS_{FAD}$ is more similar to $mNOS_{FAD}$ than flavoHb. It is possible that structural features specific to NOS_{red}, in particular the NOS_{FAD} connecting domain, could occlude $syNOS_g$ interactions modeled on flavoHb. However, the crystal structure of $syNOS_g$ has yet to be determined, and instead a homology model was

used to mimic $syNOS_{FAD}$ – $syNOS_g$ interactions. Although $syNOS_g$ shares significant similarity to the template used, Hell's Gate globin I, no functional information can be gathered from this protein. This globin is found in the acidophilic, thermophilic methanotroph *Methylacidiphilum infernorum*, and is a subject of interest as it is remarkably stable and able to bind heme under the extreme conditions where this organism thrives, but its function is currently unknown (49, 50). The $syNOS_g$ model was docked to $syNOS_{FAD}$ using the *E. coli* flavoHb structure (1GVH), because Hell's Gate globin I does not have a flavin domain. It is remarkable that the docked $syNOS_{FAD}$ and $syNOS_g$ structures do not clash severely. In fact, $nNOS_{red}$ has more backbone clashes than $syNOS_{FAD}$, and some sequence and structural variations may be a consequence of the $syNOS_{FAD}$ – $syNOS_g$ interaction. For example, $syNOS_{FAD}$ has low similarity to the beta finger of nNOS, residues 976-996. When the structure of 1TLL is aligned to 1GVH, residues 987-990 clash with the $syNOS_g$ homology model. The lack of sequence similarity in this region of syNOS could reflect a steric accommodation for $syNOS_g$ or an interaction region, however this region has no density in the $syNOS_{FAD}$ structure. The clashes between α14 and β10 of $syNOS_{FAD}$ also contain residues not conserved in other $mNOS_{red}$. In particular, a charged residue (Glu1222) replaces the leucine found in mNOS and CYPOR. These and other clashing residues (K1145, D1139, and residues 1278-1280) that are not conserved with mNOS are actually conserved in other syNOS-like proteins. These proteins can be found in cyanobacteria, *Spirosoma*, and the Proteobacteria phylum, and all contain an N-terminal NOS_g and C-terminal NOS_{red}. The observation that these clashes are conserved in other NOS_g-containing NOS is consistent with the possibility that deviations between $syNOS_{FAD}$ and $mNOS_{FAD}$ may be a consequence of $syNOS_{FAD}$ interaction with $syNOS_g$.

The exact biochemical function of Ca^{2+} remains unclear, as it is an obligate factor for NO production by $syNOS_{ox}$ (21), however it does not accelerate $syNOS_{ox}$ reduction. rather it increases the rate of $syNOS_g$ reduction. The Michaelis constant for Ca^{2+} was measured to be higher than physiological concentrations, and it was proposed that it may be substituting for some other unknown factor (21). In addition, for both the $syNOS_{FMN}$ – $syNOS_{FAD}$ and the $syNOS_{FAD}$ – $syNOS_g$ models no calcium binding site can be explicitly identified. However, one of the proteins identified in the aforementioned sequence search contains an interesting insert in the NOS_g domain. A yet unnamed *Microcoleus* species contains a NOS sequence with a Ca^{2+} binding EF-hand sequence inserted a few residues prior to the heme ligating proximal histidine of other NOS_g. Additionally, in *Microcoleus* NOS this histidine is a valine and is unlikely to bind heme, but it is not clear what purpose this may serve. The identification of *Microcoleus* NOS and the observations that Ca^{2+} is required for NO production but also acceleration of $syNOS_g$ reduction confirms that the role of Ca^{2+} in NOS enzymology is nuanced and likely intimately tied to the biological function of syNOS-like proteins. The results presented herein will be invaluable to initiate the study of $syNOS_{FAD}$ – $syNOS_g$ interactions and what governs the preferential reduction of $syNOS_g$ versus $syNOS_{ox}$.

3.5 References

1. Palmer, R. M. J., and Moncada, S. (1989) A novel citrulline-forming enzyme implicated in the formation of nitric oxide by vascular endothelial cells. *Biochem. Biophys. Res. Commun.* 158, 348–352
2. MacMicking, J., Xie, Q.-W., and Nathan, C. (2002) NITRIC OXIDE AND MACROPHAGE FUNCTION. *Annu. Rev. Immunol.* 15, 323–350
3. Bredt, D. S., and Snyder, S. H. (1990) Isolation of nitric oxide synthetase, a calmodulin-requiring enzyme. *Proc. Natl. Acad. Sci. U. S. A.* 87, 682–685
4. White, K. a, and Marletta, M. a (1992) Nitric oxide synthase is a cytochrome P-450 type hemoprotein. *Biochemistry*. 31, 6627–6631
5. Iyanagi, T., Xia, C., and Kim, J. J. P. (2012) NADPH-cytochrome P450 oxidoreductase: Prototypic member of the diflavin reductase family. *Arch. Biochem. Biophys.* 528, 72–89
6. Garcin, E. D., Bruns, C. M., Lloyd, S. J., Hosfield, D. J., Tiso, M., Gachhui, R., Stuehr, D. J., Tainer, J. a., and Getzoff, E. D. (2004) Structural basis for isozyme-specific regulation of electron transfer in nitric-oxide synthase. *J. Biol. Chem.* 279, 37918–37927
7. Crane, B. R., Arvai, a S., Ghosh, D. K., Wu, C., Getzoff, E. D., Stuehr, D. J., and Tainer, J. a (1998) Structure of nitric oxide synthase oxygenase dimer with pterin and substrate. *Science*. 279, 2121–2126
8. Crane, B. R., Arvai, A. S., Gachhui, R., Wu, C., Ghosh, D. K., Getzoff, E. D., Stuehr, D. J., and Tainer, J. A. (1997) The structure of nitric oxide synthase oxygenase domain and inhibitor complexes. *Science (80-.).* 278, 425–431
9. Campbell, M. G., Smith, B. C., Potter, C. S., Carragher, B., and Marletta, M. a (2014) Molecular architecture of mammalian nitric oxide synthases. *Proc. Natl. Acad. Sci. U. S. A.* 10.1073/pnas.1413763111
10. Yokom, A. L., Morishima, Y., Lau, M., Su, M., Glukhova, A., Osawa, Y., and Southworth, D. R. (2014) Architecture of the nitric-oxide synthase holoenzyme reveals large conformational changes and a calmodulin-driven release of the FMN domain. *J. Biol. Chem.* 289, 16855–16865
11. Volkmann, N., Martásek, P., Roman, L. J., Xu, X. P., Page, C., Swift, M., Hanein, D., and Masters, B. S. (2014) Holoenzyme structures of endothelial nitric oxide synthase - An allosteric role for calmodulin in pivoting the FMN domain for electron transfer. *J. Struct. Biol.* 188, 46–54
12. Persechini, A., Tran, Q. K., Black, D. J., and Gogol, E. P. (2013) Calmodulin-induced structural changes in endothelial nitric oxide synthase. *FEBS Lett.* 587, 297–301
13. Gusarov, I., and Nudler, E. (2005) NO-mediated cytoprotection: instant adaptation to oxidative stress in bacteria. *Proc. Natl. Acad. Sci. U. S. A.* 102, 13855–13860
14. Patel, B. a, Moreau, M., Widom, J., Chen, H., Yin, L., Hua, Y., and Crane, B. R. (2009) Endogenous nitric oxide regulates the recovery of the radiation-resistant bacterium Deinococcus radiodurans from exposure to UV light. *Proc. Natl. Acad. Sci. U. S. A.* 106, 18183–8
15. Kinkel, T. L., Ramos-Montañez, S., Pando, J. M., Tadeo, D. V., Strom, E. N., Libby, S. J., and Fang, F. C. (2016) An essential role for bacterial nitric oxide synthase in

Staphylococcus aureus electron transfer and colonization. *Nat. Microbiol.* 2, 1–7
16. Wang, Z.-Q., Lawson, R. J., Buddha, M. R., Wei, C.-C., Crane, B. R., Munro, A. W., and Stuehr, D. J. (2007) Bacterial flavodoxins support nitric oxide production by Bacillus subtilis nitric-oxide synthase. *J. Biol. Chem.* 282, 2196–2202
17. Holden, J. K., Lim, N., and Poulos, T. L. (2014) Identification of redox partners and development of a novel chimeric bacterial nitric oxide synthase for structure activity analyses. *J. Biol. Chem.* 289, 29437–29445
18. Gusarov, I., Starodubtseva, M., Wang, Z. Q., McQuade, L., Lippard, S. J., Stuehr, D. J., and Nudler, E. (2008) Bacterial nitric-oxide synthases operate without a dedicated redox partner. *J. Biol. Chem.* 283, 13140–13147
19. Agapie, T., Suseno, S., Woodward, J. J., Stoll, S., Britt, R. D., and Marletta, M. a (2009) NO formation by a catalytically self-sufficient bacterial nitric oxide synthase from Sorangium cellulosum. *Proc. Natl. Acad. Sci. U. S. A.* 106, 16221–16226
20. Correa-Aragunde, N., Foresi, N., Del Castello, F., and Lamattina, L. (2018) A singular nitric oxide synthase with a globin domain found in Synechococcus PCC 7335 mobilizes N from arginine to nitrate. *Sci. Rep.* 8, 12505
21. Picciano, A. L., and Crane, B. R. (2019) A nitric oxide synthase-like protein from Synechococcus produces NO/NO 3 - from L-arginine and NAPDH in a tetrahydrobiopterin- and Ca 2+ -dependent manner . *J. Biol. Chem.* 294, jbc.RA119.008399
22. Lechauve, C., Butcher, J. T., Freiwan, A., Biwer, L. A., Keith, J. M., Good, M. E., Ackerman, H., Tillman, H. S., Kiger, L., Isakson, B. E., and Weiss, M. J. (2018) Endothelial cell α-globin and its molecular chaperone α-hemoglobin-stabilizing protein regulate arteriolar contractility. *J. Clin. Invest.* 128, 5073–5082
23. Straub, A. C., Lohman, A. W., Billaud, M., Johnstone, S. R., Dwyer, S. T., Lee, M. Y., Bortz, P. S., Best, A. K., Columbus, L., Gaston, B., and Isakson, B. E. (2012) Endothelial cell expression of haemoglobin α regulates nitric oxide signalling. *Nature*. 491, 473–477
24. Kuma, F. (1981) Properties of methemoglobin reductase and kinetic study of methemoglobin reduction. *J. Biol. Chem.* 256, 5518–5523
25. Gardner, P. R., Gardner, A. M., Martin, L. a., and Salzman, A. L. (1998) Nitric oxide dioxygenase: an enzymic function for flavohemoglobin. *Proc. Natl. Acad. Sci. U. S. A.* 95, 10378–10383
26. Sobolewska-Stawiarz, A., Leferink, N. G. H., Fisher, K., Heyes, D. J., Hay, S., Rigby, S. E. J., and Scrutton, N. S. (2014) Energy landscapes and catalysis in nitric-oxide synthase. *J. Biol. Chem.* 289, 11725–11738
27. Guan, Z. W., Kamatani, D., Kimura, S., and Iyanagi, T. (2003) Mechanistic studies on the intramolecular one-electron transfer between the two flavins in the human neuronal nitric-oxide synthase and inducible nitric-oxide synthase flavin domains. *J. Biol. Chem.* 278, 30859–30868
28. Sabat, J., Stuehr, D. J., Yeh, S. R., and Rousseau, D. L. (2009) Characterization of the proximal ligand in the P420 form of inducible nitric oxide synthase. *J. Am. Chem. Soc.* 131, 12186–12192
29. Huang, L., Abu-Soud, H. M., Hille, R., and Stuehr, D. J. (1999) Nitric oxide-generated P420 nitric oxide synthase: Characterization and roles for tetrahydrobiopterin and substrate in protecting against or reversing the P420 conversion. *Biochemistry*. 38,

1912–1920
30. Abu-Soud, H. M., Ichimori, K., Presta, A., and Stuehr, D. J. (2000) Electron transfer, oxygen binding, and nitric oxide feedback inhibition in endothelial nitric-oxide synthase. *J. Biol. Chem.* 275, 17349–17357
31. Presta, A., Weber-Main, A. M., Stankovich, M. T., and Stuehr, D. J. (1998) Comparative effects of substrates and pterin cofactor on the heme midpoint potential in inducible and neuronal nitric oxide synthases. *J. Am. Chem. Soc.* 120, 9460–9465
32. Gardner, A. M., Martin, L. A., Gardner, P. R., Dou, Y., and Olson, J. S. (2000) Steady-state and transient kinetics of Escherichia coli nitric-oxide dioxygenase (flavohemoglobin). The B10 tyrosine hydroxyl is essential for dioxygen binding and catalysis. *J. Biol. Chem.* 275, 12581–12589
33. Garnaud, P. E., Koetsier, M., Ost, T. W. B., and Daff, S. (2004) Redox properties of the isolated flavin mononucleotide- and flavin adenine dinucleotide-binding domains of neuronal nitric oxide synthase. *Biochemistry*. 43, 11035–11044
34. Zhang, J., Martàsek, P., Paschke, R., Shea, T., Siler Masters, B. S., and Kim, J.-J. P. (2001) Crystal Structure of the FAD/NADPH-binding Domain of Rat Neuronal Nitric-oxide Synthase. *J. Biol. Chem.* 276, 37506–37513
35. BRENNAN, T. V., and CLARKE, S. (1995) Effect of adjacent histidine and cysteine residues on the spontaneous degradation of asparaginyl- and aspartyl-containing peptides. *Int. J. Pept. Protein Res.* 45, 547–553
36. Stephenson, R. C., and Clarke, S. (1989) Succinimide formation from aspartyl and asparaginyl peptides as a model for the spontaneous degradation of proteins. *J. Biol. Chem.* 264, 6164–6170
37. Porter, T. D., and Kasper, C. B. (1986) NADPH-cytochrome p-450 oxidoreductase: Flavin mononucleotide and flavin adenine dinucleotide domains evolved from different flavoproteins. *Biochemistry*. 25, 1682–1687
38. Roman, L. J., Martásek, P., Miller, R. T., Harris, D. E., De La Garza, M. A., Shea, T. M., Kim, J. J. P., and Masters, B. S. S. (2000) The C termini of constitutive nitric-oxide synthases control electron flow through the flavin and heme domains and affect modulation by calmodulin. *J. Biol. Chem.* 275, 29225–29232
39. Salerno, J. C., Harris, D. E., Irizarry, K., Patelf, B., Morales, A. J., Smith, S. M. E., Martasek, P., Roman, L. J., Masters, B. S. S., Jones, C. L., Weissman, B. A., Lane, P., Liu, Q., and Gross, S. S. (1997) An autoinhibitory control element defines calcium-regulated isoforms of nitric oxide synthase. *J. Biol. Chem.* 272, 29769–29777
40. Huang, W. C., Ellis, J., Moody, P. C. E., Raven, E. L., and Roberts, G. C. K. (2013) Redox-linked domain movements in the catalytic cycle of cytochrome P450 reductase. *Structure*. 21, 1581–1589
41. Murataliev, M. B., Feyereisen, R., and Walker, F. A. (2004) Electron transfer by diflavin reductases. *Biochim. Biophys. Acta - Proteins Proteomics*. 1698, 1–26
42. Dohr, O., Paine, M. J. I., Friedberg, T., Roberts, G. C. K., and Wolf, C. R. (2001) Engineering of a functional human NADH-dependent cytochrome P450 system. *Proc. Natl. Acad. Sci.* 98, 81–86
43. Gutierrez, A., Doehr, O., Paine, M., Wolf, C. R., Scrutton, N. S., and Roberts, G. C. K. (2000) Trp-676 facilitates nicotinamide coenzyme exchange in the reductive half-reaction of human cytochrome P450 reductase: Properties of the soluble W676H and W676A mutant reductases. *Biochemistry*. 39, 15990–15999

44. Konas, D. W., Zhu, K., Sharma, M., Aulak, K. S., Brudvig, G. W., and Stuehr, D. J. (2004) The FAD-shielding residue Phe1395 regulates neuronal nitric-oxide synthase catalysis by controlling NADP+ affinity and a conformational equilibrium within the flavoprotein domain. *J. Biol. Chem.* 279, 35412–35425
45. Adak, S., Sharma, M., Meade, A. L., and Stuehr, D. J. (2002) A conserved flavin-shielding residue regulates NO synthase electron transfer and nicotinamide coenzyme specificity. *Proc. Natl. Acad. Sci. U. S. A.* 99, 13516–13521
46. Meints, C. E., Gustafsson, F. S., Scrutton, N. S., and Wolthers, K. R. (2011) Tryptophan 697 modulates hydride and interflavin electron transfer in human methionine synthase reductase. *Biochemistry*. 50, 11131–11142
47. Meints, C. E., Simtchouk, S., and Wolthers, K. R. (2013) Aromatic substitution of the FAD-shielding tryptophan reveals its differential role in regulating electron flux in methionine synthase reductase and cytochrome P450 reductase. *FEBS J.* 280, 1460–1474
48. Gardner, P. R. (2005) Nitric oxide dioxygenase function and mechanism of flavohemoglobin, hemoglobin, myoglobin and their associated reductases. *J. Inorg. Biochem.* 99, 247–266
49. Teh, A. H., Saito, J. a., Baharuddin, A., Tuckerman, J. R., Newhouse, J. S., Kanbe, M., Newhouse, E. I., Rahim, R. A., Favier, F., Didierjean, C., Sousa, E. H. S., Stott, M. B., Dunfield, P. F., Gonzalez, G., Gilles-Gonzalez, M. A., Najimudin, N., and Alam, M. (2011) Hell's Gate globin I: An acid and thermostable bacterial hemoglobin resembling mammalian neuroglobin. *FEBS Lett.* 585, 3250–3258
50. Dunfield, P. F., Yuryev, A., Senin, P., Smirnova, A. V, Stott, M. B., Hou, S., Ly, B., Saw, J. H., Zhou, Z., Ren, Y., Wang, J., Mountain, B. W., Crowe, M. A., Weatherby, T. M., Bodelier, P. L. E., Liesack, W., Feng, L., Wang, L., and Alam, M. (2007) Methane oxidation by an extremely acidophilic bacterium of the phylum Verrucomicrobia. *Nature*. 450, 879–882

3.6 Supplemental information

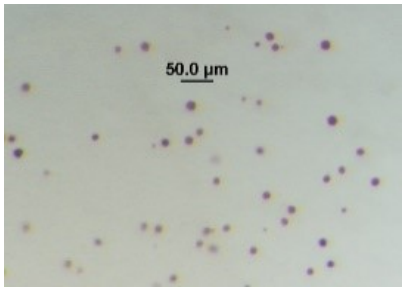

Figure 3.S1: Aggregates of full-length syNOS at 20 mg/mL, pH 6.0, 200 mM MPD, 200 mM $MgCl_2$

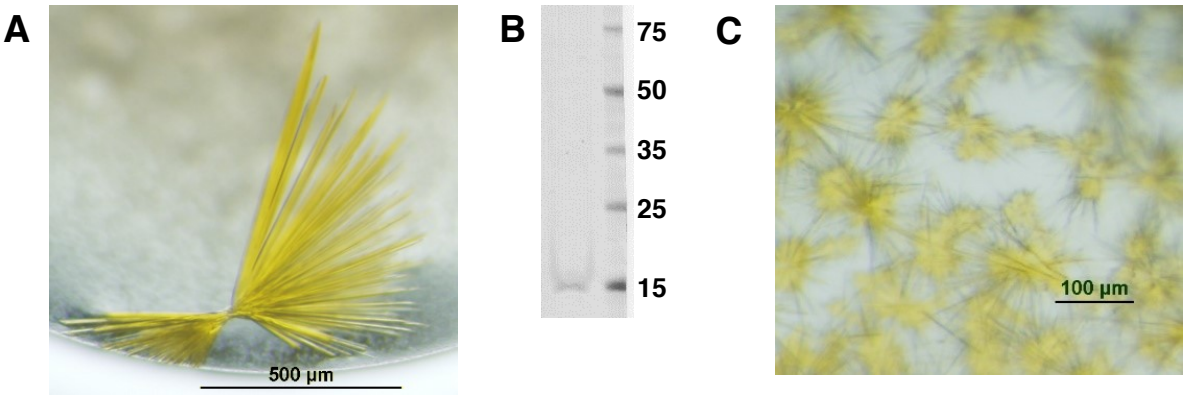

Figure 3.S2: A) Crystals of $syNOS_{FMN}$ four months after setup, containing $syNOS_{red}$ at 20 mg/mL, pH 7.5, 32% PEG 1500, and stored at 17 °C. B) gel of A. C) 11-4-15 Wizard 4 #19 10 mg/mL $syNOS_{FMN}$ domain

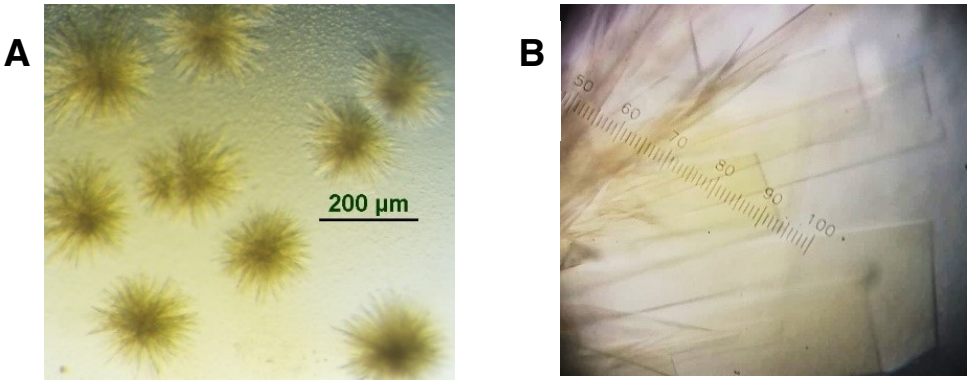

Figure 3.S3: Crystals of $syNOS_{FAD}$ in A) 3-25-16 Core 1#63 B) 8-31-16 optimization of $syNOS_{FAD}$

Figure 3.S4: Alignment of syNOS$_{FAD}$ to flavoHb in the PDB.

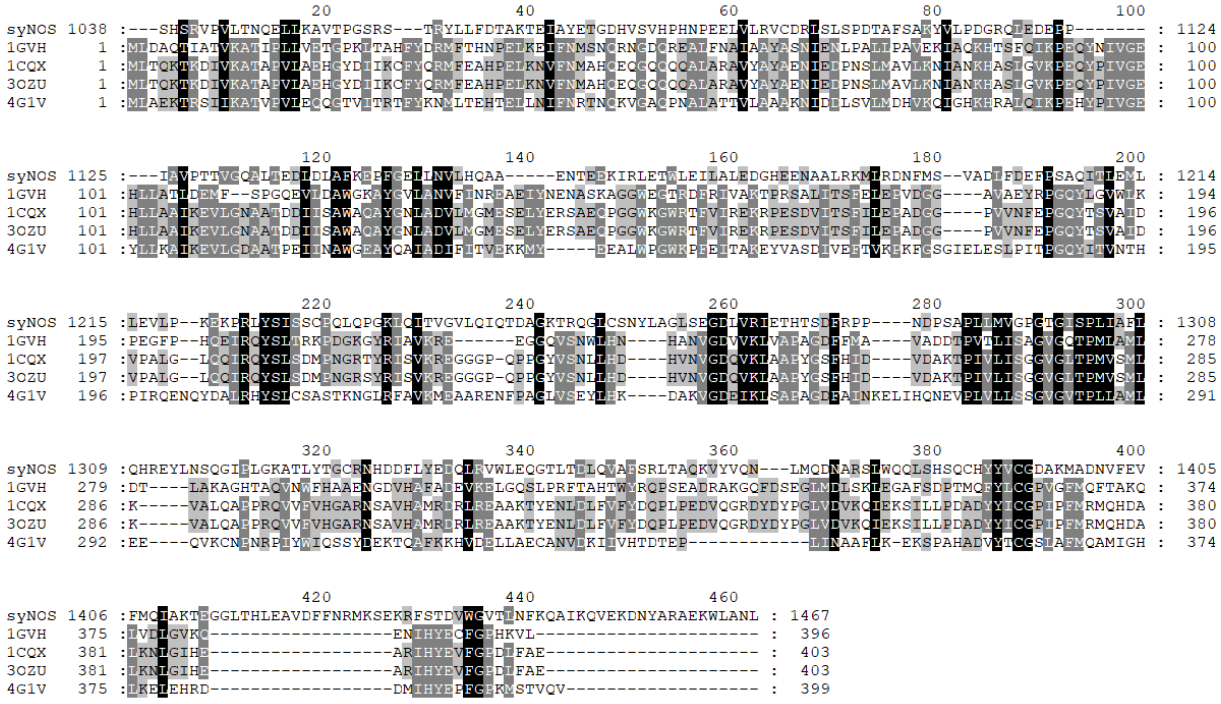

CHAPTER FOUR

Conclusions

4.1 syNOS is a challenging protein to express and purify in the active form.

Recombinantly expressed syNOS is a challenging protein to study; in spite of our best efforts, research was stalled for lack of any enzymatic activity. It was not believed to be a folding problem as syNOS was well resolved by SEC, the retention time did not vary, and little to no protein was found in the aggregate peak. Efforts focused on improving cofactor incorporation during protein expression. Remarkably, after tens of protein preparations, a few active preparations were obtained, but activity waned quickly in subsequent batches. How these active preparations differed from others was unknown; no variables were intentionally changed during protein expression or purification. This brief but auspicious event led to the recognition that inconsistent protein folding was the source of inactivity and identified GroEL/ES as the component necessary for producing consistently active syNOS (discussed in Appendix B), thus enabling all the work described in this thesis. Although co-expression with GroEL/ES has significantly decreased batch-to-batch variations, preparations of syNOS are sporadically inactive. The $syNOS_{ox}$ domain is likely to be the problematic domain. In addition to poor activity and poor heme binding in the full-length enzyme, domain truncations only exacerbate the problem resulting in very poor yields, very low heme incorporation, and formation of the inactive P420 heme.

4.2 Proposed syNOS Functions

As discussed in Chapter Two, it is highly unlikely that syNOS aids nitrogen

assimilation by *Synechococcus*, as has been proposed recently (1). The simplest reason being that *Synechococcus* sp. PCC 7335 is a diazotroph (2) and does not have a significant need for this proposed pathway. One could argue that syNOS is a supplementary N source when nitrogen fixation is limited, but this argument falls short as the concentration of dissolved arginine (tens of nanomolar (3–5)) in sea water is far less than that of dissolved $NO_2^- + NO_3^-$ (tens of micromolar (6–8)), and *Synechococcus* contains nitrate transport genes. Compared to other N acquisition pathways, syNOS is also the least efficient, as it oxidizes organic nitrogen that must be reduced back to ammonia for cellular use. Bacteria contain various more effective catabolic pathways, such as the arginine succinyl transferase (AST) pathway in *E. coli* (9), or use of arginase and urease in *Synechocystis* (10), and derive more N (two molecules of ammonia via AST, and three via arginase and urease (9, 10)) per arginine consumed than syNOS (one nitrate per arginine).

Synechococcus growth experiments suggest that syNOS may have a more significant role in *Synechococcus* biology (1). Figure 6A in the aforementioned publication reveals that *Synechococcus* growth in the presence of L-arg or nitrate is indistinguishable from growth fueled by nitrogen fixation alone (1). When the NOS inhibitor L-NAME is added to the same three growing conditions, *Synechococcus* growth is significantly slowed under all conditions independent of nitrogen source (1), strongly implying that syNOS has a more nuanced role in *Synechococcus* biology. It is certainly possible that L-NAME could be interfering with pathways unrelated to NOS, and has been documented to do such on multiple occasions, particularly in the search for plant NOS (11, 12). However, results in Chapter Two verify that L-NAME is a potent syNOS inhibitor.

The search for syNOS function may be expedited by investigating other syNOS-like

proteins. A recent NCBI-BLAST search (Appendix C, Fig. C1) reveals a number of NOS-like proteins that also contain a NOS_g domain, NOS_{red} domain, and an N-terminal region that cannot be assigned to any conserved domain. These proteins are found in the Cyanobacteria phylum (15 proteins), *Spirosoma* genus (10 proteins), and the Proteobacteria phylum (3 proteins). It is difficult to identify any one unifying characteristic among these bacteria, as many of them are poorly studied and cluster in different phyla. However, the genomes of these organism have been sequenced, and the genes neighboring these syNOS-like sequences may reveal possible functions. The operon containing syNOS in *Synechoccocus* includes a pentapeptide repeat-containing protein YjbI (whose functions are largely unknown, but include antibiotic resistance, manganese transport, and Ser/Thr phosphorylation (13)), filamentous hemagglutinin-containing protein (an adhesion factor involved in bacterial virulence (14)), and a CHAT domain-containing protein (related to peptidases and caspases (15)). However, these genes are not localized with NOS in the other syNOS-containing bacteria (Appendix C Table C1). In cyanobacteria, the most common gene neighbors are nitrate transporters and PhzF family phenazine biosynthesis proteins, responsible for the biosynthesis of phenazines which are involved in electron transport, controlling gene expression, and have antibiotic properties (16), but four cyanobacterial species have no genes on the same operon as the syNOS-like sequence. The existence of nitrate-transport genes adjacent to syNOS-like proteins adds to the evidence that syNOS and its homologues do not serve to assimilate N from arginine, as the amount of N obtained from L-arg would be marginal compared to the large amount of environmental nitrate. Each of the identified species of *Spirosoma* share the same three gene neighbors, a DNA-binding response regulator LytR/AlgR family, a PAS domain S-box protein, and a heme NO binding domain protein.

PAS domain-containing proteins sense a variety of signals, including light, oxygen, and redox potential, and are found in pathways controlling the circadian clock, bacterial chemotaxis, and nitrogen fixation (17). LytR/AlgR domains are DNA-binding domains found in the response regulators of two-component systems and control various virulence factors, including the biosynthesis of toxins and extracellular polysaccharides (18). The localization of these proteins adjacent to a syNOS-like sequence is strong evidence that syNOS may function in a signal-transduction pathway.

Three of the syNOS-like proteins identified in the BLAST search stand out in particular. *Planktothrix paucivesiculata* PCC 9631, and *Cyanobacteria* bacterium UBA9273 both contain a large C-terminal extension (~200 residues), however they cannot be assigned to any conserved domain. The NOS from *Microcoleus* (txid 1151) is particularly interesting; a ~60 residue insert is found in the NOS_g domain and is >40% identical to the Ca^{2+}-binding EF-hand family of proteins. This is the first and only Ca^{2+} binding site identified thus far in syNOS-like proteins. In addition, the EF-hand insert is located about six residues prior to where the heme-ligating proximal histidine is located in other syNOS-like proteins, however in this protein the histidine is a valine and is unlikely to bind heme. The significance of this is unclear, but it is strong evidence that the effects of Ca^{2+} observed in Chapters Two and Three are specific interactions, the effects of which may be mediated through NOS_g.

4.3 Remaining Questions and Future Directions

The identification of globin domains in NOS proteins poses many questions and reveals that our current understanding of NOS enzymology is incomplete. NO dioxygenation and Ca^{2+} dependence could replace regulation by Ca^{2+}-CaM and inhibitory structural

elements, but assigning them to this role would be premature and is likely an over-simplification. Further work is needed to identify how Ca^{2+} can influence both $syNOS_{ox}$ activity and $syNOS_g$ reduction. The crystal structures of these domains would be invaluable to this investigation, but understanding how the reduction rate of one heme is affected by the presence of the opposite heme and how Ca^{2+} factors into this is also necessary. Crystallization of full-length syNOS is unlikely, however cryo-electron microscopy may be just as enlightening to study the arrangement of NOS_g relative to NOS_{ox}, and to also observe structural movements during electron transfer, in particular electron transfer between $syNOS_g$ and $syNOS_{FAD}$. It remains to be seen if NOS_g reduction is an inter- or intra-molecular process, and if reduction is mediated by $FADH_2$ and $FADH^{\bullet}$, as in flavoHb, or if it is limited to $FADH_2$. This can be determined by measuring the reduction potentials of each cofactor, and these values may also illuminate the driving forces dictating the preference between NOS_g reduction versus NOS_{FMN}/NOS_{ox} reduction. It may also be worthwhile to explicitly confirm that *Synechococcus* can biosynthesize H_4B, which would validate the *in vitro* observations in Chapter Two. As discussed in Chapter Two, it is not clear if *Synechococcus* contains the last enzyme for H_4B synthesis, sepiapterin reductase, but it contains a homologous SDR-family protein on the same operon as GTPCH I, the first enzyme in the H_4B synthesis pathway. As the syNOS-like proteins identified in Appendix C are highly identical (more than half are >50% identical to syNOS) these proteins may also require H_4B. All but three of these genomes contain an SDR family protein that is immediately adjacent to a GTPCH I, and they are also found in operons containing all three H_4B biosynthesis genes (GTPCH I, PTPS, and SR). It is very likely that the future directions mention here will quickly lead to unexpected discoveries and new questions. This thesis is just the beginning of the investigation into a new

class of bacterial NOS-NOD proteins, which promise to expand the field of NO biology in unforeseen directions.

4.4 References

1. Correa-Aragunde, N., Foresi, N., Del Castello, F., and Lamattina, L. (2018) A singular nitric oxide synthase with a globin domain found in Synechococcus PCC 7335 mobilizes N from arginine to nitrate. *Sci. Rep.* 8, 12505
2. Rippka, R., Deruelles, J., Waterbury, J. B., Herdman, M., and Stanier, R. Y. (1979) Generic Assignments, Strain Histories and Properties of Pure Cultures of Cyanobacteria. *J. Gen. Microbiol.* 111, 1–61
3. Clark, M. E., Jackson, G. A., and North, W. J. (1972) Dissolved Free Amino Acids in Southern California Coastal Waters. *Limnol. Oceanogr.* [online] http://citeseerx.ist.psu.edu/viewdoc/download?doi=10.1.1.497.1957&rep=rep1&type=pdf (Accessed October 1, 2018)
4. Kaiser, K., and Benner, R. (2009) Biochemical composition and size distribution of organic matter at the Pacific and Atlantic time-series stations. *Mar. Chem.* 113, 63–77
5. Hubberten, U., Lara, R. J., and Kattner, G. (1994) Amino acid composition of seawater and dissolved humic substances in the Greenland Sea. *Mar. Chem.* 45, 121–128
6. Patey, M. D., Rijkenberg, M. J. A., Statham, P. J., Stinchcombe, M. C., Achterberg, E. P., and Mowlem, M. (2008) Determination of nitrate and phosphate in seawater at nanomolar concentrations. *TrAC - Trends Anal. Chem.* 27, 169–182
7. Masami Watanabe, Jun Ohtsu, A. O. (2000) Daily Variations in Nutrient Concentrations of Seawater at 321 m Depth in Toyama Bay, Japan Sea. *J. Oceanogr.*
8. Hansell, D. A., and Follows, M. J. (2008) Nitrogen in the Atlantic Ocean. in *Nitrogen in the Marine Environment*, pp. 597–630, 10.1016/B978-0-12-372522-6.00013-X
9. Schneider, B. L., Kiupakis, A. K., and Reitzer, L. J. (1998) Arginine Catabolism and the Arginine Succinyltransferase Pathway in Escherichia coli. *J. Bacteriol.* 180, 4278–4286
10. Quintero, M. J., Muro-Pastor, A. M., Herrero, A., and Flores, E. (2000) Arginine catabolism in the cyanobacterium Synechocystis sp. strain PCC 6803 involves the urea cycle and arginase pathway. *J. Bacteriol.* 182, 1008–1015
11. Barroso, J. B., Corpas, F. J., Carreras, A., Sandalio, L. M., Valderrama, R., Palma, J. M., Lupiánez, J. A., and Del Río, L. A. (1999) Localization of nitric-oxide synthase in

plant peroxisomes. *J. Biol. Chem.* 274, 36729–36733

12. Guo, F. Q., Okamoto, M., and Crawford, N. M. (2003) Identification of a plant nitric oxide synthase gene involved in hormonal signaling. *Science (80-.).* 302, 100–103
13. Vetting, M. W., Hegde, S. S., Fajardo, J. E., Fiser, A., Roderick, S. L., Takiff, H. E., and Blanchard, J. S. (2006) Pentapeptide repeat proteins. *Biochemistry*. 45, 1–10
14. Clantin, B., Hodak, H., Willery, E., Locht, C., Jacob-Dubuisson, F., and Villeret, V. (2004) The crystal structure of filamentous hemagglutinin secretion domain and its implications for the two-partner secretion pathway. *Proc. Natl. Acad. Sci. U. S. A.* 101, 6194–6199
15. Aravind, L., and Koonin, E. V. (2002) Classification of the caspase-hemoglobinase fold: Detection of new families and implications for the origin of the eukaryotic separins. *Proteins Struct. Funct. Genet.* 46, 355–367
16. Pierson, L. S., and Pierson, E. A. (2010) Metabolism and function of phenazines in bacteria: Impacts on the behavior of bacteria in the environment and biotechnological processes. *Appl. Microbiol. Biotechnol.* 86, 1659–1670
17. Taylor, B. L., and Zhulin, I. B. (1999) PAS domains: internal sensors of oxygen, redox potential, and light. *Microbiol. Mol. Biol. Rev.* 63, 479–506
18. Nikolskaya, A. N., and Galperin, M. Y. (2002) A novel type of conserved DNA-binding domain in the transcriptional regulators of the AlgR/AgrA/LytR family. *Nucleic Acids Res.* 30, 2453–2459

APPENDIX A

Experimental Methods

Chapter 2

Materials

Synechococcus PCC 7335 (ATCC 29403) was purchased from the American Type Culture Collection. *E. coli* strain JW2536 was purchased from Dharmacon and BW25113 was from the Coli Genetic Stock Center at Yale University. NOC-7 and N-(dithiocarbamoyl)-N-methyl-D-glucamine (MGD) were purchased from Santa Cruz Biotechnology. Nitrate reductase was purchase from Roche. L-NNA, L-NAA, L-citrulline, N-hydroxy arginine, and ortho-phthaldialdehyde (OPA) were purchased from Sigma-Aldrich. Tetrahydrobiopterin (H_4B) was purchased from Cayman Chemical. 2',5' ADP Sepharose 4B and Superdex 200 resins was purchased from GE Healthcare Life Sciences. Ni-NTA was purchased from Thermo Scientific.

Genomic DNA extraction, cloning

Genomic DNA extraction was performed following the method of Singh et al (73). *Synechococcus* (50 mL) was grown for one week and then harvested by centrifugation at 2000 G. Cells were resuspended in 400 µL of lysis buffer (4 M urea, 0.2 M TRIS, pH 7.4, 20 mM NaCl, 0.2 M EDTA) supplemented with 50 µL of 20 mg/mL proteinase K. The sample was incubated for one hour at 55 °C and mixed by gentle inversion every 15 min. One mL of the extraction buffer (3% CTAB, 1.4 M NaCl, 20 mM EDTA, 0.1 M TRIS, pH 8.0, 1% sarkosyl) heated to 55 °C was added to the sample. The resulting sample was subsequently incubated at 55 °C for one hour with gentle inversion every ten min. Once the sample cooled to room temperature, two volumes of

chloroform/isoamyl alcohol (24:1) solution were added and the sample was mixed by inversion. The sample was centrifuged for five min at 10,000 G and the upper aqueous phase was removed. Two volumes of ethanol + 0.1 volumes 3 M sodium acetate (pH 5.2) were added to the aqueous phase. This was incubated at -20 °C for one hour, then centrifuged for three min at 10,000 G. The pellet was washed with 500 µL cold 70% ethanol. After evaporating the ethanol, the DNA was dissolved in 50 µL water, and the purity was assessed by the absorbance ratio 260 nm/280 nm.

Full-length syNOS (residues 1 - 1468, NCBI Protein database accession number WP_006458277) was cloned from base pair 486069 to 490475 (NCBI Nucleotide database accession number NZ_DS989905) and inserted into the following vectors: 1) pET28 (Novagen) using the restriction sites NdeI and EcoRI, and 2) pCW-LIC (a gift from Cheryl Arrowsmith, Addgene plasmid # 26098) using BamHI and KpnI. Point mutations were constructed by primer overlap extension PCR.

Each domain of syNOS was subcloned into expression vectors by PCR. NOS_g (residues 337-469), NOS_{ox} (residues 475-795), and NOS_{red} (residues 856-1468) were inserted into the vector pET28 using the restriction sites NdeI and XhoI.

Protein expression and purification

E. coli BL21 DE3 cells were cotransformed with syNOS (in either pCW-LIC or pET28) or its heme domain truncations, plus the *E. coli* chaperonins GroEL/ES and Trigger Factor in pACYCDuet (Addgene plasmid #83923). The reductase domain truncation was transformed into BL21 DE3 without GroEL/ES. Lysogeny broth Miller was inoculated with an overnight culture and incubated at 37 °C until the $OD_{600\ nm}$ reached ~0.6. Protein expression was induced by the addition of 25 µg/mL isopropyl β-D-1-thiogalactopyranoside (IPTG), 80 µg/mL δ-aminolevulinic

acid, 4 μg/mL hemin, 2 μg/mL flavin adenine dinucleotide (FAD), 2 μg/mL flavin mononucleotide (FMN), and incubated at 17 °C overnight. Hemin and δ-aminolevulinic acid were excluded from NOS_{red} expression, and flavins were excluded from the expression of either heme domain. Cells were harvested 18 hours after induction by centrifugation at 5,000 G, then frozen at -20 °C.

The cell pellet from a 2 L growth was resuspended in 50 mL lysis buffer (200 mM NaCl, 50 mM TRIS, pH 7.5, 10% glycerol) with 174 μg/mL phenylmethylsulfonyl fluoride (PMSF), 1.5 μg/mL pepstatin A, and 1 μg/mL leupeptin. Cells were lysed on ice by sonication using a Fisher Scientific Sonic Dismembrator 550 (amplitude of 7, pulsed 2 sec on, 2 sec off) for a total sonication time of five min. Lysate was centrifuged for one hour at 48,000 G at 4 °C. For the full-length constructs the soluble portion was applied in batch to a 2',5' ADP Sepharose resin pre-equilibrated with lysis buffer and then incubated at 4 °C for two hours with gentle rocking. The resin was collected and washed with five column volumes of lysis buffer, then eluted with 5 mM NADPH. Domain truncations were lysed in the same manner, with 5 mM imidazole in the lysis buffer. After centrifugation, the soluble portion was applied to Ni-NTA and the resin was washed with five column volumes of lysis buffer with 20 mM imidazole, then eluted with lysis buffer plus 200 mM imidazole.

The eluent was concentrated, then further purified on a Superdex 200 (full-length constructs) or 75 (truncations) 26/60 size exclusion column by isocratic elution using gel filtration buffer (25 mM TRIS pH 7.5, 150 mM NaCl, 10% glycerol). Protein was concentrated using a 50 kDa (full-length constructs) or 10 kDa (truncations) cutoff Amicon Ultra centrifugal filter.

Multiangle Light Scattering

MALS was performed using a Phenomenex BioSep SEC-s3000 column (5 μm, 290 Å, 300

mm × 7.8 mm) with a Phenomenex SecurityGuard guard column, connected to an Agilent 1200 series HPLC with G1314D variable wavelength detector. Light scattering was detected using a Wyatt DAWN HELEOS-II and dRI measured by a Wyatt Optilab T-rEX refractometer. The mobile phase contained 100 mM TRIS, pH 7.5, 200 mM NaCl with either 5 mM arginine, 5 mM $CaCl_2$, or 250 μM H_4B with 1.5 mM DTT. A solution of bovine serum albumin (BSA) monomer (5 mg/mL) was used as the standard to control for peak alignment and molecular weight calculations. Data were collected for 30 min at a flow rate of 1 mL/min at 25 °C. ASTRA V software was used to analyze the molecular weight and polydispersity of each peak.

UV-vis analysis of purified syNOS

Heme content was measured using the pyridine hemochrome method. Twenty microliters of protein at 1 mg/mL were diluted to 100 μL in 20% pyridine 0.2 M NaOH. An Agilent 8453 UV-vis spectrophotometer was blanked with this solution, then ~ 0.5 mg solid dithionite was added and the absorbance difference at 557 - 573 nm was recorded (extinction coefficient 32.4 mM^{-1} cm^{-1}). Protein concentration was measured using the Bradford assay (Bio-Rad protein assay dye) and the calculated extinction coefficient of the denatured protein ($\varepsilon_{280\ nm}$ = 0.24053 μM^{-1} cm^{-1}). The protein was denatured in 4 M urea, then unbound cofactors were removed by concentrating in a spin column and diluting in 4 M urea, which was repeated three times. The protein concentration calculated from the absorbance at 280 nm agreed with that of the Bradford assay.

As syNOS does not appear to be fully loaded with heme, the concentration of active protein was estimated based on the amount of NOS_{oxy} heme bound in the H422A variant. The heme concentration of a syNOS sample was measured as stated previously, and the Soret intensity at 415 nm was recorded. Thirty-nine percent of the measured heme concentration was presumed to

originate from the NOS_{oxy} heme, and thus represents the concentration of active protein. This concentration and the Soret intensity were used to calculate an extinction coefficient that was used to quantify active protein in subsequent assays.

The spectra for the ferrous and ferrous-carbonmonoxy syNOS were taken after the ferric enzyme was sparged with argon and reduced with ~ 0.5 mg solid dithionite, then carbon monoxide gas was gently bubbled into the solution. Difference spectra were constructed by subtracting the spectrum of the ferric species from that of the ferrous-carbonmonoxy species.

NOS enzymatic reaction

NOS activity was assayed following the method of Moreau et al (74), using 250 μM H_4B, 5 mM arginine, 5 mM $CaCl_2$, 1.5 mM DTT, and 1 mM NADPH in 100 mM TRIS, pH 7.5, 200 mM NaCl. Where specified, THF was used at 250 μM, and CaM at 10 μg/mL. The reaction proceeded for 30 min at room temperature and was stopped by rapid heating to 60−70 °C for five min. Samples were centrifuged at 16,000 G for five min to remove any insoluble debris.

Nitrate and nitrite measurement by Griess assay

Nitrate was measured by adding 75 μL 0.2 U/mL nitrate reductase, 1 mM NADPH, and 0.1 mM FAD to 150 μL of sample, then incubated for two hours at 37 °C. Nitrite was quantified similarly but in the absence of nitrate reductase. NADPH was removed by zinc acetate precipitation (75, 76). To each sample 100 μL 0.5 M zinc acetate in 50% ethanol was added and the samples were vortexed. Subsequently, 100 μL 0.5 M sodium carbonate was added, followed by vortexing. After five min of centrifugation at 16,000 G, 150 μL of each sample were plated in duplicate and 25 μL 2% sulfanilamide 1 M HCl were added, followed by 25 μL 0.2% naphthyl-

ethylenediamine. The absorbance at 540 nm was recorded immediately afterwards using a Biotek Synergy HT plate reader. A standard curve was prepared from nitrate and nitrite standards under the same conditions as the experimental samples. The standard curve was used to convert the absorbance at 540 nm to concentration.

HPLC product detection

The NOS reaction was performed as stated above, with the substitution of 50 mM HEPES (pH 7.5) for TRIS. HPLC detection of derivatized citrulline was performed using the method of Davydov et al (77) with the following modifications. Using an Agilent 1100 series HPLC equipped with an Agilent 1260 fluorescence detector, an Agilent Eclipse Plus reverse phase column (150 mm × 4.6 mm; equipped with a Supelguard LC-18-DB guard column) was equilibrated with 50 mM trichloroacetic acid (pH 4.0) and 15% acetonitrile at 1 mL/min. The derivatization agent ortho-phthaldialdehyde (OPA) was dissolved in methanol (8 mg/mL), then 100 µL of the OPA reagent was added to 900 µL of 100 mM sodium borate (pH 10.0) and 6 µL β-mercapto ethanol. Then, 20 µL OPA was added to 10 µL filtered sample. Following three min of incubation at room temperature, the mixture was injected onto the column. After injection, the concentration of acetonitrile was increased to 25% over 20 min and fluorescence was detected at $\lambda_{excitation}$= 360 nm and $\lambda_{emission}$= 455 nm. Derivatized citrulline eluted at 8.58 min, followed by NOHA at 12.01 min, and L-arg 13.34 min. A standard curve was prepared from citrulline standards under the same conditions as the experimental samples. The standard curve was used to convert the peak area to concentration.

Fe-MGD spin trap and ESR detection

The NOS reaction was performed as stated above, with the addition of 0.7 mM iron (II) sulfate and 2.7 mM MGD (78). After reacting for 30 min at room temperature glycerol was added to the sample to 15% w/v. The sample was immediately transferred to an X-band electron spin resonance (ESR) tube, and flash frozen in liquid nitrogen. Continuous-wave ESR spectra were acquired using a Bruker Elexsys E500 CW ESR spectrometer with an ER4131VT variable temperature unit at 150 K and 9.4 GHz, with a modulation amplitude of 1.5 G and modulation frequency of 100 kHz.

NO detection by electrochemistry

NO oxidation was measured using an Innovated Instruments amiNO-2000 electrode and a CH Instruments Electrochemical Analyzer CH1630B potentiostat. The electrode was submerged in buffer (100 mM TRIS, pH 7.5, 200 mM NaCl, 1 mM NADPH) while stirring, and a 0.85 V potential was applied for about five min to prime the electrode. Data collection was initiated, and the current was measured at a sampling interval of two per sec. The baseline current was recorded for about five min. Upon baseline stabilization, 10 μM NOC-7 was added and the current was allowed to plateau (about five min). syNOS was then added to initiate NO oxidation and data collection continued for approximately ten min. Signal decay was fit to a mono exponential equation using Matlab and the rate constants were extracted.

Reduction of NOS_g and NOS_{ox} by NOS_{red}

All solutions were sparged with argon then degassed in an anaerobic COY chamber for six hours. NOS_{ox} was added to two molar equivalents of NOS_{red} and 1 mM NADPH, with or without

5 mM $CaCl_2$. NOS_g was added to two molar equivalents of NOS_{red} with 1 mM NADPH. Samples were transferred to an anaerobic cuvette and the absorbance spectra were recorded before and after sparging with carbon monoxide.

Minimal media growth assay

The growth assay described by Lamattina et al (30) was carried out with the following modifications. *E. coli* BL21 (DE3) pLysS cells were transformed with either pET-28a containing syNOS or the empty vector. Ten milliliters of LB broth were inoculated with 100 µL of an overnight culture, with 50 µg/mL kanamycin and 30 µ/mL chloramphenicol, and the culture was incubated at 37 °C until the $OD_{600\ nm}$ was approximately 0.3-0.4. Protein expression was induced with 0.1 mM IPTG, 500 µM δ-aminolevulinic acid, and 1 mM arginine, and incubated at 37 °C for 1.5 hours. Cells were pelleted by centrifugation at 2000 G for ten min then washed three times with five milliliters of minimal media (5.44 g KH_2PO_4, 2 g glucose, and 6 ml salt solution dissolved in one liter of distilled water, pH 7.4; The salt solution contained 10 g $MgSO_4 \cdot 7H_2O$, 1.0 g $MnCl_2 \cdot 4H_2O$, 0.4 g $FeSO_4 \cdot 7H_2O$ and 0.1 g $CaCl_2 \cdot 2H_2O$ dissolved in one liter of distilled water). The cells were resuspended in minimal media and supplemented with 0.1 mM IPTG, 500 µM δ-aminolevulinic acid, and 1 mM arginine in an effort to maintain the conditions specified by Lamattina et al (30). The culture was diluted 1/100 in minimal media containing either 0.2% w/v arginine, 0.3% NH_4Cl, or 0.018% NH_4Cl and incubated at 37 °C. (Washing with minimal media was strictly required; the 1/100 dilution in minimal media contained enough nitrogen to allow for significant growth.) $OD_{600\ nm}$ was recorded using an Agilent 8453 UV-vis spectrophotometer to monitor cell density.

NO minimum inhibitory concentration

The vector pCW-LIC containing syNOS was transformed into cells of the flavohemoglobin deficient *E. coli* strain JW2536 or of the wild-type strain BW25113. LB containing 100 μg/mL ampicillin (and 50 μg/mL kanamycin for strain JW2536) was inoculated with an overnight culture (1:200 dilution) and incubated at 37 °C until the $OD_{600\ nm}$ was approximately 0.6. Cells were diluted to 10^6 CFU/mL ($OD_{600\ nm}$ 1 = 10^8 colony forming units/mL) in LB supplemented with antibiotics and 0, 6.25, 12.5, or 25 μg/mL IPTG. DETA nonoate was diluted in 10 mM NaOH, and 20 uL of each dilution was added to 180 uL of each solution of cells in a 96 well plate. Final concentrations of DETA NONOate were 2.7, 1.35, 0.675, 0.338, 0.169, 0.084, 0.042, and 0 mM. Microplates were wrapped with parafilm to prevent excess evaporation and incubated at 37 °C for 18 hours. The $OD_{600\ nm}$ was recorded using a Biotek Synergy HT plate reader.

Chapter Three

Materials

Crystallization sparse matrix screens were purchased from Rigaku Reagents (Wizard classic screens) and Qiagen (JCSG Core Suite). Glucose oxidase and catalase were purchased from Sigma-Aldrich. NADPH was purchased from Cayman Chemical. Superdex 75 resin was purchased from GE Healthcare Life Sciences. Ni-NTA was purchased from Thermo Scientific.

Protein expression and purification

E. coli BL21 DE3 cells were cotransformed with $syNOS_{red}$, $syNOS_{FMN,}$ or $syNOS_{FAD}$. Lysogeny broth Miller was inoculated with an overnight culture and incubated at 37

°C until the $OD_{600\ nm}$ reached ~0.6. Protein expression was induced by the addition of 25 μg/mL isopropyl β-D-1-thiogalactopyranoside (IPTG), 2 μg/mL flavin adenine dinucleotide (FAD) (excluded from NOS_{FMN} expression), and 2 μg/mL flavin mononucleotide (FMN) (excluded from NOS_{FAD} expression), and incubated at 17 °C overnight. Cells were harvested 18 hours after induction by centrifugation at 5,000 G, then frozen at -20 °C.

The cell pellet from a 2 L growth was resuspended in 50 mL lysis buffer (200 mM NaCl, 50 mM TRIS, pH 7.5, 5 mM imidazole, 10% glycerol) with 174 μg/mL phenylmethylsulfonyl fluoride (PMSF), 1.5 μg/mL pepstatin A, and 1 μg/mL leupeptin. Cells were lysed on ice by sonication using a Fisher Scientific Sonic Dismembrator 550 (amplitude of 7, pulsed 2 sec on, 2 sec off) for a total sonication time of five min. Lysate was centrifuged for one hour at 48,000 G at 4 °C. The soluble portion was applied to Ni-NTA and the resin was washed with five column volumes of lysis buffer with 20 mM imidazole, then eluted with lysis buffer plus 200 mM imidazole.

The eluent was concentrated, then further purified on a Superdex 75 26/60 size exclusion column by isocratic elution using gel filtration buffer (25 mM TRIS pH 7.5, 150 mM NaCl, 10% glycerol). Protein was concentrated using a 10 kDa cutoff Amicon Ultra centrifugal filter.

UV-vis spectra of flavin domains

UV-vis spectra were recorded with an Agilent 8453 UV-vis spectrophotometer. The $syNOS_{FMN}$ semiquinone was obtained by reduction with dithionite and re-oxidation to the air-stable semiquinone. $syNOS_{FAD}$ semiquinone was obtained by reduction with five molar equivalents of NADPH and re-oxidation by air. The stable semiquinone can be isolated by stopping the re-oxidation by the addition of 5 mM glucose to NOS_{FAD} samples containing 25 μg/mL glucose

oxidase and 50 μg/mL catalase (GOD/CAT system). Isolation of the NOS_{red} disemiquinone was attempted in the same manner as NOS_{FAD}, but was unsuccessful.

Reduction of NOS_g and NOS_{ox} by NOS_{red}

All solutions contained the GOD/CAT system and were incubated in an anaerobic COY chamber for 30 minutes. $syNOS_g$ was added to three molar equivalents of $syNOS_{red}$ or three molar equivalents of $syNOS_{FAD}$. Samples were transferred to an anaerobic cuvette with a septum cap and the absorbance spectra were recorded before and after the addition of 1 mM NADPH anaerobically with a gas-tight syringe..

Reduction kinetics

All solutions contained the GOD/CAT system and were incubated in an anaerobic COY chamber for 30 minutes. $syNOS_g$ was added to three molar equivalents of $syNOS_{red}$ or three molar equivalents of $syNOS_{FAD}$. Five millimolar $CaCl_2$ was added to C539A and H422A, and five millimolar of L-arg was added to H422A. Samples were transferred to an anaerobic cuvette with a septum cap and stir flea, and samples of H422A were sparged with CO. Data collection was initiated (recording 413 nm, 425 nm, and 560 nm every 0.5 s for NOS_g and C539A, and 417 nm, 444nm every 5 s for H422A) then 1 mM NADPH was added anaerobically with a gas-tight syringe.

Crystallization of NOS_{FMN} and NOS_{FAD}

Crystallization screens were constructed using the Art Robbins Instruments Gryphon robot and the Wizard Classic 1-1V and JCSG Core Suite 1-4 sparse matrix screens. Fifty microliters of

each crystallization solution were dispensed into the reservoirs of a sitting drop intelli-plate 96-3 LVR (Hampton Research) and 0.3 µL was dispensed into each of the three crystallization wells, then 0.3 µL of protein solution was added to each crystallization well. The plates were sealed with and stored at 17 °C.

The first crystals of $syNOS_{FMN}$ were grown in conditions using the $syNOS_{red}$ truncation. The initial hit was in the Wizard Classic 4 screens from Rigaku Reagents, condition #19 containing 100 mM MMT buffer (malic acid, MES, and TRIS in a 1:2:2 molar ratio) pH 6.5, 25% PEG 1500 and 15 mg/mL $syNOS_{red}$. Two months after setting up the screen, a cluster of birefringent crystals was observed. Crystal growth was optimized using hanging drop diffusion with 24-well plates (Hampton Research). Each reservoir contained 400-500 µL of crystallization solution and 1 µL of the solution was added to 1 µL of protein solution on siliconized coverslips. Wells were sealed with vacuum grease. X-ray diffraction was collected on 10-9-15 at CHESS line F1 with the Quantum 270 CCD detector (beam center x 133.8, y 120.0) using crystals grown in 32% PEG 1500, 100 mM MMT buffer pH 7.0, 20 mg/mL NOS_{red} stored at 17°C). The structure was phased using molecular replacement with Phenix Phaser-MR and the model 3HR4 of the human iNOS FMN domain and calmodulin complex (TFZ 6.1, LLG 48).). The structure was built through cycles of manual editing in COOT and refinement with Phenix Refine.

Crystals of $syNOS_{FAD}$ were grown in Qiagen JCSG Core I condition #63 containing 200 mM magnesium formate pH 8.5, 20% w/v PEG 3350, and 25 mg/mL NOS_{FAD} stored at 17°C. These diffracted poorly, and were optimized using hanging drop diffusion. X-ray diffraction was collected on 7-28-16 at the Northeastern Collaborative Access Team (NE-CAT) facility at the Advanced Photon Source using the ADSC Quantum 315 CCD detector with crystals grown in 200 mM magnesium formate pH 8.5, 23-26% w/v PEG 3350, 200 µL paraffin oil, and the hanging

drop contained 1:2 or 1:3 v/v protein (20-25 mg/mL): reservoir stored at 17°C. The structure was phased using molecular replacement with Phenix Phaser-MR and the model 3QFS of the human NADPH-Cytochrome P450 Reductase FAD/NADPH domain (TFZ 15.3, LLG 232). The structure was built through cycles of manual editing in COOT and refinement with Phenix Refine.

Homology modeling syNOS$_g$

The syNOS$_g$ homology model was built using SWISS-MODEL and the structure of Hell's Gate globin I from the methanotroph *Methylacidiphilum infernorum*. syNOS$_g$ and syNOS$_{FAD}$ were docked relative to one another by alignment to the structure of the *E. coli* flavoHb, hmp (PDBID:1GVH).

APPENDIX B

Identification of syNOS misfolding

The syNOS inactivity problem was not thought to be a folding problem as its retention time on SEC did not vary, and it did not elute in the void, indicating aggregation. What aided identification of this problem was the isolation of active protein purely by chance. This sample eluted similarly to inactive protein on SEC and had similar cofactor incorporation (an average of 1 heme per syNOS monomer). The active and inactive samples were analyzed using circular dichroism in Fig. B.1, which confirmed that there was variable protein folding between batches.

After the addition of GroEL/ES to syNOS expression, a significant contaminating band at ~60-70 kDa was observed. This band had always been present in syNOS purifications and had varied in intensity, but the overall amount was low and it was thought to be degraded syNOS. The contaminant bands (Fig. B2) were sent to the Cornell Biotechnology Resource Center Proteomics Facility for identification. The larger band predominantly contained the *E. coli* chaperone DnaK, the next band was glutamine--fructose-6-phosphate aminotransferase, and the lowest band was GroEL. The presence of two folding chaperones co-purifying with syNOS reaffirms that activity problems may have been caused by poor folding.

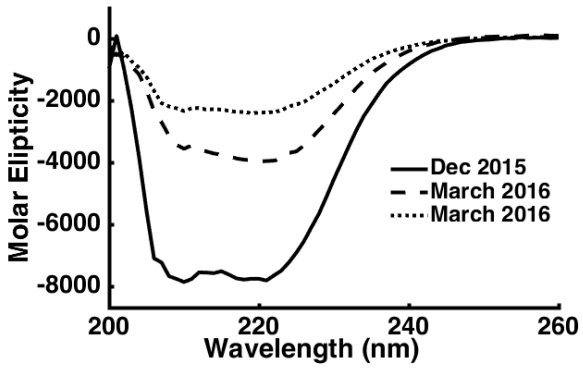

Figure B1: Circular dichroism of syNOS preparations. Dec 2015 is an active syNOS sample, and both samples prepared in March 2016 are inactive.

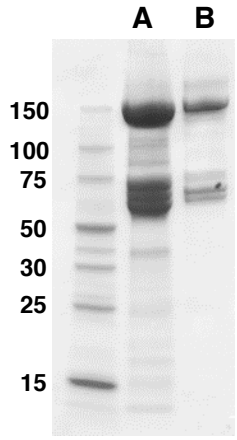

Figure B2: SDS-PAGE of syNOS after SEC and anion exchange

Table B1 Mass spectrometry results from the ~70 kDa band

Accession	Description	Score	Coverage	# Unique Peptides	MW [kDa]
P0A6Y8	Chaperone protein DnaK Escherichia coli K12	12323.21	82.13	52	69.1
P77398	Bifunctional polymyxin resistance protein ArnA Escherichia coli K12	10203.12	76.82	40	74.2
P17169	Glutamine--fructose-6-phosphate aminotransferase [isomerizing] Escherichia coli K12	5159.96	63.71	26	66.9
B4WU43	Nitric oxide synthase, oxygenase domain protein Synechococcus sp. (strain ATCC 29403 / PCC 7335	2552.65	35.83	32	166.1
P0A6F5	60 kDa chaperonin Escherichia coli K12	1108.18	50.36	17	57.3
P0AG67	30S ribosomal protein S1 Escherichia coli K12	494.80	35.37	14	61.1
P27302	Transketolase 1 Escherichia coli K12	167.66	9.05	4	72.2
P0A8M3	Threonine--tRNA ligase Escherichia coli K12	91.80	8.10	6	74.0
P0A6Z3	Chaperone protein HtpG Escherichia coli K12	27.28	8.17	3	71.4
P07024	Protein UshA Escherichia coli K12	0.00	12.00	2	60.8

Table B2: Mass spectrometry results from the larger band at ~60kDa

Accession	Description	Score	Coverage	# Unique Peptides	MW [kDa]
P17169	Glutamine--fructose-6-phosphate aminotransferase [isomerizing] Escherichia coli K12	32949.85	80.13	46	66.9
P0A6F5	60 kDa chaperonin groL Escherichia coli K12	5607.06	72.99	28	57.3
P77398	Bifunctional polymyxin resistance protein ArnA Escherichia coli K12	2196.94	67.12	30	74.2
B4WU43	Nitric oxide synthase, oxygenase domain protein Synechococcus sp. (strain ATCC 29403 / PCC 7335)	2033.03	29.36	26	166.1
P0A6Y8	Chaperone protein DnaK Escherichia coli K12	186.27	16.30	5	69.1
P0A6X3	RNA-binding protein Hfq Escherichia coli K12	70.28	57.84	2	11.2

Table B3: Mass spectrometry results for the smaller band at ~60 kDa

Accession	Description	Score	Coverage	# Unique Peptides	MW [kDa]
P0A6F5	60 kDa chaperonin groL Escherichia coli K12	23201.97	77.92	35	57.3
P17169	Glutamine--fructose-6-phosphate aminotransferase [isomerizing] Escherichia coli K12	6434.58	67.16	30	66.9
P0A8N3	Lysine--tRNA ligase Escherichia coli K12	162.96	20.20	7	57.6
P10902	L-aspartate oxidase Escherichia coli K12	129.83	13.33	6	60.3
P0AC38	Aspartate ammonia-lyase Escherichia coli K12	129.49	10.67	6	52.3
B4WU43	Nitric oxide synthase, oxygenase domain protein Synechococcus sp. (strain ATCC 29403 / PCC 7335)	94.70	3.54	4	166.1
P77398	Bifunctional polymyxin resistance protein ArnA Escherichia coli K12	93.28	5.91	3	74.2
P0A9B2	Glyceraldehyde-3-phosphate dehydrogenase A Escherichia coli K12	79.10	16.92	2	35.5
P0A6Y8	Chaperone protein DnaK Escherichia coli K12	53.02	8.62	2	69.1
P0A6X3	RNA-binding protein Hfq Escherichia coli K12	50.08	57.84	2	11.2
P0A799	Phosphoglycerate kinase Escherichia coli K12	39.78	21.19	3	41.1

APPENDIX C

Additional syNOS-Like Proteins

Sequences with high identity to syNOS can be found in several other organisms. Using the NCBI basic local alignment search tool (BLAST) 28 sequences are identified that are 30-60% identical to syNOS (more than half are >50% identical), and that also contain a NOS_{red} and a globin-like domain. These proteins are primarily found in cyanobacteria (15 proteins, 6 found in *Nostoc*), *Spirosoma* (10 proteins), and the Proteobacteria phylum (3 proteins). Although eight different proteins from the order Oscillatoriales are identified in the search, they are actually the same protein from one organism (a yet unnamed *Microcoleus* species). The genome of this organism is assembled into 29 scaffolds, and the sequence for this protein is located where several separate scaffolds overlap, resulting in redundant search hits.

These syNOS-like proteins have a few gene neighbors in common, which may aid in the search for its biological role. In cyanobacteria the most common genes are annotated as nitrate transporters and PhzF family phenazine biosynthesis proteins. Four species have no genes on the operon containing the syNOS-like sequence. All species of *Spirosoma* have the same gene neighbors, a DNA-binding response regulator LytR/AlgR family, a PAS domain S-box protein, and a heme NO binding domain protein. The genomes of three species, *Planktothrix paucivesiculata* PCC 9631, *Cyanobacteria bacterium* UBA9273, and *Deltaproteobacteria bacterium*, were not searchable using the BLAST and their master genomic records in the NCBI Nucleotide database contains no sequence data. It is unclear

why the genomes of these organisms are difficult to search, but may be another situation where sequence data is not yet assembled into a full genome.

Table C1: Genes on the same operon as syNOS-like proteins

syNOS homologue Accession Number	Organism	Gene Neighbors/Shared Operon
WP_006458277.1	*Synechococcus* sp. PCC 7335 (txid 91464)	WP_006457826.1 pentapeptide repeat-containing protein YjbI WP_006458003.1 filamentous hemagglutinin N-terminal domain-containing WP_006458447.1 CHAT domain-containing protein
WP_104909534.1	*Nostoc* sp. 'Lobaria pulmonaria' (txid 1618022)	WP_104909533.1 hypothetical protein No accession number NOSox Pseudo, Partial start WP_104909535.1 cyclic nucleotide-binding domain-containing protein
WP_015114580.1	*Nostoc* sp. PCC 7107 (txid 317936)	WP_015114578.1 hypothetical protein WP_015114579.1 PhzF family phenazine biosynthesis protein WP_015114581.1 binding-protein-dependent transport system inner membrane protein
WP_103125914.1	*Nostoc cycadae* (txid 1861711)	WP_096578673.1 nitrate transporter TM_PBP2 super family WP_103125915.1 PhzF family phenazine biosynthesis protein
WP_096578671.1	*Anabaenopsis circularis* (txid 1085406)	WP_096578673.1 nitrate transporter NrtB TM_PBP2 super family WP_096578669.1 PhzF family phenazine biosynthesis protein
BBD59461.1	*Nostoc* sp. HK-01 (txid 196308)	BBD59460.1 nitrate transporter TM_PBP2 super family BBD59462.1 Phenazine biosynthesis PhzC/PhzF protein

WP_086835556.1	*Nostoc* sp. RF31YmG (txid 1932668)	WP_086756461.1 glutathione S-transferase family protein WP_086835555.1 extracellular solute-binding protein WP_086835557.1 type II toxin-antitoxin system RelE/ParE family toxin WP_086756467.1 addiction module protein
WP_015203917.1	*Crinalium epipsammum* (txid 1173022)	WP_015203916.1 LysR family transcriptional regulator WP_015203915.1 anthranilate phosphoribosyl-transferase family protein WP_015203914.1 Y1_Tnp transposase super family WP_015203918.1 hypothetical protein
WP_096587030.1	*Calothrix* sp. NIES-2098 (txid 1954171)	None
HBB31497.1	*Cyanobacteria bacterium* UBA9273 (txid 2055791)	
WP_086756463.1	*Nostoc* sp. 106C (txid 1932667)	WP_086756461.1 glutathione S-transferase family protein WP_086756459.1 type II toxin-antitoxin system RelE/ParE family toxin WP_086756465.1 type II toxin-antitoxin system RelE/ParE family toxin WP_086756467.1 addiction module protein
WP_106459034.1	*Aphanothece hegewaldii* (txid 2107694)	None
WP_079677205.1	*Planktothrix* sp. PCC 11201 (txid 1729650)	
CUR10041.1	*Planktothrix paucivesiculata* PCC 9631 (txid 671071)	None
TAE71529.1, TAG96987.1, TAE44401.1, TAG67719.1, TAG03486.1, TAE10379.1, TAH31248.1, TAE54265.1	*Microcoleus* species 1 (txid 1151)	None
WP_017750148.1	*Scytonema hofmannii* (txid 128403)	WP_017750188.1 hypothetical protein WP_017750147.1 PenP super family WP_081403012.1 hypothetical protein WP_017750146.1 HTH_XRE super family WP_148662840.1 YjiC super family

WP_148562528.1	*Spirosoma radiotolerans* (txid 1379870)	WP_046375372.1 DNA-binding response regulator, LytR/AlgR family WP_046375371.1 PAS domain S-box protein WP_046375370.1 heme transporter CcmB
WP_100989393.1	*Spirosoma pollinicola* (txid 2057025)	WP_100989392.1 DNA-binding response regulator, LytR/AlgR family WP_100989391.1 PAS domain S-box protein WP_100989390.1 Heme NO binding domain protein
WP_080240382.1	*Spirosoma rigui* (txid 564064)	WP_080240383.1 DNA-binding response regulator, LytR/AlgR family WP_080240384.1 PAS domain S-box protein WP_080240385.1 Heme NO binding domain protein
WP_097128788.1	*Spirosoma fluviale* (txid 1597977)	WP_097128786.1 DNA-binding response regulator, LytR/AlgR family WP_097128784.1 PAS domain S-box protein WP_097128782.1 Heme NO binding domain protein
ADB42227.1	*Spirosoma linguale* DSM 74 (txid 504472)	ADB42228.1 DNA-binding response regulator, LytR/AlgR family ADB42229.1 multi-sensor hybrid histidine kinase ADB42230.1 Heme NO binding domain protein ADB42231.1 hypothetical protein ADB42232.1 hypothetical protein
WP_106138807.1	*Spirosoma oryzae* (txid 1469603)	WP_106138806.1 DNA-binding response regulator, LytR/AlgR family WP_106138805.1 PAS domain S-box protein WP_106138804.1 Heme NO binding domain protein WP_106138808.1 hypothetical protein
WP_077133057.1	*Spirosoma montaniterrae* (txid 1178516)	WP_077133058.1 DNA-binding response regulator, LytR/AlgR family WP_077133059.1 PAS domain S-box protein WP_077133060.1 Heme NO binding domain protein
WP_129603966.1	*Spirosoma* sp. TY50 (txid 2502893)	WP_077921356.1 DNA-binding response regulator, LytR/AlgR family WP_077921355.1 PAS domain S-box protein WP_077921354.1 Heme NO binding domain protein WP_129603970.1 5-(carboxyamino)imidazole ribonucleotide synthase
WP_077921357.1	*Spirosoma* sp. 209 (txid 1955701)	WP_077921356.1 DNA-binding response regulator, LytR/AlgR family WP_077921355.1 PAS domain S-box protein WP_077921354.1 Heme NO binding domain protein WP_077921358.1 5-(carboxyamino)imidazole ribonucleotide synthase

WP_138502128.1	*Spirosoma lacussanchae* (txid 1884249)	WP_138502130.1 DNA-binding response regulator, LytR/AlgR family WP_138502132.1 PAS domain S-box protein WP_138502134.1 Heme NO binding domain protein WP_138502126.1 5-(carboxyamino)imidazole ribonucleotide synthase
MBU51551.1	*Deltaproteobacteria bacterium* (txid 2026735)	
WP_142082592.1	*Roseinatronobacter monicus* (txid 393481)	WP_142082593.1 YaiI/YqxD family protein
TVQ01599.1	*Roseinatronobacter* sp. (txid 1945755)	TVQ01602.1 YaiI/YqxD family protein

Figure C1: Sequence alignment of syNOS and homologous sequences

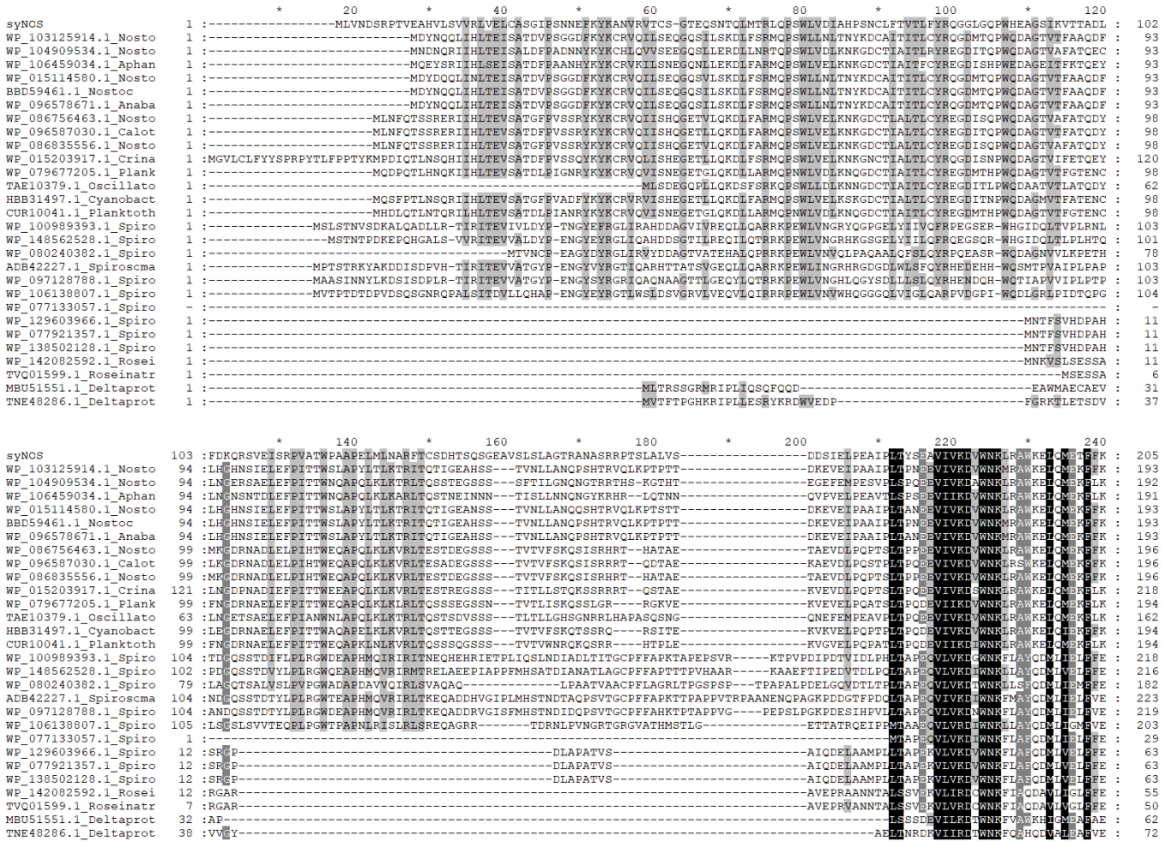

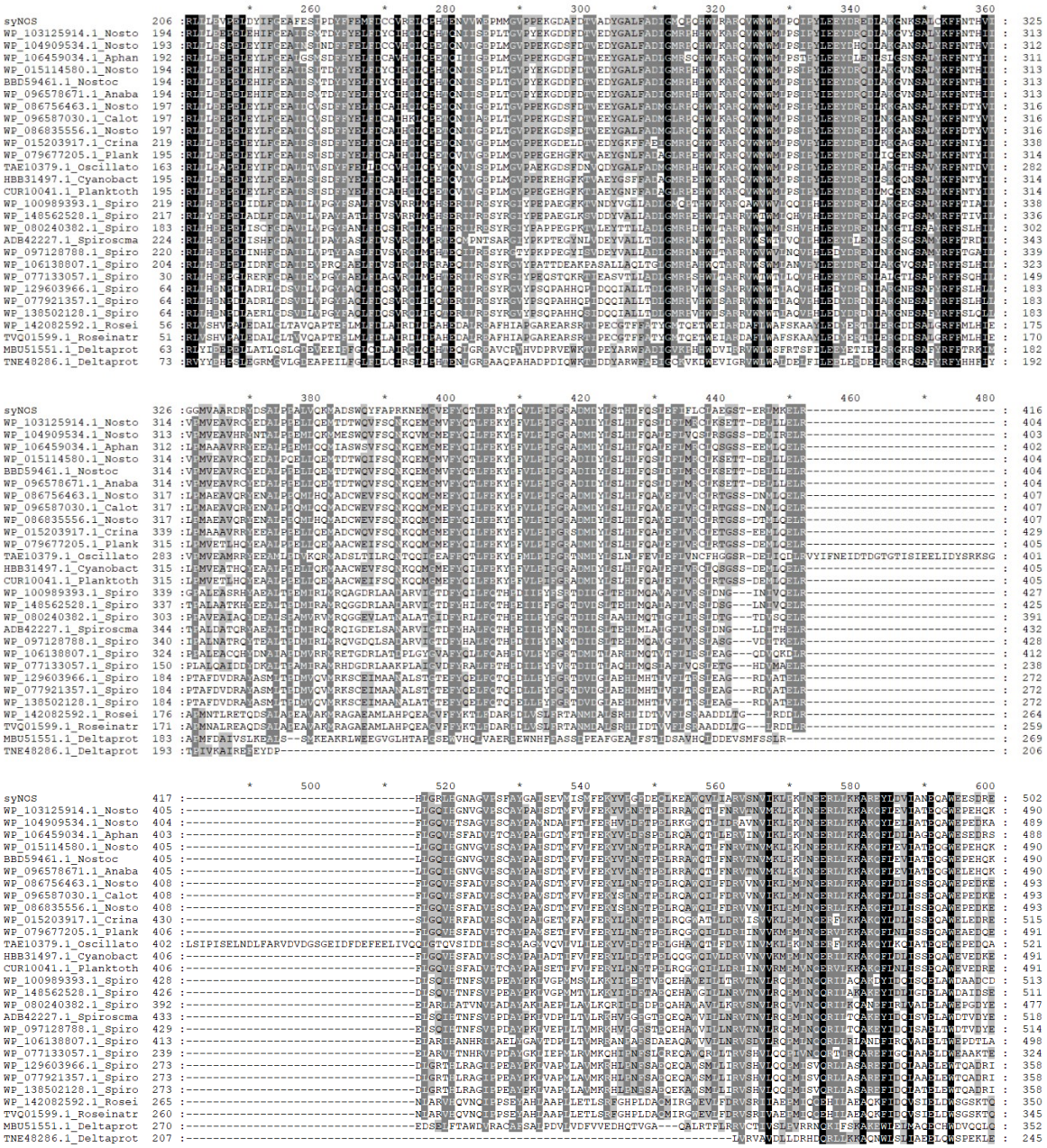

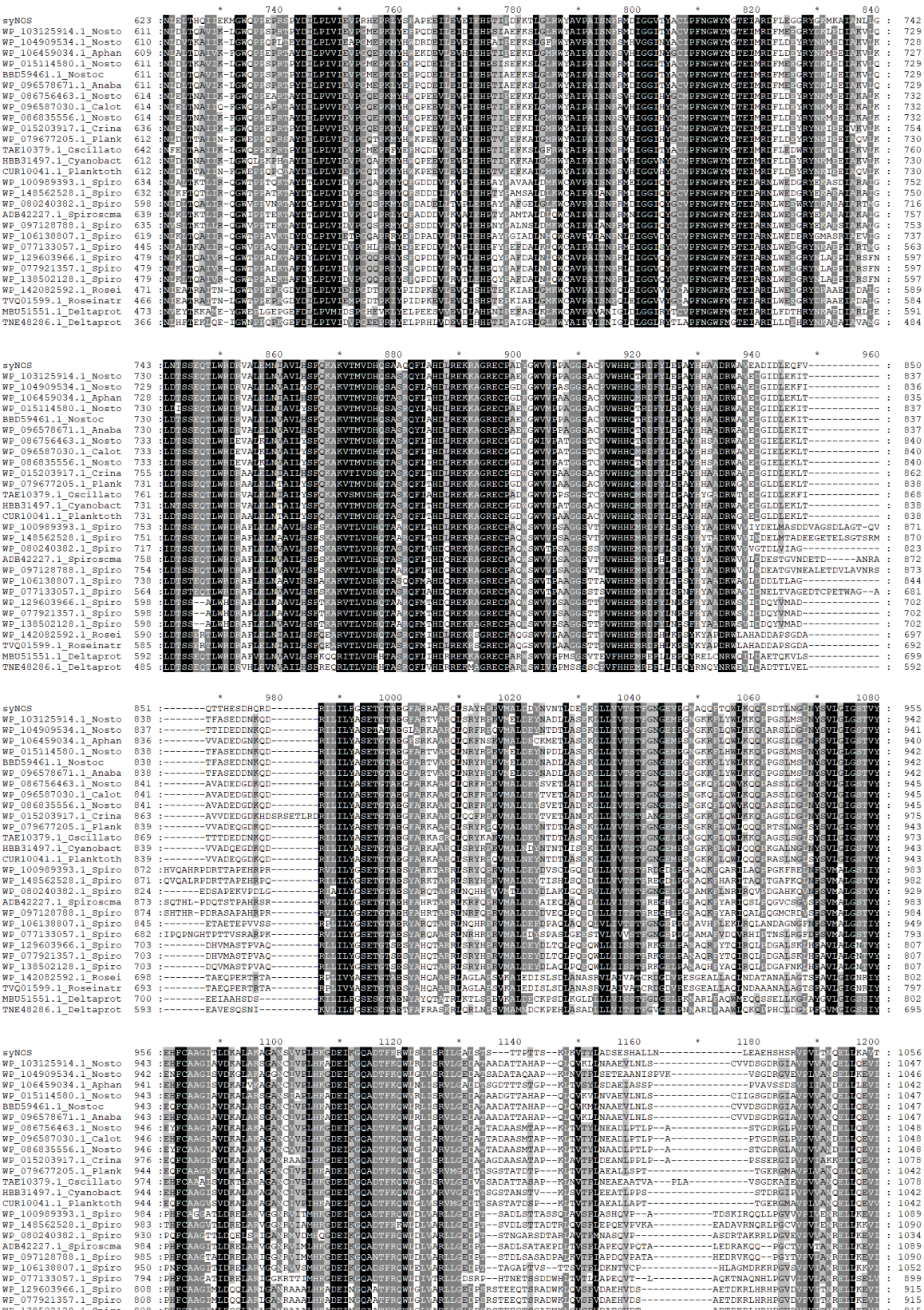

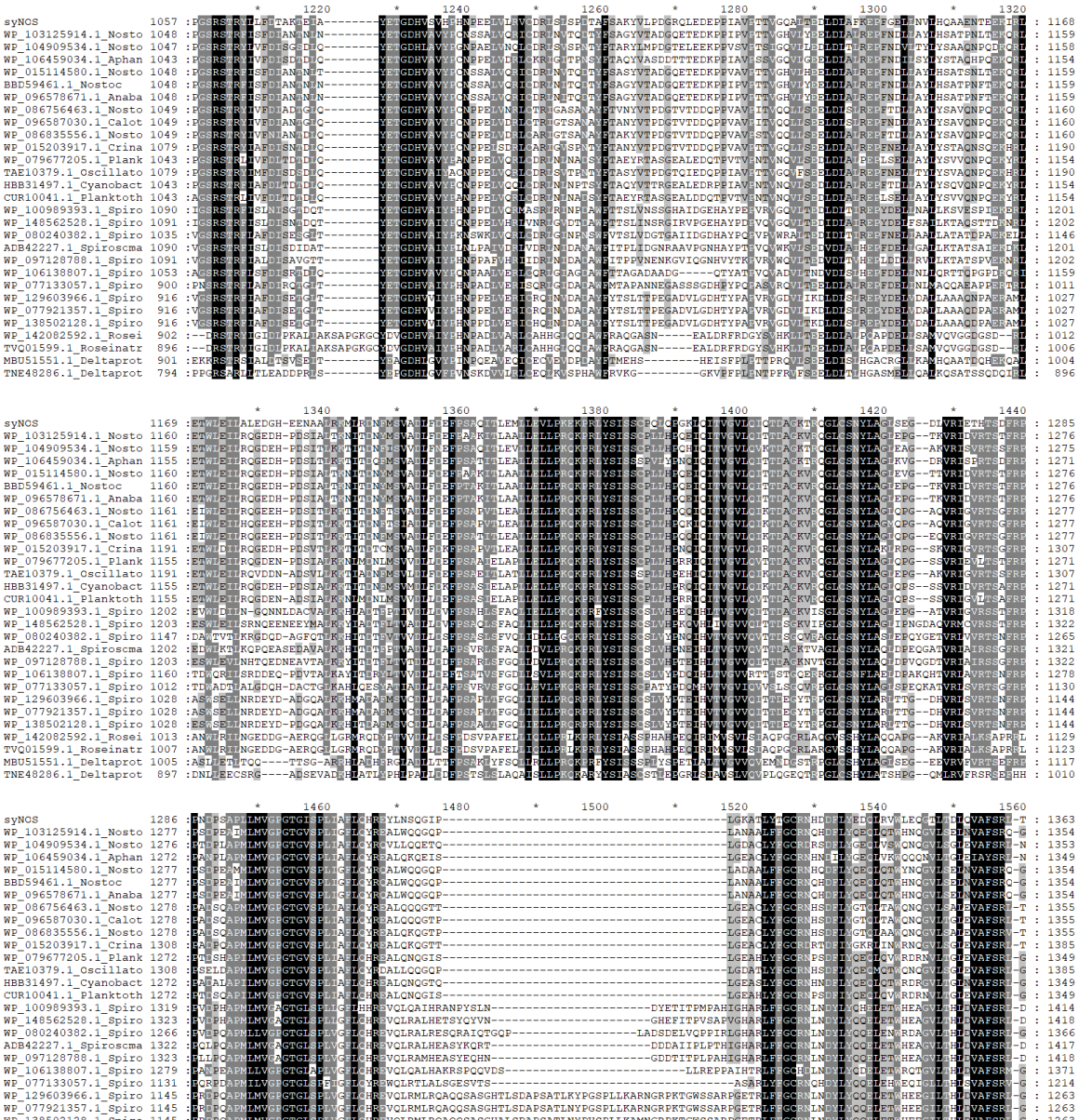

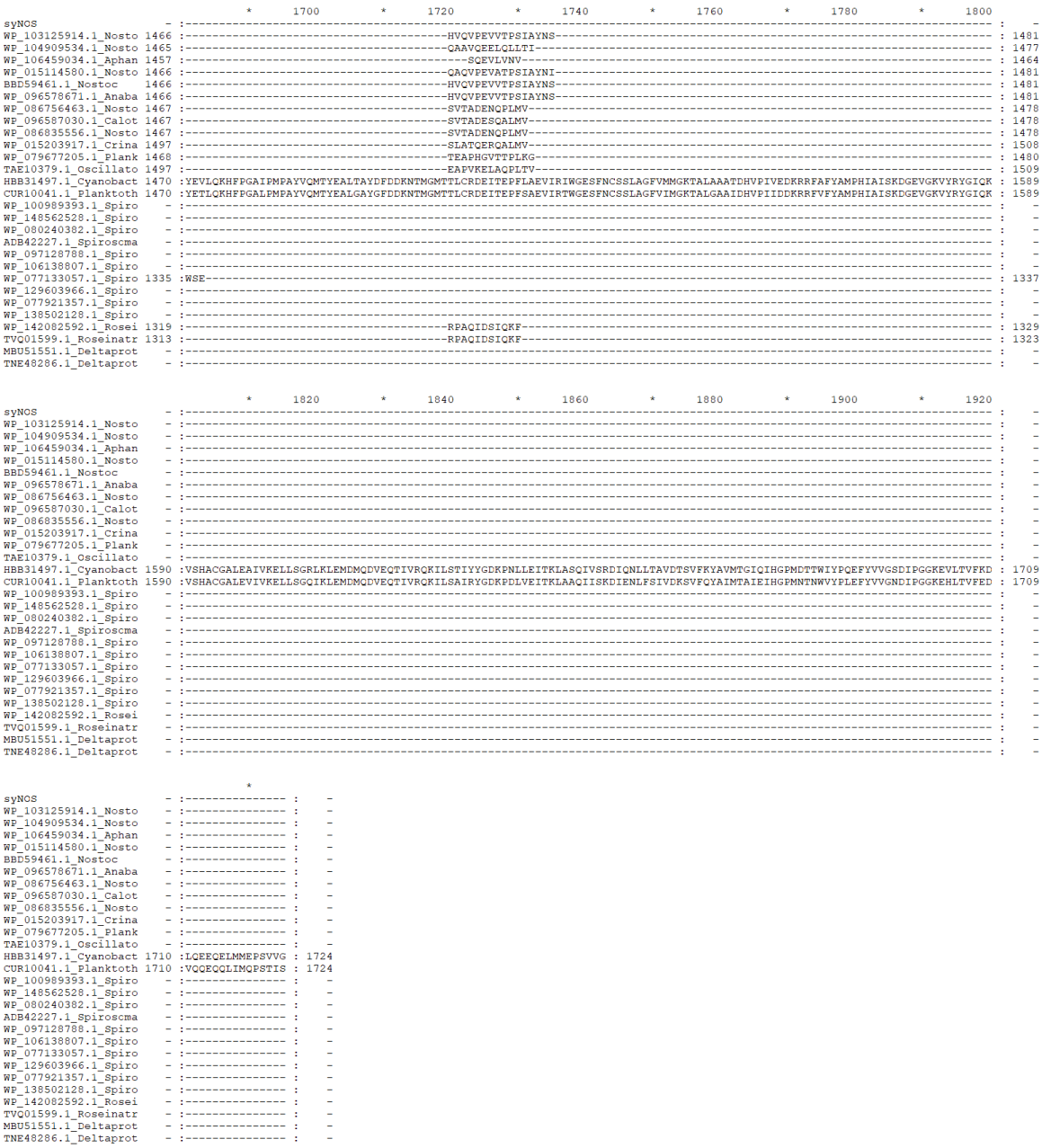
syNOS
WP_103125914.1_Nosto
WP_104909534.1_Nosto
WP_106459034.1_Aphan
WP_015114580.1_Nosto
BBD59461.1_Nostoc
WP_096578671.1_Anaba
WP_086756463.1_Nosto
WP_096587030.1_Calot
WP_086835556.1_Nosto
WP_015203917.1_Crina
WP_079677205.1_Plank
TAE10379.1_Oscillato
HBB31497.1_Cyanobact
CUR10041.1_Planktoth
WP_100989393.1_Spiro
WP_148562528.1_Spiro
WP_080240382.1_Spiro
ADB42227.1_Spiroscma
WP_097128788.1_Spiro
WP_106138807.1_Spiro
WP_077133057.1_Spiro
WP_129603966.1_Spiro
WP_077921357.1_Spiro
WP_138502128.1_Spiro
WP_142082592.1_Rosei
TVQ01599.1_Roseinatr
MBU51551.1_Deltaprot
TNE48286.1_Deltaprot

APPENDIX D

Abbreviations

AST	arginine succinyl transferase pathway
baNOS	*Bacillus anthracis* nitric oxide synthase
BLAST	basic local alignment search tool
bsNOS	*Bacillus subtilis* nitric oxide synthase
Ca^{2+}-CaM	calcium-bound calmodulin
CaM	calmodulin
CO	carbon monoxide
CYP450	cytochrome P450
CYPOR	cytochrome P450 reductase
drNOS	*Deinococcus radiodurans* nitric oxide synthase
ESR	electron spin resonance
ET	electron transfer
FAD	flavin adenine dinucleotide
flavoHb	flavohemoglobin
FMN	flavin mononucleotide
FNR	ferredoxin-$NADP^+$ reductase
GOE	great oxidation event
GTPCH I	guanosine triphosphate cyclohydrolase I
H_4B	(6R,1'R,2'S)-5,6,7,8-tetrahydrobiopterin
H-NOX	heme nitric oxide/oxygen binding proteins

HPLC	high pressure liquid chromatography
iNOS	inducible nitric oxide synthase
L-Arg	L-arginine
L-Cit	L-citrulline
L-NAA	N^G-amino-L-arginine
L-NAME	N^G-nitro-L-arginine methyl ester
L-NNA	N^G-nitro-L-arginine
MGD	N-methyl-d-glucamine dithiocarbamate
mNOS	mammalian NOS
NADPH	nicotinamide adenine dinucleotide phosphate
NOD	nitric oxide dioxygenase
NOHA	N^{ω}-hydroxy-L-arginine
nNOS	neuronal NOS
NO	nitric oxide
NOS	nitric oxide synthase
NOS_g	nitric oxide synthase globin domain
$NOS_{g/ox}$	nitric oxide synthase globin and oxygenase domains
NOS_{NOC}	*Nocardia* nitric oxide synthase
NOS_{ox}	nitric oxide synthase oxygenase domain
$NOS_{ox/red}$	nitric oxide synthase oxygenase and reductase domains
NOS_{red}	nitric oxide synthase reductase domain
OPA	*o*-phthaldialdehyde
otNOS	*Ostreococcus tauri* nitric oxide synthase

PTPS	6-pyruvoyl tetrahydrobiopterin synthase
saNOS	*Staphylococcus aureus* nitric oxide synthase
SEC	size exclusion chromatography
siliNOS	*Silicibacter* nitric oxide synthase
scNOS	*Sorangium cellulosum* nitric oxide synthase
SDR	short-chain dehydrogenase/reductase
SR	sepiapterin reductase
syNOS	*Synechococcus* sp. PCC 7335 nitric oxide synthase
THF	tetrahydrofolic acid